



# Evaluating climate change impacts on the upper Yukon River basin

Projecting future conditions using glacier,  
climate and hydrological models



**Northern Climate ExChange**  
YUKON RESEARCH CENTRE • Yukon College



**This publication may be obtained online at [yukoncollege.yk.ca/research](http://yukoncollege.yk.ca/research).**

**This publication may be obtained from:**

Northern Climate ExChange  
Yukon Research Centre, Yukon College  
500 College Drive, PO Box 2799  
Whitehorse, Yukon Y1A 5K4  
867.668.8895 or 1.800.661.0504

**Recommended citation:**

Samuel, J., J. Kavanaugh, B. Benkert, M. Samolczyck, S. Laxton, R. Evans, S. Saal, J. Gonet, B. Horton, J. Clague, Z. Harmer and L. Kinnear. 2016. *Evaluating climate change impacts on the upper Yukon River basin: Projecting future conditions using glacier, climate and hydrological models*. Whitehorse, Yukon: Northern Climate ExChange, Yukon Research Centre.

**Photo credit:** Stephanie Saal, Northern Climate ExChange, Yukon Research Centre

**Photo location:** Llewellyn Glacier, British Columbia

## **Project team**

### **Lead authors**

Jos Samuel Northern Climate ExChange, Yukon Research Centre, Yukon College  
Jeffrey Kavanaugh Department of Earth and Atmospheric Sciences, University of Alberta;  
Adjunct Faculty, Yukon College  
Bronwyn Benkert Northern Climate ExChange, Yukon Research Centre, Yukon College  
Mary Samolczyck Centre for Northern Innovation in Mining, Yukon College

### **Contributors**

Sarah Laxton Yukon Geological Survey, Department of Energy Mines and Resources,  
Government of Yukon  
Randal Evans Northern Climate ExChange, Yukon Research Centre, Yukon College  
Stephanie Saal Northern Climate ExChange, Yukon Research Centre, Yukon College  
Jared Gonet Northern Climate ExChange, Yukon Research Centre, Yukon College  
Brian Horton Northern Climate ExChange, Yukon Research Centre, Yukon College  
John Clague Department of Earth Sciences, Simon Fraser University  
Zach Harmer Department of Sustainability Science and Society, Brock University  
Lacia Kinnear Northern Climate ExChange, Yukon Research Centre, Yukon College

### **Technical advisors**

John Pomeroy Centre for Hydrology, University of Saskatchewan  
Chris DeBeer Global Institute for Water Security, University of Saskatchewan  
Ric Janowicz Water Resources Branch, Department of Environment, Government of  
Yukon

### **Technical editing and production**

Patricia Halladay, Patricia Halladay Graphic Design (editing and layout)  
Guinevieve Lalena, Lalena Graphic Design (cover design)

### **Disclaimer**

This report, including any associated maps, tables and figures (the “Information”) conveys general comments and observations only. The Information is provided by the Yukon Research Centre on an “AS IS” basis without any warranty or representation, express or implied, as to its accuracy or completeness. Any reliance you place upon the information contained here is your sole responsibility and strictly at your own risk. In no event will the Yukon Research Centre be liable for any loss or damage whatsoever, including without limitation, indirect or consequential loss or damage, arising from reliance upon the Information.

## **Acknowledgements**

We gratefully acknowledge the financial support from Natural Sciences and Engineering Research Council of Canada (NSERC) and Yukon Energy Corporation (YEC).

This project would also not have been possible without contributions from staff and students at the Yukon Research Centre, including Bob Sagar, Alison Perrin, Eirik Sharp, Alex Mischler, Tannicka Reeves, Kyla Foster and Clint Sawicki. Thank you for your commitment and enthusiasm.

The Cold Regions Hydrological Model and both technical support for and changes to this model were provided free of charge by the Centre for Hydrology, University of Saskatchewan. We thank Xing Fang, Dhiraj Pradhananga, Kabir Rasouli and Tom Brown of the Centre for Hydrology for their technical assistance with preparation of the model for the upper Yukon River Basin.

The staff of Yukon Energy, past and present, were a driving force behind this project and helped ensure the excellence of the final product.

Our thanks to all of you!

## Contents

Executive Summary	v
Glossary of terms	viii
<b>1. Introduction and project objectives</b>	<b>1</b>
1.1 Research context and climatic setting	2
1.1.1 Studies in the area	7
1.1.2 Development of the hydrological model	8
1.2 Report outline	10
<b>2. Contemporary studies in water isotope tracers</b>	<b>11</b>
2.1 Water isotope tracers and hydrology	11
2.2 Isotope sampling and analysis, Yukon River headwaters	12
2.3 Water isotope results	13
2.4 Juneau to Atlin glacial traverse	18
2.5 Conclusions	19
<b>3. Late Holocene fluctuations of Llewellyn Glacier's north lobe</b>	<b>20</b>
3.1 Introduction	20
3.2 Methods	20
3.3 Results	22
3.4 Conclusions	24
<b>4. Present glacier area and volume</b>	<b>25</b>
4.1 Context	25
4.2 Ground-penetrating radar (GPR)	26
4.3 Ablation wires	32
4.4 Conclusions	33
<b>5. Developing and applying the Cold Regions Hydrological Model</b>	<b>34</b>
5.1 Model description	34
5.2 Meteorological and hydrometric data	34
5.2.1 Station installation and data collection	34
5.2.2 The existing network	38
5.2.3 GEM-LAM and grid correction	39
5.3 Model set-up and parameter definition	42
5.3.1 Delineating the basin	42
5.3.2 Determining model structure	47
5.3.3 Glacier mass balance	51
5.3.4 Estimating model parameters	52
5.4 Model evaluation and results	53
5.4.1 Model evaluation	53
5.4.2 Flow variation	56
5.4.3 SWE variation	60
5.4.4 Glacier mass balance	63
5.5 Understanding and interpreting model uncertainties	68
5.6 Conclusions	69

<b>6. Climate scenario analysis</b>	<b>70</b>
6.1 Climate data	70
6.2 Predicting hydrological responses to climate forcing using CRHM	72
6.2.1 Interpolation, bias correction, and disaggregation methods	72
6.2.2 Glacier cover change model: simulating glacier retreat and advance	74
6.2.3 Workflow of the coupled CRHM, BCM and GCCM	74
6.3 Results of climate analysis	75
6.3.1 Potential future climate conditions	76
6.3.2 Estimates of future changes in glacier cover and volume	89
6.4 Conclusions	99
<b>7. Considering uncertainties and recommendations for future work</b>	<b>100</b>
7.1 Hydrological characteristics of the upper Yukon River basin	100
7.2 Anticipated climate changes	100
7.3 Future glacier cover and changes in river flow	101
7.4 Model uncertainty	101
7.5 Recommendations for future research	102
7.5.1 Reducing the uncertainty of climate projections	102
7.5.2 Improving estimates of spatial distribution of ice thickness and glacier cover	103
7.5.3 Improving the density of meteorological station networks	103
7.5.4 Improving river flow estimates	104
7.5.5 Model limitations and model development	104
<b>References</b>	<b>105</b>

## Executive Summary

The central importance of hydroelectricity to the energy security of Yukon, combined with the increasing awareness of the impacts of a changing climate, provide the context for this project. With the bulk of Yukon's hydropower generated at the Whitehorse Hydro Facility, it is of critical importance to understand how continued changes in regional climate could modify the magnitude and timing of the flow of the upper Yukon River. For this reason, the Northern Climate Exchange (NCE), part of Yukon Research Centre at Yukon College, led a three-year study with four linked objectives:

1. to improve weather and snowpack monitoring in the upper Yukon River watershed;
2. to advance the understanding of past fluctuations of the Llewellyn Glacier and examine the use of stable water isotopes for determining basin-scale hydrological patterns through field data collection studies;
3. to more accurately characterize the volume and mass balance of the region's glaciers; and
4. to develop a regional hydrological model that supports examination of hydrological responses to anticipated changes in climate.

In order to meet these objectives, the NCE engaged with collaborators from other parts of Yukon College, and with Government of Yukon, University of Alberta and University of Saskatchewan. The project began in 2013 and was co-funded by Yukon Energy Corporation and Canada's Natural Sciences and Engineering Research Council (NSERC).

The approach taken in this project merges a multi-disciplinary field study with an advanced hydrological model. Data collected during fieldwork provide an improved understanding of the timing and magnitude of glacier change in the past 2,000 years, test the ability to determine the relative contributions of river flow using stable water isotopes, and provide a greater understanding of present-day glacier geometry and mass balance. The glacier work also provides key inputs to the hydrological model.

### **1. Improving weather and snowpack monitoring in the upper Yukon River watershed**

Earlier studies noted a significant lack of robust meteorological data for the study area, particularly in the high-elevation headwater regions. To address this gap, NCE installed four permanent automated weather stations between 2012 and 2014. A fifth station was installed for the duration of the study to provide information about energy balance at a location immediately adjacent to the Llewellyn Glacier. YEC, the owner of two of these stations, and NCE will continue to collaborate in order to maintain these stations so that they can be a source of long-term data for interested groups. Details regarding the weather station installation are provided in Section 5. Station metadata can be accessed online at <http://envirodata.yukoncollege.yk.ca>.

### **2. Advancing the understanding of past fluctuations of the Llewellyn Glacier and examining the use of stable water isotopes for determining basin-scale hydrological patterns through field data collection studies**

In order to reconstruct a record of past advances and retreats of the Llewellyn Glacier, living and sub-fossil wood were collected and dated using radiocarbon isotopes and dendrochronology (Section 3). This work showed that the north lobe of Llewellyn Glacier advanced during the first half of the first millennium AD, and came within 70 m of its Little Ice Age maximum down-valley limit as early as

the 16th century; it also suggests that the main lobe of Llewellyn Glacier was advancing as early as AD 1035. As the climate continues to change, information on past glacier responses to climate variations highlights the importance of improving our understanding of present-day glacier geometry. In addition to this paleoclimate reconstruction, the project was able to establish the potential for using stable isotopes of water to understand the separate contributions of glaciers and snowmelt to flow (Section 2).

### **3. More accurately characterizing the volume and mass balance characteristics of the region's glaciers**

Fieldwork was also conducted to better understand the volume and mass balance of the glaciers in the upper Yukon River basin (Section 4). The project was planned to complement previous work co-funded by YEC in the region in order to more fully understand the relationships between glacier volume and area for both small and large glaciers. The region's total glacier surface area and volume are currently estimated at 1,030 km<sup>2</sup> and 210 km<sup>3</sup>, respectively. The Llewellyn and Willison glaciers, the largest and hydrologically most significant glaciers in the Upper Yukon River watershed, have a combined surface area of ~564 km<sup>2</sup> and volume of ~141 km<sup>3</sup>. The two glaciers are estimated to have similar maximum thickness values of approximately 500 m in their middle portions, and an average thickness of 274 m. On average, the smaller Fantail Glacier (~50 km<sup>2</sup>) is thinner, with estimated maximum and average thickness values of 500 m and 157 m, respectively. Knowledge of the region's glacier area and volume is critical in order to accurately project their future meltwater production.

### **4. Develop a regional hydrological model to examine hydrological responses to anticipated changes in climate**

Three criteria were used when selecting a hydrological model: its ability to model a complex cold-region environment; limited input data requirements (both to calibrate and validate the model and to drive the model); and the ability to efficiently manage the large and complex upper Yukon River Basin. The Cold Regions Hydrological Model (CRHM), developed at University of Saskatchewan, met these criteria. It is specifically designed for use in areas that are dominated by cryospheric processes, and has the ability to model melt and wastage derived from glacierized areas. The structure of the model allows areas with similar hydrological characteristics to be grouped into hydrological response units (HRUs), which minimizes the data requirements for calibration and validation, and the model is scalable to the area of the upper Yukon River basin (~19,600 km<sup>2</sup>). CRHM has the added advantage of having been developed using data from the Wolf Creek Research Basin, meaning that it has already been successfully applied in a sub-basin of the study area. Details regarding the model setup, and the calibration and validation scheme are found in Section 5.

Tests of model performance were robust enough to support its use in projecting future flow regimes in response to change in climate. The project used fifth-generation Coupled Model Intercomparison Project (CMIP5) projections from two organizations (IPSL and GFDL) and for two emissions scenarios (RCP4.5 and RCP8.5) to project a range of potential future climate conditions. These four projected conditions were used to estimate mean flow between 2014–30 and 2031–45. As shown in Section 6, the average losses of glacier surface area and volume for the Llewellyn and Willison glaciers, estimated by both models and both scenarios, were approximately 18 km<sup>2</sup> and 23 km<sup>3</sup>, respectively, at the end of 2045 compared to the end of 2013. Higher river flow is estimated to occur in the future, with increases ranging from 15 to 18% for 2014–30 and 18 to 26% for 2031–45, relative to 2006–13.

Testing of the model revealed that it is more sensitive to temperature and precipitation, but also responsive to relative humidity and wind speed (Section 6). Temporal variations of the climate variables depended on the scenario, model and time period. Air temperature is the dominant contributor to changes in future flow in May and June. Air temperature and precipitation influenced flow in April and July, and precipitation was the dominant contributor to changes in flow for the other months.

The report closes with recommendations for future work, including suggested steps to develop short-term forecasting using the CRHM model, and to build an approach to mass balance monitoring to better detect glaciers' response to climate change. Key recommendations for further work are as follows:

- Investigate alternative approaches to projecting future climate conditions in order to limit uncertainty in the glacier cover and hydrological models, and evaluate options for physical, statistical, or hybrid approaches to downscaling and bias correction.
- Improve measurement, monitoring and modelling of glacier thickness, flow and mass balance. Although the study did make progress on this, particularly with the modelling of glacier cover, higher-resolution modelling and improved monitoring would be informative for YEC. This would require both field measurement and computer simulation.
- Study the need for additional meteorological monitoring, particularly in eastern and north-central regions of the basin.
- Employ 2D and 3D hydraulic models, coupled with the hydrological model, in order to better estimate the impacts of climate change on the timing of flow.
- Advance the modelling of glacial contributions to flow by treating glaciers as dynamic (moving, while growing and melting) rather than static (growing and melting in place).

This project has met its stated objectives and provides a strong basis for long-term planning by YEC. Although this is not addressed in this project, the CRHM model, with appropriate modifications, could also provide an excellent basis for short-term planning and forecasting.

## Glossary of terms

AD	Anno Domini
AMS	accelerator mass spectrometry
AO	Arctic Oscillation
asl	above sea level
BP	Before Present
BSI	Blue System Integration
CaPA	Canadian Precipitation Analysis
CMIP	Coupled Model Intercomparison Project
CRHM	Cold Regions Hydrological Model
DDF	degree-day factor
DEM	digital elevation model
DETIM	Distributed Temperature Index Model
d-excess	deuterium excess (S2)
DHSVM	Distributed Hydrology Soil Vegetation Model
ELA	Equilibrium Line Altitude
ENSO	El Nino Southern Oscillation
G	glacierized model structure
GCM	global climate model
GEM	Global Environmental Multiscale Model
GEM-LAM	limited-area model version of GEM
GFDL	Geophysical Fluid Dynamics Laboratory
GIS	Geographic Information System
GMWL	Global Meteoric Water Line (S2)
GPR	ground penetrating radar
GRASS	Geographic Resources Analysis Support System
HBV	<i>Hydrologiska Byråns Vattenbalansavdelning</i>
HRU	hydrological response unit
IP3	Improving Processes and Parameterization for Prediction in Cold Regions Hydrology
IPCC	Intergovernmental Panel on Climate Change
IPSL	<i>Institut Pierre Simon Laplace</i>
LEL	Local Evaporation Line (S2)
LIA	Little Ice Age
LWi	incoming long-wave radiation
LWo	outgoing long-wave radiation
masl	metres above sea level
NARR	North American Regional Reanalysis
NCE	Northern Climate ExChange
NG	non-glacierized model structure
NSE	Nash-Sutcliffe Efficiency
PDO	Pacific Decadal Oscillation
RDPS	Regional Deterministic Prediction System
RH	relative humidity
RMSE	root-mean-square error
SWE	snow water equivalent
SWi	incoming short-wave radiation
SWo	outgoing short-wave radiation
VSMOW	Vienna Standard Mean Ocean Water
WAAS	Wide Area Augmentation System

# 1. Introduction and project objectives

Hydroelectricity is a central part of the energy mix in Yukon. Variability in flow, the dominance of snow and glacier melt, a lack of multi-year storage in Yukon River reservoirs, and increasing demand for renewable electricity make it necessary to carefully plan and manage the use of water for hydroelectric production. In addition, the impacts of climate change are already evident in Yukon rivers, and are expected to increase in coming decades. These changes in climate have the potential to affect hydroelectric production.

Recognizing this, Yukon Energy Corporation (YEC), the primary generator of electricity in the territory, has partnered with researchers at Northern Climate ExChange (NCE) to study the potential impacts of climate change in the upper Yukon River basin. This report documents research that took place between July 2013 and December 2016. Results from previous field studies in the Fantail and Wheaton glaciers conducted in August 2011 are also included in this report. The outcomes of the project include the completion of a hydrological model that projects potential changes in the timing and volume of flow of the Yukon River upstream of the dam in Whitehorse, Yukon; the installation and maintenance of automated weather stations in remote locations in order to build the observational network to fill observational data gaps and determine hydrological model parameters (such as elevational air temperature lapse rates); and the advancement of the fundamental knowledge of the hydrology of the Yukon River.

The strategic importance of the Whitehorse Hydro Facility to the energy security of Yukon, and the history of collaboration between YEC and NCE, provide a strong foundation for this study. The two organizations share a desire to advance the understanding of climate change impacts on Yukoners. A precursor to this project in 2011–12 focused primarily on quantifying the hydrological role of glaciers in the watersheds that feed the upper Yukon River (between the headwaters and the Whitehorse dam) and on modelling potential climate change impacts on glaciers. This current project expanded that work to cover climate change impacts for the full basin, and to fill knowledge gaps regarding glacier geometry, glacier mass balance characteristics, and contributions to river discharge at the Whitehorse dam. The specific objectives of the study were as follows:

1. Install automated weather and snowpack monitoring stations in three new locations in the upper Yukon River watershed. This results in a total of five automated weather stations; two were placed in a previous collaborative study between NCE and YEC (NCE 2014). The objective of these stations is to add to the existing network of hydrometric and meteorological stations, with metadata and data made available to the public, and to gain a better understanding of potential changes in snow conditions;
2. Conduct field studies and modelling studies of the past fluctuations and current form and mass balance characteristics of glaciers in the upper Yukon River basin. The project focused on Llewellyn Glacier, British Columbia (BC), the most significant reservoir of frozen water in the catchment, and on its potential responses to future climatic scenarios, but work was extended to other glaciers where possible. This allowed for study of the potential responses of glaciers in the upper Yukon River basin to future climate scenarios;
3. Develop a regional hydrological model that supports examination of hydrological responses to anticipated changes in climate.

In order to meet these objectives, the NCE engaged with collaborators from Yukon College, the Government of Yukon (Department of Environment, Water Resources Branch, Yukon Geological Survey), University of Alberta, and University of Saskatchewan.

## 1.1 Research context and climatic setting

The study area includes all of the Yukon River headwaters upstream of Whitehorse, Yukon, an area of approximately 19,600 km<sup>2</sup> that extends from the Llewellyn Glacier in northwest British Columbia (BC) to Whitehorse in the southwestern Yukon (Figure 1.1).

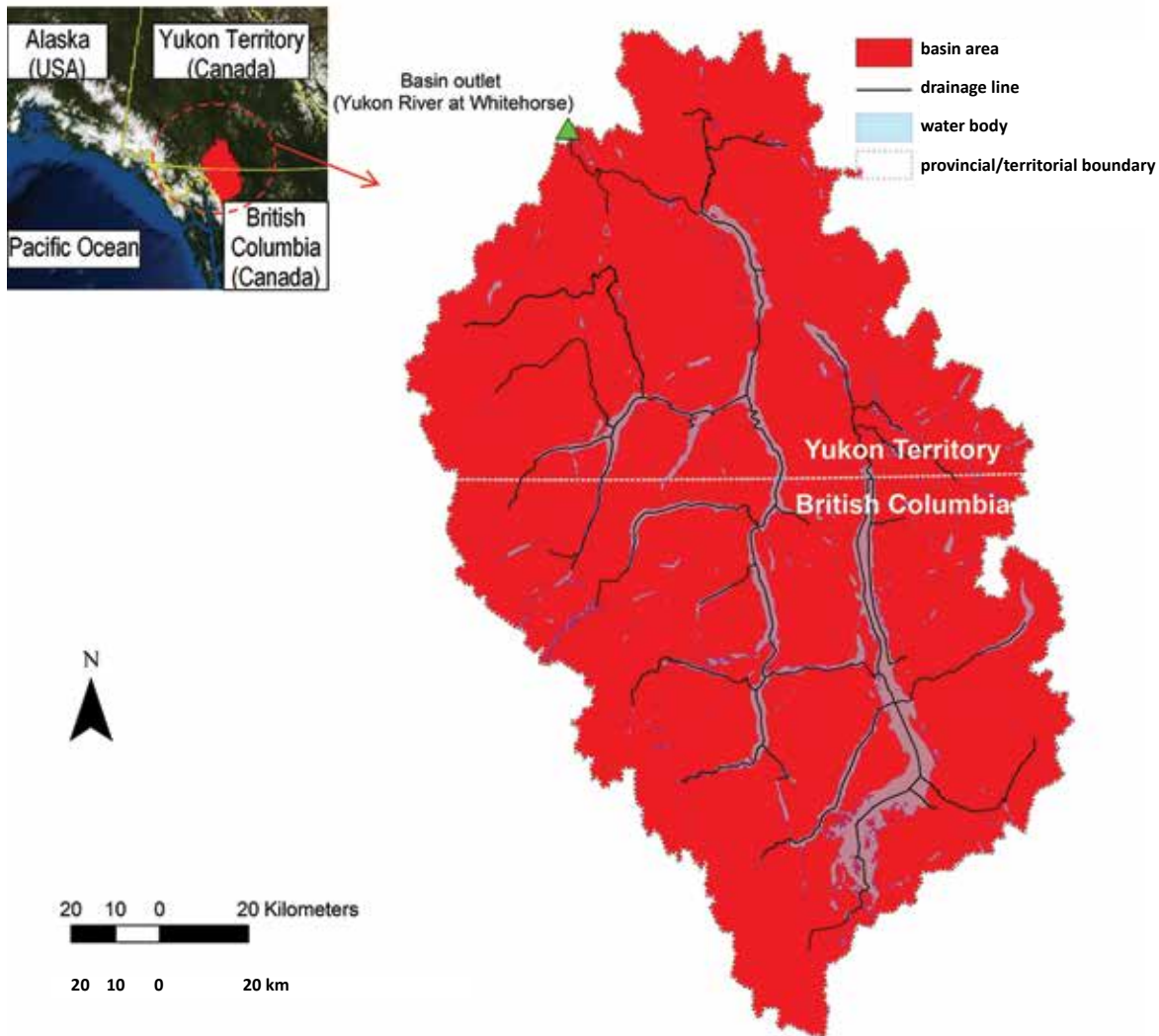


**Figure 1.1** Area map showing basin boundaries, major drainage lines and water bodies.

The basin's climate includes moderately cold regions as well as moist to mild temperate, very wet and cold alpine areas (NCE 2014). Based on output from the Global Environmental Multiscale Model (GEM), a gridded climate data source that covers the whole upper Yukon River basin, the spatially averaged eight-year (2006–13) mean annual air temperature was approximately  $-1.6^{\circ}\text{C}$ , with monthly means ranging from  $-11.9^{\circ}\text{C}$  in January to  $+10^{\circ}\text{C}$  in July. Colder mean monthly air temperatures are found at higher elevations and farther inland, away from the warming influence of the Pacific Ocean. The annual precipitation for the study area for 2006–13 had a mean of approximately 480 mm, ranging between 340 mm in the lower-elevation (central and eastern) regions and 1,400 mm at the highest elevations near the Llewellyn and Willison glaciers.

The hydrology of the basin is dominated by cold mountain region processes, but the southwest portion of the basin is also influenced by Pacific maritime weather systems that produce higher precipitation and more moderate temperatures than in other parts of Yukon (NCE 2014; Carey et al. 2010; Smith et al. 2004; Rouse et al. 1997). The spatial variability of climate in this region is also influenced by the Coast Mountains, which force moisture-laden air approaching from the west upwards, resulting in precipitation at high elevations and a shadow of dryness on the lee side of these mountain ranges (Klock et al. 2011).

The upper Yukon River Basin covers a heterogeneous mix of boreal, subalpine taiga (shrubland), alpine tundra, alpine rockland and glacier, and lakes and wetland land-cover types (Smith et al. 2004). As shown in Figure 1.2, the glacierized portion of the basin represents about 5% (980 km<sup>2</sup>) of the total study area; approximately 60% of the glacierized area is made up of the two largest glaciers in the area, the Llewellyn (450 km<sup>2</sup>) and Willison (160 km<sup>2</sup>). The dominant land cover is boreal forest, which covers approximately 42% of the basin (8,200 km<sup>2</sup>) with an average stand height of 15 m.

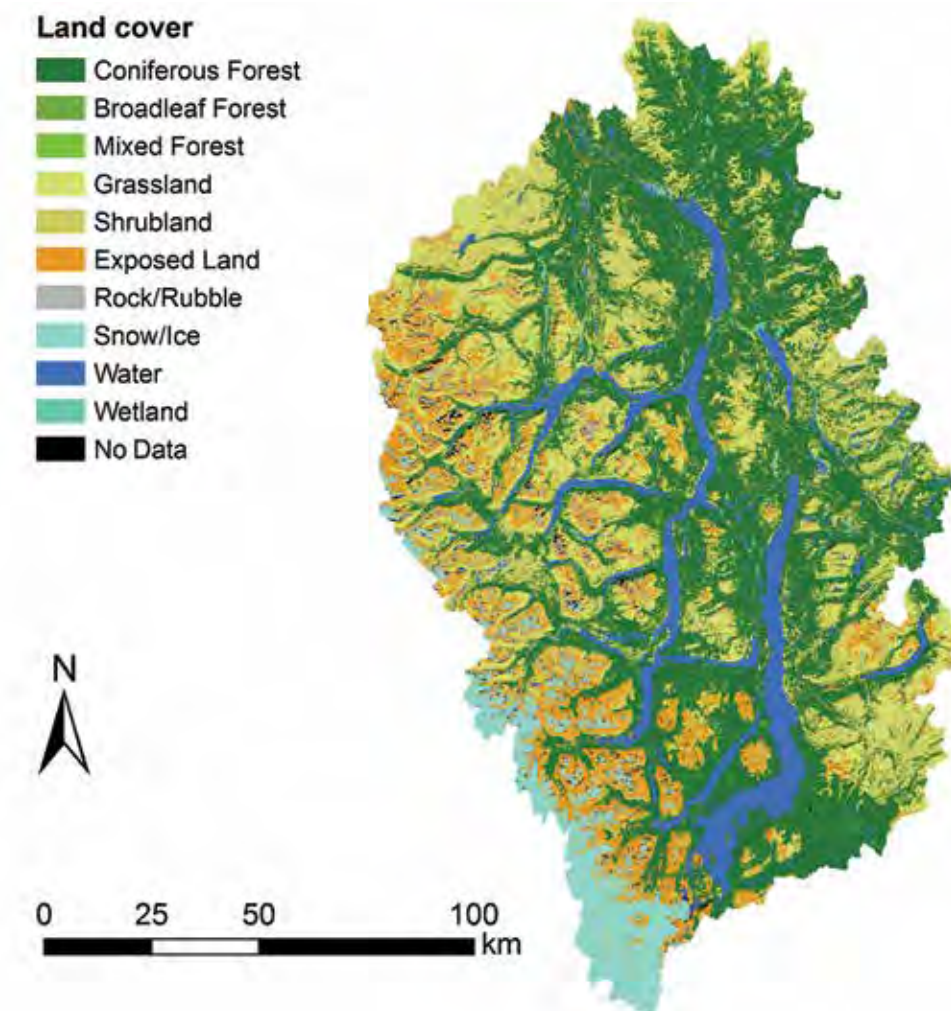


**Figure 1.2** Land cover distribution in the upper Yukon River basin.

The second most significant land cover is shrubland, which covers approximately 20% (4,000 km<sup>2</sup>) of the basin: 16% with shrub height ≤2 m and 4% with shrub height >2 m. The basin's dominant soil type is sandy loam, according to the Harmonized World Soil database (Nachtergaele et al. 2012). The basin has a mix of low- and high-relief areas, with elevations ranging from 640 m at the Yukon River's Whitehorse outlet to 2,466 m in the headwater areas (see Section 5, Figure 5.5), and with slopes varying from 0° to 80° (see Section 5, Figure 5.12). Substantial portions of the basin, particularly those at higher elevations, are underlain by discontinuous permafrost (Lewkowicz et al. 2012; Bonnaventure and Lewkowicz 2011); this can modify flow by affecting the infiltration of water and limiting the effective depth of soil.

Scientists have observed changes in climate in the upper Yukon River basin over the past 60 years. A reliable indicator of change and variability in climate is the Adjusted and Homogenized Canadian Climate dataset produced by Environment and Climate Change Canada (Vincent et al. 2012). This dataset uses standard Government of Canada meteorological observations that have been corrected to account for slight changes over time in factors such as station location and changes in sensors and technology. For Whitehorse, the location in the upper Yukon River basin with the longest observational record, statistically significant increases are evident in mean spring, summer, winter and annual air temperatures (Figure 1.3).

The annual observed increase in air temperature has been 1.7°C/decade over the past 60 years; the observed winter increase has been 4.9°C/decade. Similarly, there has been an increase of 6.0 mm/decade in mean annual precipitation (Figure 1.4). This change is primarily seen in fall and winter, with 3.2 and 2.8 mm increases, respectively. In fall, more of the change in precipitation can be attributed to an increase in snow water equivalent (SWE). In spring, there has been little change in overall precipitation: an increase in rain has been offset by a decrease in snow. Although these data are useful to provide a context of climate change in Yukon, they cannot be used directly in the Cold Regions Hydrological Model (CRHM) used in this project since they are observations from a single point and are not spatially distributed. Gaps in the observational record make it impossible to test the statistical significance of observed trends for precipitation records.

The observed temperature trends are statistically significant at the 95% confidence level and an F-test indicates a low likelihood that the trend is occurring by chance. However, the coefficient of determination ( $R^2$ ) value is generally low for all seasons. This is an indication that there is high variability; visual inspection of the precipitation data indicates similar characteristics. Temperature variability is most apparent in fall and winter, whereas precipitation appears to be the most variable in summer.

# 1. INTRODUCTION AND PROJECT OBJECTIVES

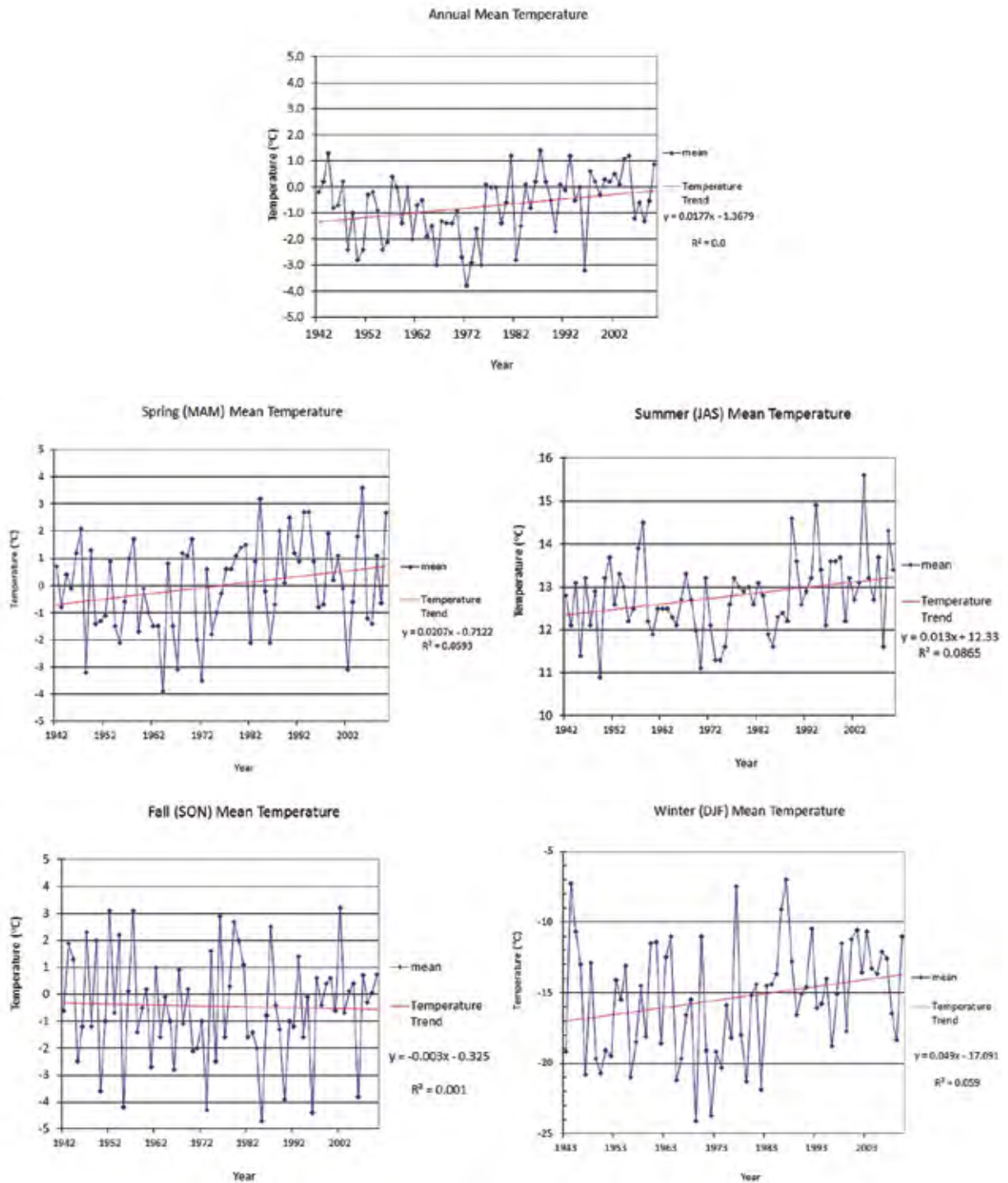


**Figure 1.3** Air temperature summarized as seasonal and annual means.

Note: Plotted using adjusted homogenized climate data from Vincent et al. (2012).

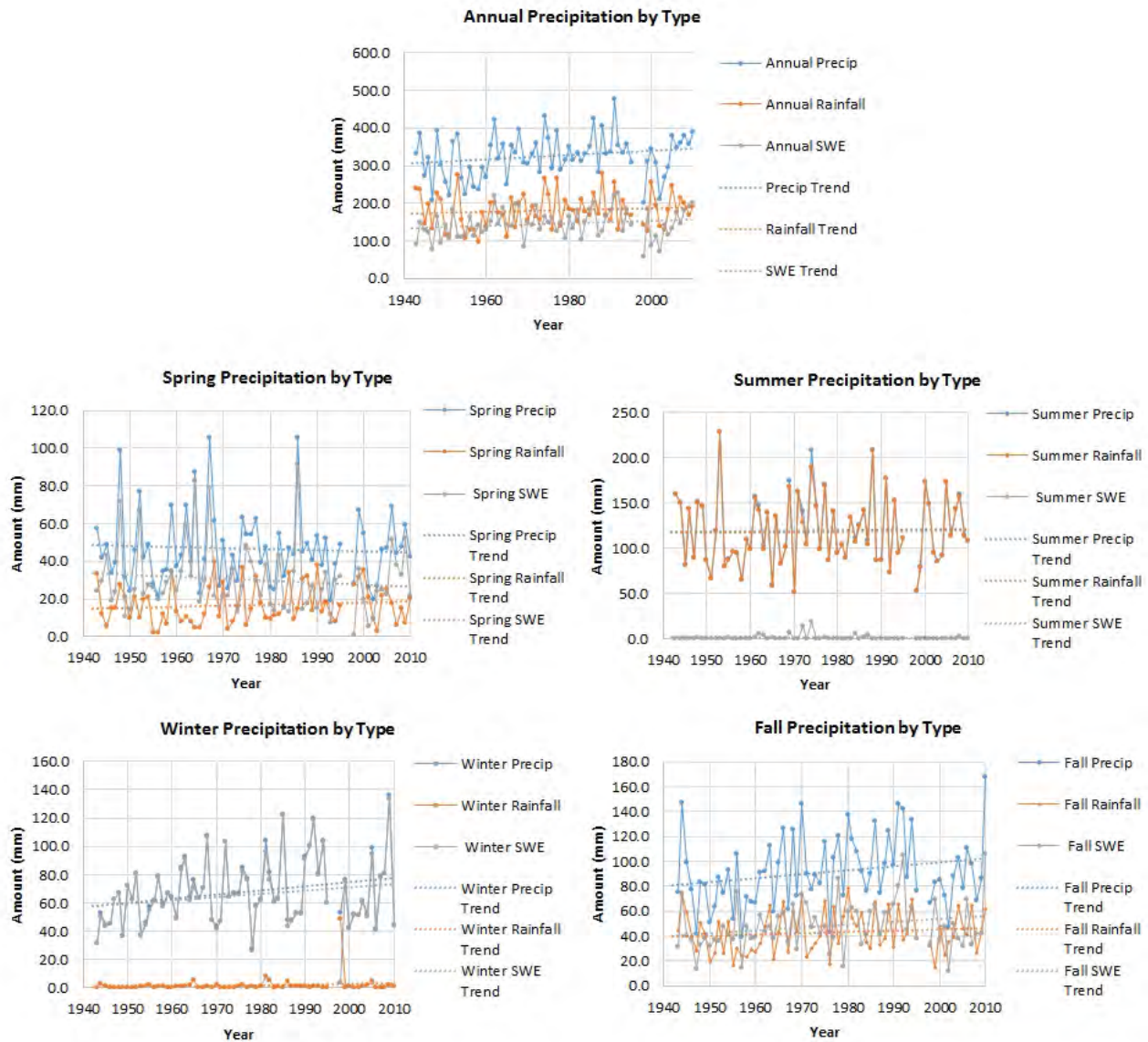


**Figure 1.4** Observed precipitation from Whitehorse Airport summarized as seasonal and annual means. Note: Plotted using adjusted homogenized climate data from Vincent et al. (2012).

Large-scale variations or oscillations in ocean and atmospheric conditions are frequently invoked as causes of variability in local conditions (Bitz and Battisti 1999; Trenberth 1990). The Pacific Decadal Oscillation (PDO), Arctic Oscillation (AO), and El Niño Southern Oscillation (ENSO) can affect local patterns of precipitation and air temperature. Because these oscillations vary in time scales, ranging from months to decades, they can combine to contribute to a large departure from normal conditions, or can cancel each other out (Jianqi and Huijun 2006; Trenberth 1990). These large-scale oscillations have an impact on seasonal weather; they have also been linked to periods of gain or loss of glacier mass (Fleming and Clarke 2003; Neal et al. 2002; Moore and Demuth 2001; Bitz and Battisti 1999) and to variation in river discharge (Brabets and Walvoord 2009; Fleming et al. 2006). Increases in winter and spring flow have been statistically linked with the warm (positive) phase of the PDO (Brabets and Walvoord 2009).

The observation of past trends and variability gives some indication of what future conditions may be like. Past research on the potential response of northern rivers to climate change have used methods such as perturbing mean temperature and precipitation values at set intervals to determine the response (or sensitivity) of northern streams (Janowicz et al. 2016), or have taken a hybrid approach that combines regional climate modelling and perturbation of variables (NCE 2014). However, these methods use past data records and assume linear changes that might introduce uncertainties for non-linear variables such as precipitation (Rasouli et al. 2014). This project uses global climate model projections that form the basis of the fifth assessment report (AR5) for the Intergovernmental Panel on Climate Change (IPCC) to evaluate the potential response of Yukon River to further changes in climate (IPCC 2013). The AR5 climate projections are the present-day standard for modelling studies of this type.

Due to the many complex physical characteristics of the upper Yukon River basin, uncertainties and sensitivities associated with the transfer of water through the basin to the stream outlet are not easily understood (NCE 2014). Meteorological and flow monitoring stations are also limited in the region, which means that the fundamental data required to establish current hydro-meteorological conditions in the region are poorly represented, especially at high elevations (NCE 2014). In addition, few hydrological studies have been conducted in basins of this size and complexity, particularly with respect to developing and determining physically-based distributed hydrological models that examine relevant cold-region processes, such as flow variations due to snowpack dynamics and glacier mass balance and their interactions.

### **1.1.1 Studies in the area**

Recent studies have explored hydrological variability and change across the North. Changes in the flow of northern rivers have been attributed to the warming of winter and spring temperatures, earlier melting of snow, decreasing snow cover and retreating of glacier termini (DeBeer et al. 2016; Berthier et al. 2010; Brown et al. 2010; Brabets and Walvoord 2009; Déry et al. 2009; Moore et al. 2009; Prowse and Furgal 2009; Fleming and Clarke 2003; Serreze et al. 2000; Whitfield and Cannon 2000). In Yukon, there has been an overall increase in observed flow, particularly in winter (Janowicz 2008). In the upper Yukon River basin specifically, NCE (2014) found that the Llewellyn Glacier is the single largest glacial contributor of water, from both melt and wastage, to the Yukon River discharge at Whitehorse. The Llewellyn Glacier contributes more to flow than other glaciers in the area do because it has the largest ablation-zone surface area in the basin, and its terminus extends to a relatively low elevation, which increase the intensity and duration of the melt season (NCE 2014). Ice wastage from this glacier was found to be greater than that of other glaciers in the region over the last few decades (NCE 2014).

Despite the widely acknowledged inter-relationship between climate and hydrology and the specific properties of cold-climate hydrology, there remain large uncertainties associated with data limitations and with complex physical and hydrological characteristics. These pose challenges to quantitatively projecting the hydrological response to changing climate. Hydrological responses to modern-day variability in precipitation and temperature are not completely understood, and climate change is anticipated to impose further complexity on these relationships.

Recognizing these knowledge gaps, researchers from the University of Saskatchewan and the Government of Yukon established a project to intensively study northern, high-elevation hydrology

in a real-world setting. The University of Saskatchewan established the Wolf Creek Research Basin outside of Whitehorse in 1993 (Pomeroy et al. 2010). In the ensuing decades, researchers from all over the world have participated in research there. Results from an array of monitoring stations, and from a wealth of studies of specific phenomena have provided substantial insight into key hydrological processes in cold region mountain environments.

These studies have provided important insight into topics that include snowmelt hydrology in alpine, subalpine and boreal environments (Carey and Woo 2005), interactions between snowmelt and discontinuous permafrost (Carey and Quinton 2004), and modelling of snowpack evolution, sublimation processes and redistributions through the full accumulation and ablation cycle (MacDonald et al. 2009; McCartney et al. 2006; Pomeroy et al. 2002). Long-term data from this site have also been used to directly quantify the sensitivity of northern rivers to a changing climate (Rasouli et al. 2014).

### **1.1.2 Development of the hydrological model**

The knowledge gained from the Wolf Creek Research Basin has been central to the development of the Cold Regions Hydrological Model, or CRHM (Pomeroy et al. 2010), the model selected for use in this project. Today, the Wolf Creek Research Basin continues to operate as a Water, Ecosystem, Cryosphere and Climate Observatory as part of the Changing Cold Regions Network led by University of Saskatchewan.

Scaling from the relatively small area of the Wolf Creek Research Basin ( $\approx 220 \text{ km}^2$ ) to the entire upper Yukon River basin (approximately  $19,600 \text{ km}^2$ ) presents a number of challenges. The sparse observational network and lack of high-elevation monitoring sites in the upper Yukon River basin, where a significant portion of runoff is generated, make it difficult to verify the baseline hydrometeorological conditions. Without a clear understanding of current conditions, it is difficult to project hydrological responses to climate change. This was a fundamental motivation for achieving Objective 1 of this project.

The hydrological role of cryospheric processes (such as snow accumulation, snowmelt and glacier storage and melt) and their potential sensitivity to climate change are only partially understood in this region. Recent scientific advances in the understanding of cold region hydrology and glaciology in western North America have been made by studies such as those by Improving Processes and Parameterization for Prediction (IP3) in Cold Regions Hydrology (IP3 2010) and the Western Canadian Cryospheric Network (WC2N 2010), both of which conducted research in the Wolf Creek Research Basin. However, the need remains to integrate some of the findings and tools developed through these initiatives for predicting hydrological changes in the glacierized headwaters of the Yukon River.

IP3 has shown that predictive hydrological modelling in cold regions needs to incorporate physical process descriptions and process interactions to improve reliability under non-stationary conditions. The Wolf Creek Research Basin is non-glacierized, and foundational scientific investigations are required in glacial and periglacial environments if the quantitative understanding of associated processes is to improve. This further underscores the need for establishing a monitoring network in the region (Objective 1), and provides the motivation for Objective 2. These issues represent some of the principal problems that must be addressed in order to support better water management and future hydrosecurity in Yukon.

Computer-based models are needed in order to quantitatively project the impacts of climate change on the upper Yukon River basin. However, not all models are equal. This project considered the use of both simple and physically-based models. Although a simple model may be tuned to fit a hydrograph, it can be difficult to ascertain the underlying reasons why it fits, and whether it will be able to accurately represent future processes if climate inputs change. Physically-based distributed hydrological models are valuable tools for studying the hydrological responses to climate inputs, such as precipitation, air temperature and wind speed. The use of these models is more complex, but their more realistic treatment of hydrological processes make them more robust if inputs change (Beven 2001; Beven 1985; Beven and O'Connell 1982).

Several physically-based distributed models have been used in snow-dominated regions (particularly in Canada). These include the Distributed Hydrology Soil Vegetation Model (Wigmosta et al. 1994), the *Modélisation Environnementale Communautaire* (MEC)–Surface Hydrology developed by Environment Canada (Pietroniro et al. 2007; Soulis et al. 2000), the Variable Infiltration Capacity model (Liang et al. 1994), and the Cold Regions Hydrological Model (Pomeroy et al. 2007). In general, the first three models use the same hydrological structure for the entire model domain and depend mainly on calibration/validation schemes. Such schemes require relatively long data time-series records, and their use can increase uncertainty about model parameters and hinder understanding of hydrological processes (Beven 2001). In addition, the first three models compute water and energy balances in a grid system, in which the results depend on the grid resolutions and may not be appropriate for heterogeneous basins with complex river geometries.

CRHM is able to operate with minimal or no calibration, and allows flexibility in assembling the hydrological model structure by providing a wide selection of physically-based processes modules. Instead of computing on a grid system, CRHM computes water and energy balances in hydrological response units (HRUs). These units are hydrologically unique model elements for configuring the spatial variability of physical attributes and drainage conditions (Pomeroy et al. 2007). In addition, CRHM includes a full set of physically based representations of cold hydrological processes, such as direct and diffuse radiation to slopes, long-wave radiation in complex terrain, intercepted snow, blowing snow, sub-canopy turbulent and radiative transfer, sublimation, energy balance snowmelt, infiltration to frozen and unfrozen soils, rainfall interception, evapotranspiration, subsurface flow, depressional storage fill and spill, saturation excess overland flow and routing of surface, subsurface and streamflow waters (Pomeroy et al. 2007).

CRHM has been widely applied in cold regions across Canada, including British Columbia, Yukon, Alberta and Northwest Territories, and in other parts of the world, including Tibet, Patagonia, the Pyrenees and the Alps (Zhou et al. 2014; Fang et al. 2013; López-Moreno et al. 2012; Ellis et al. 2010; Dornes et al. 2008; Ellis and Pomeroy 2007). Due to its benefits and its suitability for study needs, CRHM was used in this project. Although it is well suited to study needs, its application to the region remains challenging. The model had not previously been applied in a large, heterogeneous and glacierized basin in the Yukon region.

## 1.2 Report outline

The primary focus of this report is to synthesize the methods and results of the modelling work conducted in the last three years (Objective 3). However, this would not have been possible without the work conducted under Objectives 1 and 2. As a result, this report provides a basic overview of all work conducted as part of the project.

Section 2 provides an overview of how stable water isotope tracers ( $^{18}\text{O}$ ,  $^2\text{H}$ ) offer an effective way to assess water balance conditions over large-scale systems. Sampling can be conducted rapidly, and in conjunction with other activities, and isotopic partitioning in the hydrological cycle is well understood (see Edwards et al. 2004). This project used isotope tracers to attempt to distinguish the importance of glacier melt and snowpack runoff, and of precipitation and groundwater inputs, to discharge on the Yukon River. Such approaches have been applied effectively in other areas with glacierized river systems, including the Wind River Range, Wyoming (Cable et al. 2011) and Okstindan, Norway (Theakstone 1998).

Section 3 describes what is understood about how glaciers in the upper Yukon River basin have responded to fluctuations in climate during the late Holocene Epoch (approximately the past 2,000 years). A record of past advances and retreats of the north lobe of the Llewellyn Glacier was constructed by dating both living and sub-fossil wood found in lateral and end moraines located beside and down valley from the present-day glacial toe using radiocarbon isotopes and dendrochronology.

Section 4 summarizes results from work to better delineate the present-day geometry and mass balance of the Llewellyn and Fantail glaciers. During this study, ground penetrating radar (GPR) was used to survey the ice depth of key glaciers in the basin. These surveys were complemented by installation and periodic measurement of ablation wires in order to monitor glacier mass balance.

Section 5 describes in detail how the CRHM model has been implemented for the upper Yukon River Basin. Input data are described in detail, the modules using their base equations are summarized, and results showing model performance are presented.

Section 6 describes how climate projections were used to investigate potential future hydrological conditions. Climate-induced changes in the timing and volume of flow were modelled for 2014–30 and 2031–45.

Section 7 discusses results, summarize sources of uncertainty, and recommends future actions, both by YEC and for more fundamental research.

## 2. Contemporary studies in water isotope tracers

### 2.1 Water isotope tracers and hydrology

Preliminary studies of water isotopes were conducted in conjunction with other research in this project to investigate the effectiveness of water isotope tracers as a tool for understanding local hydrological processes. Stable water isotope tracers ( $^{18}\text{O}$ ,  $^2\text{H}$ ) offer an effective way to assess local hydrological conditions over large-scale systems; sampling can be conducted rapidly in conjunction with other activities, and isotopic partitioning in the hydrological cycle is well understood (see Gibson and Edwards 2002).

Mass-dependent fractionation of different hydrological species of water as they move through the water cycle is the result of water molecules formed by different combinations of the isotopic species of oxygen ( $^{16}\text{O}$ ,  $^{17}\text{O}$  and  $^{18}\text{O}$ ) and hydrogen ( $^1\text{H}$  and  $^2\text{H}$  and  $^3\text{H}$ ) —  $^3\text{H}$ , or tritium, is a radioactive species of hydrogen that is produced via nuclear reactions. Put simply, the lighter isotopes are slightly more likely to evaporate than the heavier variants ( $^{18}\text{O}$  and  $^2\text{H}$ ), which are proportionally less likely to condense and precipitate. As a result, the isotopic composition of a water sample can be used to understand hydrological processes both spatially and temporally.

The isotopic composition of a water sample is expressed as a delta ( $\delta$ ) value in parts per thousand (‰, or per mil), reflecting the ratio of  $^{18}\text{O}/^{16}\text{O}$  or  $^2\text{H}/^1\text{H}$  in a water sample versus a globally accepted standard (Vienna Standard Mean Ocean Water, or VSMOW, on a scale normalized to Standard Light Arctic Precipitation; see Coplen 1996). Negative values, which are typical of high latitudes and cold regions, indicate that the sample has less of the heavy isotope than the standard (in this case, mainly as a result of rainout between the ocean source and the study region). Results are typically discussed in terms of enrichment and depletion of the heavy isotope relative to other samples, and a series of metrics have been developed to support interpretation (explained in more detail below).

Water isotope results are typically interpreted using a  $\delta$ - $\delta$  plot, which plots the composition of  $\delta^{18}\text{O}$  versus  $\delta^2\text{H}$  for a given sample. Several supporting elements are superimposed on this framework to help interpret results. These include the Global Meteoric Water Line (GMWL), which reflects the relationship between  $\delta^{18}\text{O}$  and  $\delta^2\text{H}$  arising from the global ocean source and collected from points around the globe (Craig 1961). Because of secondary fractionation effects, both locally and during atmospheric transport (including re-evaporation and precipitation), the local evaporation line (LEL) is also a useful metric. The slope of the LEL is calculated based on local climate conditions and fractionation factors, and reflects the role of evaporation in controlling local water balances.

The intersection of the GMWL and the LEL typically reflects the composition of amount-weighted mean annual precipitation for an area ( $\delta_p$ ), although in the upper Yukon River basin, this value is closer to amount-weighted mean summer precipitation ( $\delta_{ps}$ ). The more enriched end of the LEL is bounded by the isotopic composition of the last drop of water before complete desiccation ( $\delta^*$ ). Importantly,  $\delta_{SSL}$ , or the isotopic composition of a water body at isotopic and hydrological steady state (with an evaporation-to-inflow ratio of 1:1) is also used to evaluate relative water balance conditions. For more details, see Edwards et al. 2004 and Brock et al. 2007. These framework parameters appear on several figures in this section.

## 2.2 Isotope sampling and analysis, Yukon River headwaters

Water samples were collected during field activities carried out as part of this project (see Figure 2.1). They were collected primarily between February 2014 and October 2015 from surface water bodies including lakes, rivers and standing meltwater pools. Some snow samples were also collected from locations where snow was present at the time of sampling. Two synoptic sampling surveys of specific lake and river locations were conducted by helicopter during the project. Those surveys were conducted in September 2014 and September 2016, with the intention of comparing results between years and exploring variability in isotopic composition within sites. Results from a total of 61 sample sites are presented in this report. Lab analysis of samples from fieldwork in September 2016 were not available at the time this report was written, but data can be obtained from the Yukon Research Centre.

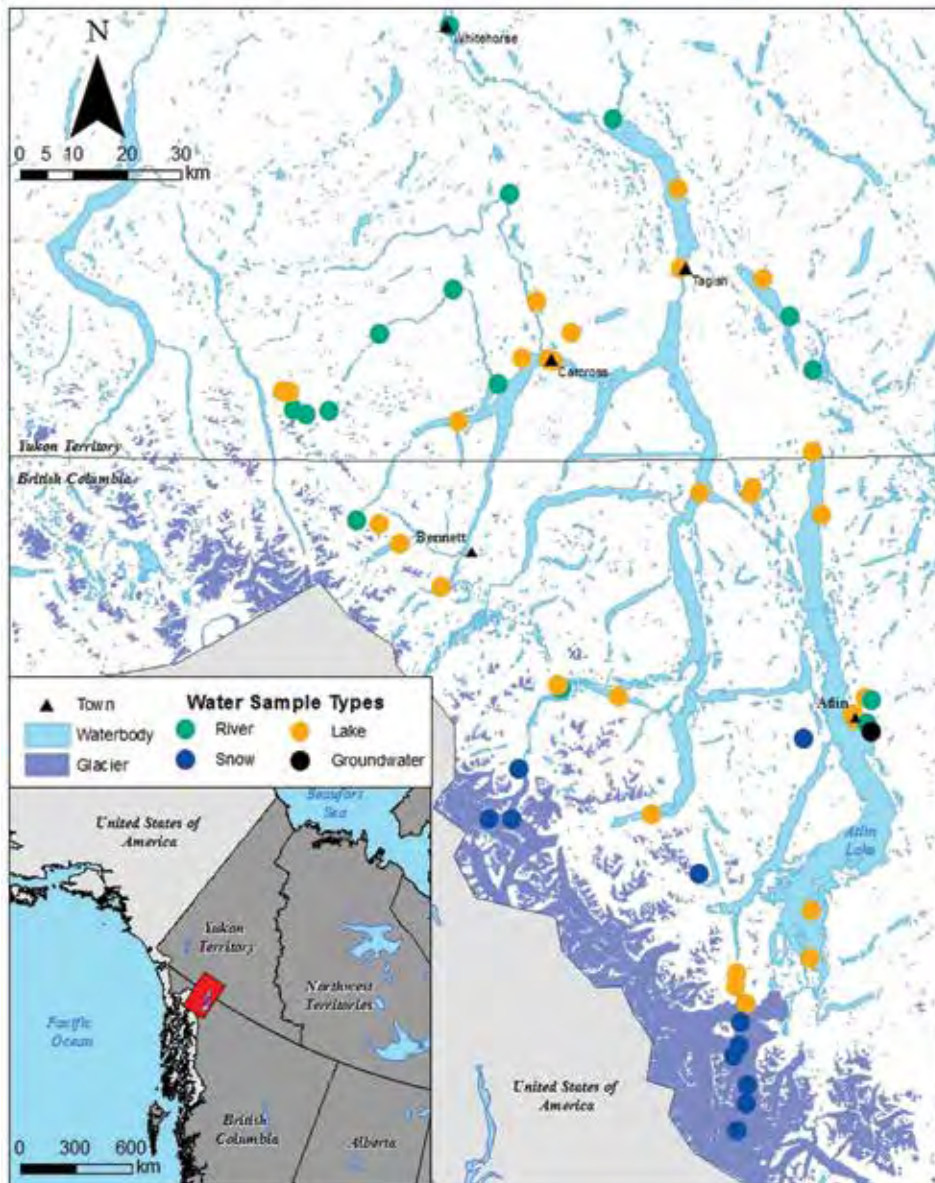


Figure 2.1 Map of sites where water isotope samples were collected.

Additional snow samples from regional glaciers were collected during a glacial traverse by the Juneau Icefields Research Program from Juneau, Alaska to Atlin, BC in summer 2015. These results are summarized in Section 2.4.

All samples were analyzed by the Environmental Isotope Laboratory at the University of Waterloo.

### 2.3 Water isotope results

Water isotope results from analyzed samples were superimposed on a  $\delta$ - $\delta$  plot, which was constructed using local hydroclimatic parameters (see Brock et al. 2007 for details regarding calculation of input parameters and framework construction).

Figure 2.2 shows the results for both water and snow samples collected from the headwater region. Snow sample results (Figure 2.2a) range between  $-16.7\text{‰}$   $\delta^{18}\text{O}$  ( $-126\text{‰}$   $\delta^2\text{H}$ ) and  $-22.9\text{‰}$   $\delta^{18}\text{O}$  ( $-180\text{‰}$   $\delta^2\text{H}$ ). They cluster along the GMWL; this reflects minimal fractionation, which is to be expected. Many samples cluster around the composition of amount-weighted mean annual precipitation ( $\delta_p$ ), which is also unsurprising; however, several snow samples are more enriched than  $\delta_{ps}$ . This may be a result of sublimation effects after deposition, or of snow samples being collected early in the sampling season, when conditions were relatively warm. Re-evaporation after sample collection is unlikely, given the close positioning of the sample results to the GMWL.

River sample results (Figure 2.2b) are quite similar to those of snow samples. River sample results range between  $-16.6\text{‰}$   $\delta^{18}\text{O}$  ( $-125\text{‰}$   $\delta^2\text{H}$ ) and  $-21.5\text{‰}$   $\delta^{18}\text{O}$  ( $-166\text{‰}$   $\delta^2\text{H}$ ). These samples typically fall close to the GMWL, and are more depleted than average amount-weighted summer precipitation ( $\delta_{ps}$ ). Their positioning in d-d space points to snowmelt being the predominant input to rivers locally.

Lake sample results (Figure 2.2c) range between  $-9.0\text{‰}$   $\delta^{18}\text{O}$  ( $-106\text{‰}$   $\delta^2\text{H}$ ) and  $-21.6\text{‰}$   $\delta^{18}\text{O}$  ( $-168\text{‰}$   $\delta^2\text{H}$ ), and reflect more variability than snow and river samples. Sample results indicate two types of lake: one that clusters close to  $\delta_{ps}$ , and one that spans the LEL. Typically, those that cluster close to  $\delta_{ps}$  include the larger lakes in the headwater region – Tagish, Marsh, Bennett and Atlin lake samples are all in this area of the d-d plot. Hydrologically, these lakes are relatively open; in other words, they have large inlets and outlets, and receive notable amounts of river water as part of their input water source. Consequently, evaporation plays only a small role in lake water balance, regardless of the large surface area of these lakes.

Conversely, results from small lakes and ponds in the headwater region fall along the LEL, indicating evaporative enrichment and the increased importance of evaporation to their water balances (Figure 2.3a). Hydrologically, these lakes are typically closed (i.e., with no flow-through inlets and outlets) and likely receive spring snowmelt inputs from their catchments rather than year-round river inputs. They are shallow, and in some cases (e.g., Llewellyn terminal moraine, the marsh near Tagish Lake), evaporation exceeds inflow (reflected in compositions that exceed  $\delta_{SSL}$ ). This suggests that after several seasons with comparable hydroclimatic conditions, these lakes would dry up. Interestingly, the isotopic compositions of some lakes are more enriched than  $\delta_{ps}$ , but do not fall along the LEL (i.e., high alpine pond, Homan Lake and Lindeman Lake on Figure 2.3b). These lakes are located at a relatively high elevation (1,521 m, 836 m and 676 m, respectively), and are close together.

It is possible that local atmospheric moisture controls, or local variability in snowmelt input, are creating a local microclimate that creates water balance conditions at these lakes that differ from those in other areas of the Yukon River headwaters.

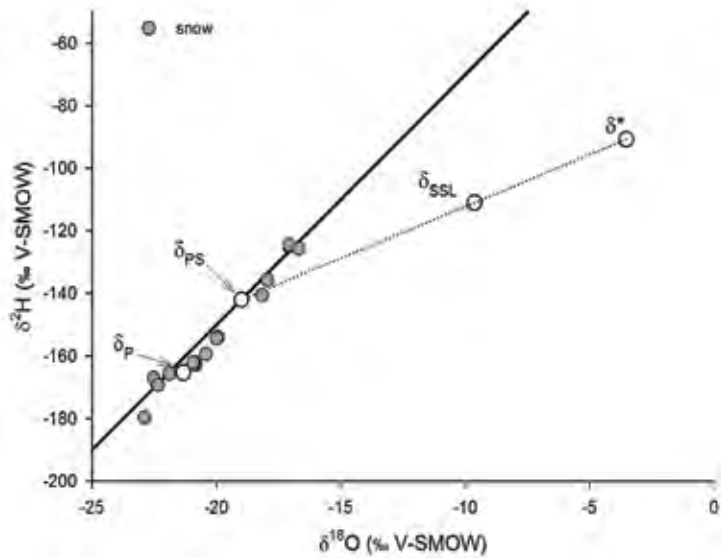


**Figure 2.2a** Water isotope results from Yukon River headwater samples, showing snow samples.

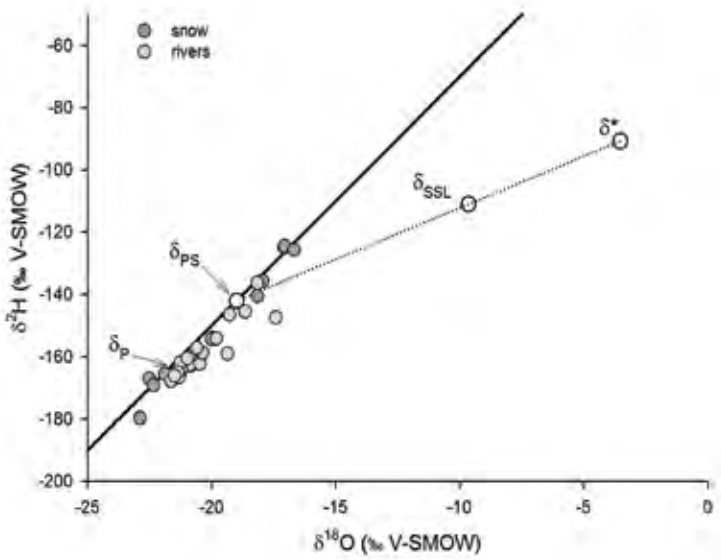


**Figure 2.2b** Water isotope results from Yukon River headwater samples, showing river samples.

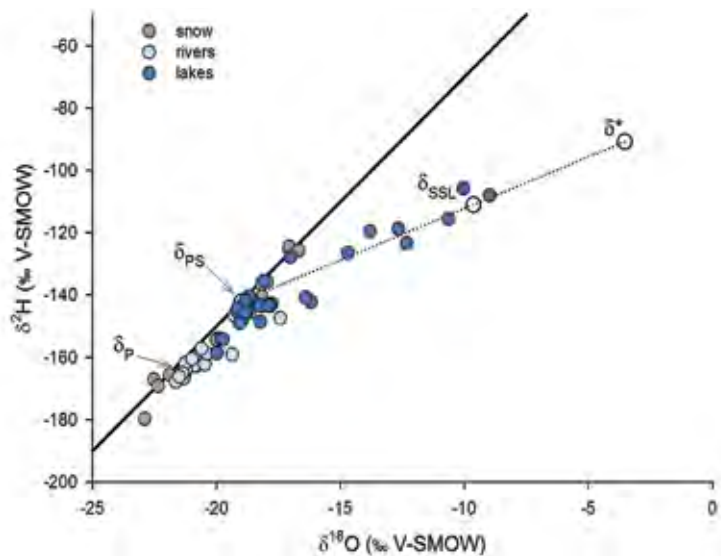


**Figure 2.2c** Water isotope results from Yukon River headwater samples, showing lake samples.

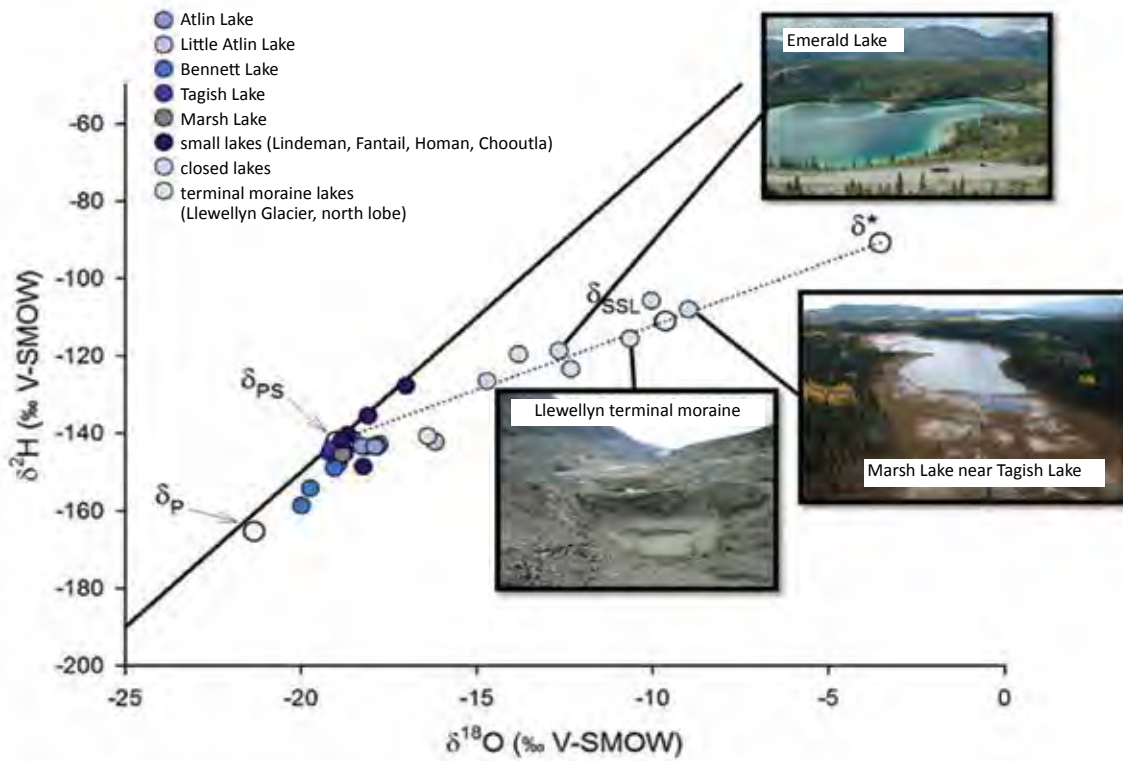


Figure 2.3a Lake water isotope results showing results from small ponds.

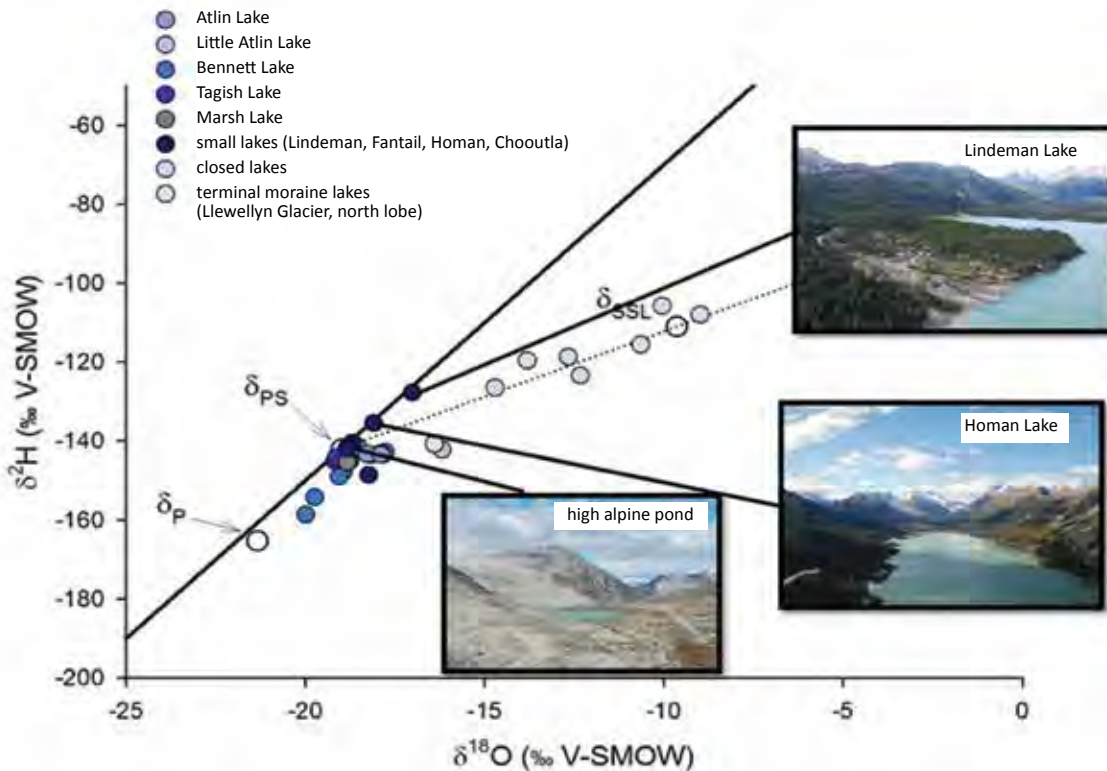
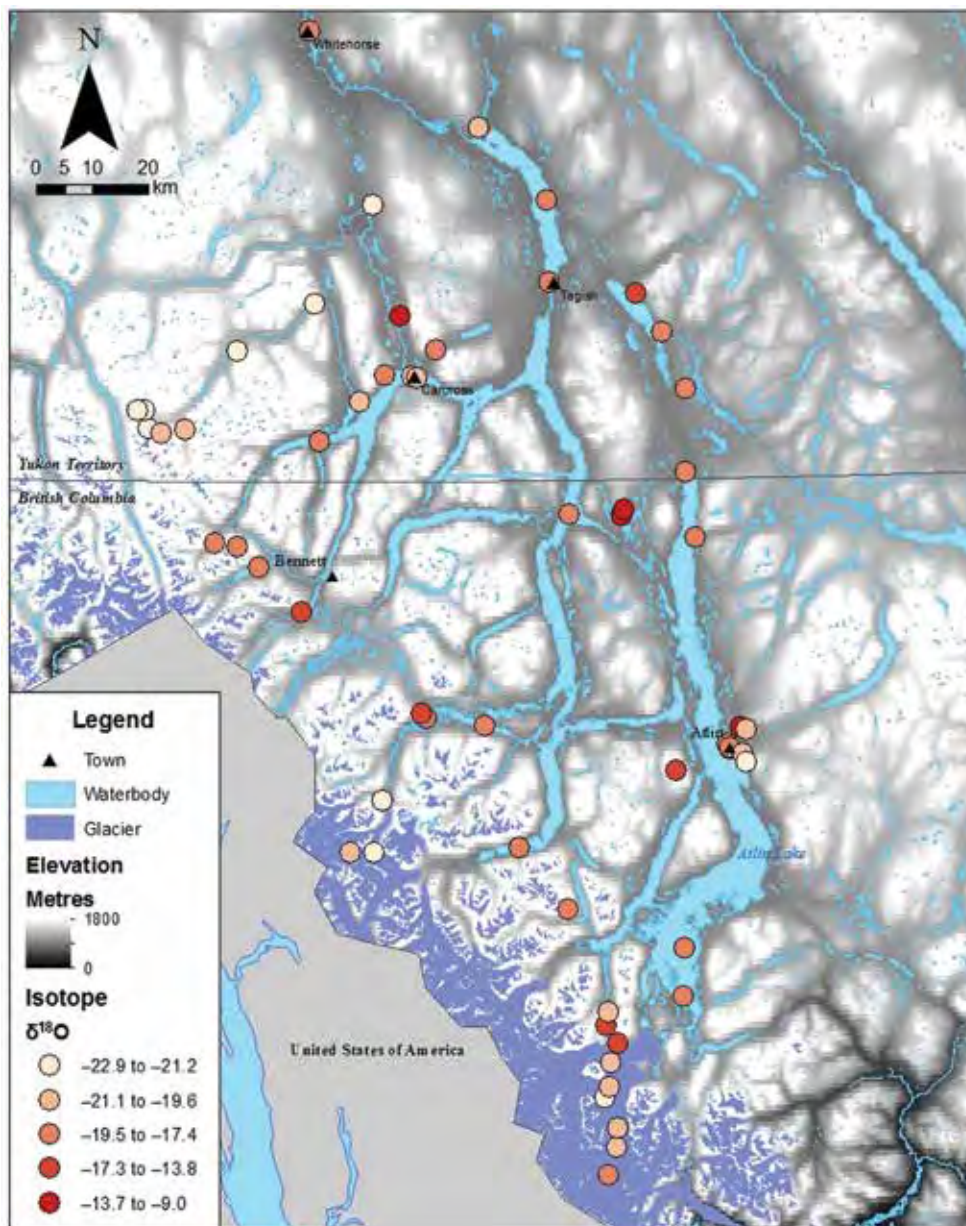


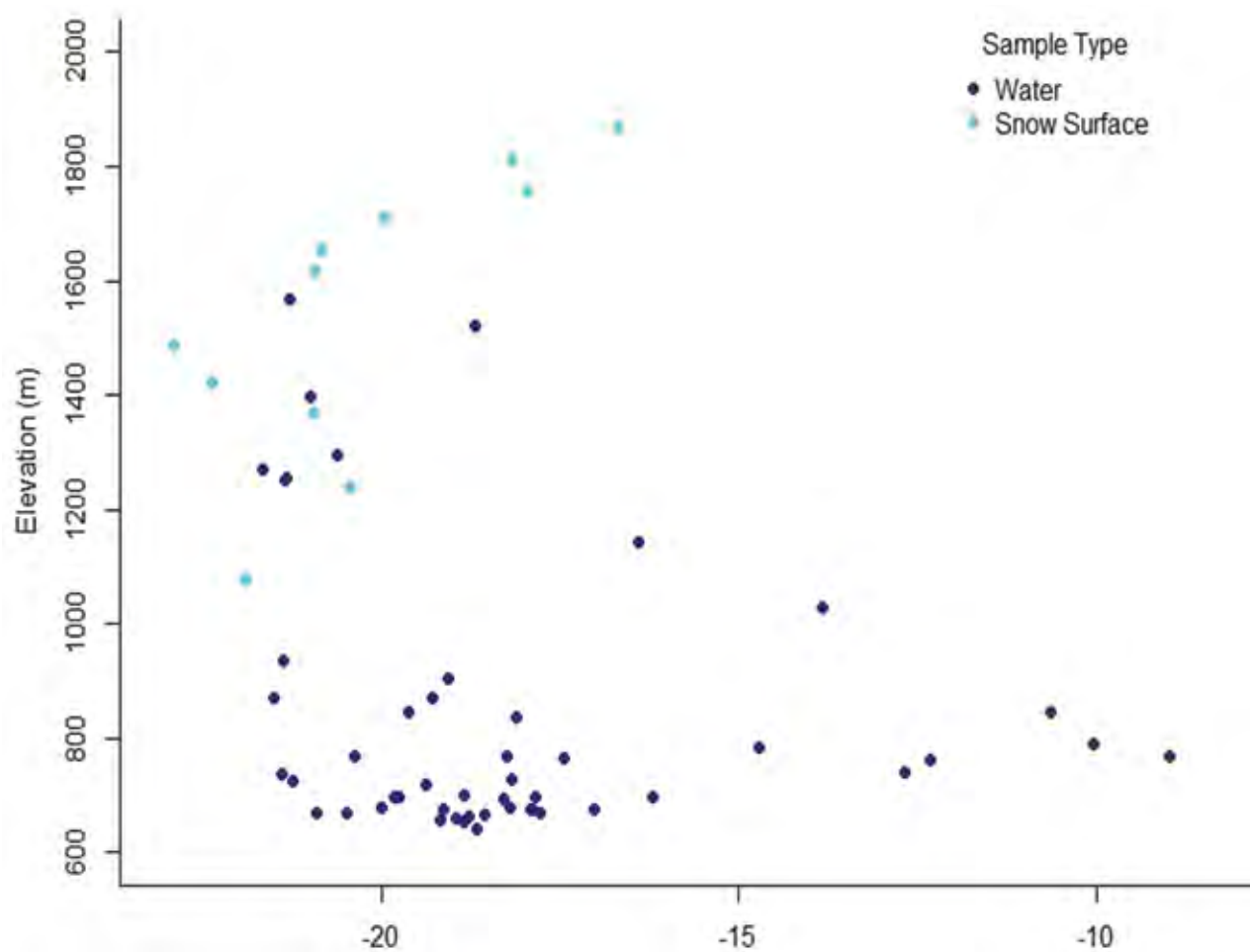
Figure 2.3b Lake water isotope results showing results from high-elevation ponds.

Figure 2.4 shows sample results ( $\delta^{18}\text{O}$ ) mapped by distribution across the Yukon River headwater region. It shows that the most isotopically depleted samples are typically situated at high elevations, close to headwater glaciers. As water moves downstream from this area, samples show that it typically become more isotopically enriched; this reflects the increased influence of evaporation (particularly on smaller, hydrologically closed lakes). River sample sites (especially along the Wheaton River in the northwest quadrant of Figure 2.4) continue to exhibit relatively isotopically depleted signatures, which reflect high headwater snow/glacial inputs. The isotopically depleted sample point close to Atlin represents a sample of groundwater taken from a spring near the community. The relatively depleted signature of this sample reflects the composition of groundwater, which is typically close to that of amount-weighted mean annual precipitation ( $\delta_p$ ).



**Figure 2.4**  $\delta^{18}\text{O}$  compositions of water sample sites in the upper Yukon River basin.

Data plotted in Figure 2.4 suggests that there is some relationship between elevation and isotopic composition in the headwater area of the Yukon River basin. Figure 2.5, which plots sample elevation against  $\delta^{18}\text{O}$ , explores this relationship. River samples tend to be relatively isotopically depleted, regardless of elevation. This is consistent with the strong clustering of river sample sites along the GMWL, as represented in Figure 2.2b. There appears to be a limited relationship between the elevation of lake sample sites and isotopic composition. This relationship is not statistically significant; nonetheless, it is consistent with general patterns of isotopic enrichment as water moves from the higher-elevation headwaters of the upper Yukon River basin toward lower-elevation sampling points downstream.



**Figure 2.5** Water and snow sample elevations plotted against  $\delta^{18}\text{O}$  compositions for upper Yukon River basin samples.

## 2.4 Juneau to Atlin glacial traverse

Snow samples were taken during a glacial traverse from Juneau to Atlin during the summer of 2015. The expedition originated at the Lemon Creek Glacier near Juneau, Alaska (elevation 17 m, with a maritime climate). It then traversed the Taku and Matthes glaciers, over the Matthes-Llewellyn divide, and across the Llewellyn Glacier near Atlin, B.C. (elevation 668 m, with a subarctic climate), over a two-month period. Samples were taken from the surface of the glaciers at semi-regular intervals during the traverse.

Preliminary examination of spatial patterns in results indicates progressive isotopic depletion in samples from Juneau to Atlin (Figure 2.6). The most enriched of the samples collected ( $-11.8\text{‰}$   $\delta^{18}\text{O}$ ,  $-88\text{‰}$   $\delta^2\text{H}$ ) come from the Taku Glacier, while the most depleted sample ( $-19.8\text{‰}$   $\delta^{18}\text{O}$ ,  $-152\text{‰}$   $\delta^2\text{H}$ ) comes from the Llewellyn Glacier. Results suggest that rainout of heavy isotopes increases with distance from Juneau; this is particularly apparent when examining sample results grouped by position relative to the Matthes Divide. Samples from the Lemon Creek, Taku and Matthes glaciers, which were all collected from the oceanic side of the Matthes Divide, range between  $-1.8\text{‰}$  and  $-16.8\text{‰}$   $\delta^{18}\text{O}$  ( $-89\text{‰}$  and  $-124\text{‰}$   $\delta^2\text{H}$ ) with the average being  $-14.3\text{‰}$   $\delta^{18}\text{O}$ ,  $-107\text{‰}$   $\delta^2\text{H}$ .

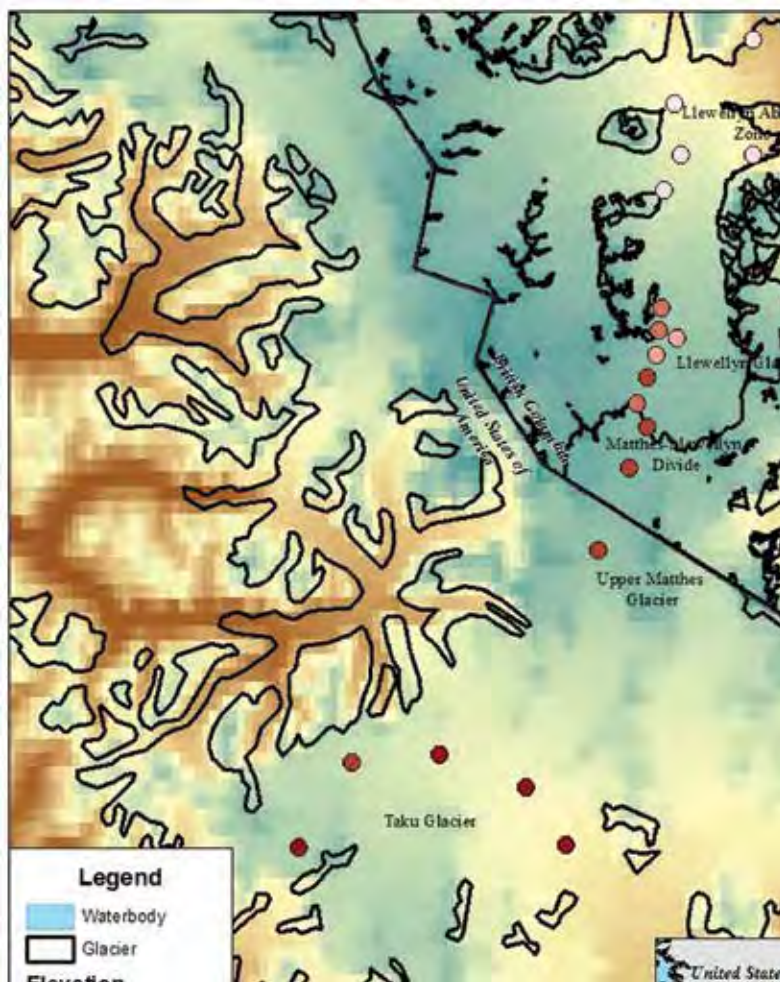


**Figure 2.6**  $\delta^{18}\text{O}$  compositions of snow samples collected during a traverse from Juneau to Atlin.

In contrast, samples collected on the continental side of the Matthes Divide range between  $-14.3\text{‰}$  and  $-19.8\text{‰}$   $\delta^{18}\text{O}$  ( $-111\text{‰}$  and  $-151\text{‰}$   $\delta^2\text{H}$ ), with the average being  $-16.3\text{‰}$   $\delta^{18}\text{O}$ ,  $-124\text{‰}$   $\delta^2\text{H}$ . Progressive rainout of heavy isotopes on the oceanic side of the Matthes Divide results in more isotopically depleted signatures in snow samples collected from the continental side. Consequently, glacial runoff from the Llewellyn Glacier to Atlin Lake in the headwaters of the upper Yukon River basin is relatively isotopically depleted.

Additional examination of these data, including samples collected from snow pits along the traverse, would yield more information regarding within-glacier variability in isotopic composition, and might support further hydrograph separation activities.

### 2.5 Conclusions

There is substantial scope for more isotope-based work in the upper Yukon River basin. The samples collected during this project provide an independent quantitative verification that the hydrologic composition of river water is primarily snowmelt and glacial runoff. These are some other key findings:

- Samples collected from large, flow-through lakes (e.g., Atlin, Tagish, and Marsh lakes) fall along the Global Meteoric Water Line, meaning that their primary hydrological input source is precipitation and groundwater. They are minimally affected by evaporation, despite having large surface areas.
- Samples from smaller lakes in the region show varying evidence of evaporation. The degree of control that evaporation has in the water balance of these lakes likely reflects the size of the lake's catchment and the amount of spring snowmelt input. In some lakes, evaporation exceeds inflow to these small lakes. This suggests that they could be susceptible to drying up, especially after several seasons with low snowpack or hot, dry summers.
- Samples taken from high elevation lakes suggest that controls on water balance are different from those for lower elevation lakes. It is possible that different atmospheric moisture conditions create different conditions than at lower elevations in the region.
- Results indicate that glacial influence is most important closest to the glacier. Unfortunately, the data available are not yet sufficient to trace the relative contribution of glacial meltwater as it moves downstream (i.e., hydrograph separation).

The analysis of results presented here is relatively simple; a more detailed investigation of site-by-site variability and nuances in the dataset presented above would yield additional detail regarding hydrological processes in the basin. Continued regular sampling would assist in the detection of hydrological change in the region.

Importantly, there is the potential to use water isotope tracers to work on hydrograph separation activities, which might result in the ability to better understand the contributions of glaciers versus snowmelt to river discharge. Comparable work in other regions (e.g., Cable et al. 2011; Theakstone 1998) suggests that this type of work is feasible in glaciated basins, given the right sampling design, frequency and expertise. Such work could supplement hydrological modelling activities, and assist Yukon Energy Corporation in the detection of changes in glacial contribution to the upper Yukon River basin over time.

### 3. Late Holocene fluctuations of Llewellyn Glacier's north lobe

#### 3.1 Introduction

Glaciers advance and retreat in response to changes in climate. Information about the timing and extent of a glacier's past fluctuations can provide baseline data for comparison to current and future fluctuations, and to understand how a glacier may respond to future climate change.

A fluctuation record of the Llewellyn Glacier over the last two millennia was constructed by dating lateral and end moraines located beside and down valley from the present-day glacial toe. A total of seven sites were examined: six in the area of the north lobe and one adjacent to the main lobe (Figure 3.1). The results build on previous work by Clague et al. (2010), who constructed a record of glacial fluctuations based on geological evidence from the main and south lobes of the glacier. A more detailed analysis of data and discussion is presented in Samolczyk et al. (2016).

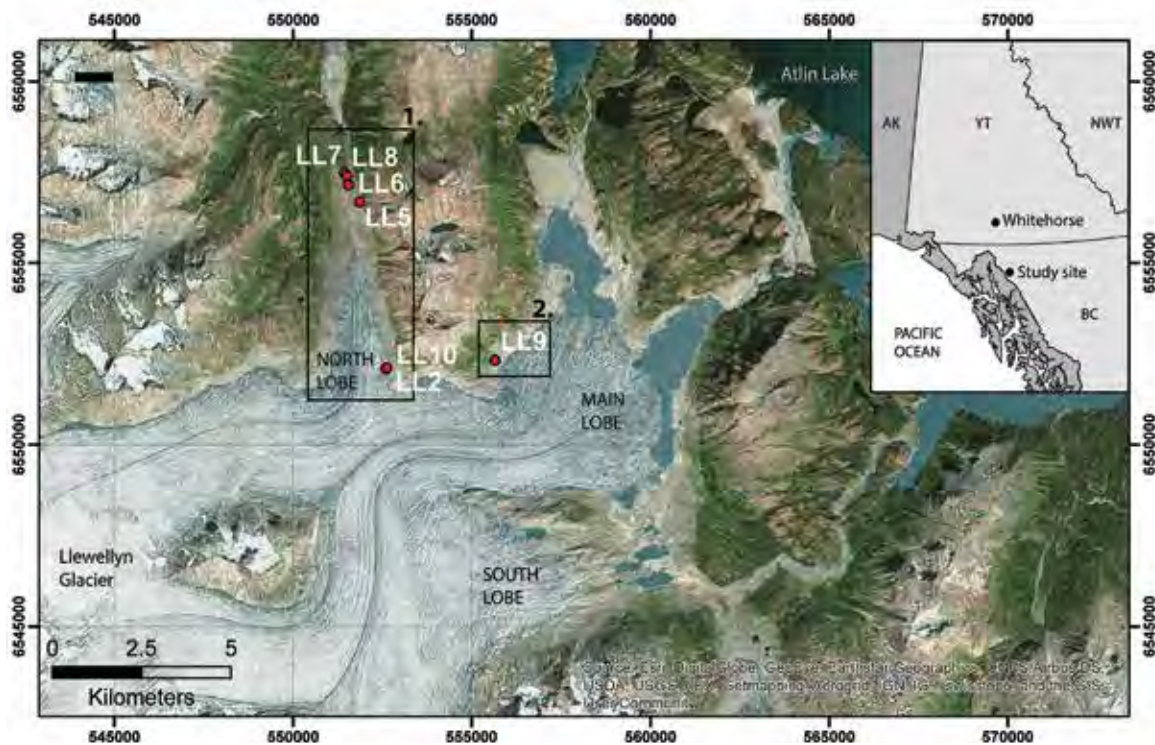


**Figure 3.1** Llewellyn Glacier, British Columbia, with study areas 1 (north lobe) and 2 (main lobe).

Note: Red dots mark sample site locations.

#### 3.2 Methods

The study team examined sediment geometry and layering within the lateral and end moraines of the Llewellyn Glacier. End moraines mark the maximum down-valley extent of a glacier at the time of deposition. Lateral moraines, which are deposited along the sides of glaciers, may be composite features built by several periods of glacial advance. During glacial advance, the ice surface grows in elevation and the glacier deposits sediments, referred to as glacial till, on existing lateral moraine surfaces. These newly deposited tills may bury and preserve vegetation and soils.

Former soil horizons buried in lateral moraines are referred to as paleosols. Radiocarbon dating the in-situ rooted wood contained within paleosols, and the detrital wood fragments found unrooted within till, can provide information about the timing of moraine-building events. In addition, counting the annual growth rings of live and dead trees rooted on the end moraine of the north lobe of the Llewellyn Glacier in this region, generally dating from the Little Ice Age, can determine the timing of moraine building and stabilization.

The Little Ice Age (LIA) was a prolonged period of cold climate (relative to the present day) that occurred across the Northern Hemisphere between approximately AD 1570 and 1900. The timing of the LIA varied by location; some regions, particularly central Europe, entered this cold period a century or more earlier (Matthews and Briffa 2005).

A total of eleven wood samples were radiocarbon-dated using accelerator mass spectrometry (AMS) at Beta Analytic Ltd. and the Keck Carbon Cycle AMS Facility (Table 3.1).

**Table 3.1** Radiocarbon dates, eleven wood samples, Llewellyn Glacier

Radiocarbon age ( $^{14}\text{C}$ yr BP) <sub>a</sub>	Calendric age (AD) <sub>b</sub>	Laboratory no. <sub>c</sub>	Site no. (Figure 3.1)	UTM coordinate (zone 8N)	Elevation (m)	Dated material
1705 ± 30	252–401	UCI-AMS-149293	LL2	552612, 6552090	1,099	Branch or root <sub>d</sub>
1750 ± 30	222–385	Beta-384639	LL2	552612, 6552090	1,099	Branch or root <sub>e</sub>
1665 ± 30	258–506	UCI-AMS-149294	LL2	552612, 6552090	1,099	Woody organic fragments
185 ± 30	1650–present	UCI-AMS-149295	LL5	551867, 6556683	949	Branch or root <sub>e</sub>
80 ± 30	1690–1926	UCI-AMS-149296	LL6	551555, 6557143	797	Tree stump <sub>e,f</sub>
370 ± 30	1446–1634	UCI-AMS-149297	LL6	551555, 6557143	797	Tree stump <sub>d,f</sub>
145 ± 30	1668–1948	UCI-AMS-149298	LL7c	551427, 6557486	874	Tree trunk <sub>d,g</sub>
155 ± 30	1666–present	UCI-AMS-149300	LL8	551503, 6557383	875	Branch or root <sub>e</sub>
910 ± 30	1033–1204	UCI-AMS-149301	LL9	555636, 6552368	834	Branch or root <sub>e</sub>
1775 ± 30	138–339	UCI-AMS-149302	LL10	552622, 6552092	unknown	Tree trunk <sub>d</sub>
1785 ± 30	134–332	UCI-AMS-149303	LL10	552622, 6552092	unknown	Tree trunk <sub>e</sub>

Source: Samolczyk et al. (2016)

Notes: <sub>a</sub> error terms reported by Laboratories are  $1\sigma$ ; <sub>b</sub> age determined from the calibration curve of Reimer et al. (2013) in OxCal v.4.2.4 ( $2\sigma$  ranges reported); <sub>c</sub> laboratories: UCIAMS, Keck Carbon Cycle AMS Facility; Beta, Beta Analytic Inc.; <sub>d</sub> inner wood; <sub>e</sub> outer wood; <sub>f</sub> sample contains 136 rings; <sub>g</sub> sample contains 147 rings; BP: Before Present; AD: Anno Domini

Radiocarbon ages were calibrated using the calibration dataset of Reimer et al. (2013) in OxCal v. 4.2.4 (Bronk Ramsey 2013). Calibrated ages are reported as  $2\sigma$  (95% confidence interval) ranges and rounded to the nearest decade or mid-decade year. Tree rings were counted at the University of Victoria Tree-Ring Laboratory using the WinDENDRO tree-ring imaging system (Guay et al. 1992).

### 3.3 Results

The radiocarbon ages of eleven wood samples from seven sites spanned the interval between the first millennium AD and the twentieth century (AD 135–1950); see Table 3.1 and Figure 3.1). The north lobe of Llewellyn Glacier deposited till on its east lateral moraine — about 70 m above the present ice surface and about 500 m down valley from where the north lobe separates from the main lobe — between AD 260 and AD 505. This date is based on a radiocarbon-dated paleosol exposed at site LL2 and a rooted stump at site LL10 (Figure 3.2). The evidence indicates that the glacier was advancing during the first half of the first millennium AD, which agrees with evidence that the main and south lobes were advancing into mature forest in the first half of the first millennium AD between AD 300 and AD 500 (Clague et al. 2010).



**Figure 3.2** Sheared tree stump at site LL10.

A radiocarbon-dated in situ root from a paleosol at site LL5 (Figure 3.3), 4.8 km down valley from LL10 and LL2, indicates that the glacier overtopped its lateral moraine and buried a vegetated surface under till sometime after AD 1650 during the time period of the LIA.



**Figure 3.3** Dipping paleosol and organic horizon at site LL5.

At site LL6, the north lobe of Llewellyn Glacier overrode a mature forest growing about 5–10 m above the present valley floor and about 70 m up valley from the LIA end moraine between AD 1690 and AD 1925. A sheared stump at this site contains 136 rings, indicating that the tree was likely killed as early as the late 16th century (Figure 3.4).



**Figure 3.4** Stump sheared by glacial advance at site LL6.

Only metres down valley from site LL6, but approximately 80 m above the valley floor on a bedrock knob, radiocarbon-dated detrital wood was collected from a veneer of till at site LL8. It had a calibrated age of younger than AD 1665 (Figure 3.5). This indicates that the glacier overrode the surface of the bedrock knob at this location sometime after the 17th century.

Two scarred and tilted subalpine firs were growing on the LIA end moraine at site LL7, approximately 2.6 km from the present-day toe of the north lobe of the Llewellyn Glacier. They had 147 and 95 rings, respectively; this suggests that the glacier was actively depositing material on its LIA end moraine as recently as the 20th century.

The main lobe of the Llewellyn Glacier was advancing again at the start of the first millennium AD. A dated stem or branch protruding from a contact between till and underlying fluvial sediments at site LL9, located on the north lateral moraine, indicates that the glacier was advancing and reached an elevation of 65 m above the present ice surface between AD 1035 and AD 1205 (Figure 3.6). The data from the North lobe are in agreement with evidence for an advance of the main lobe of the Llewellyn Glacier into mature forest between AD 1030 to and AD 1210 (Clague et al. 2010).

### 3.4 Conclusions

Radiocarbon ages of wood from the lateral and end moraines of Llewellyn Glacier provide a record of fluctuations that spans the last two millennia. Data indicate that the north lobe advanced during the first half of the first millennium AD, sometime between AD 260 and AD 505, and came within 70 m of its Little Ice Age maximum down-valley limit as early as the 16th century. An advance of the main lobe occurred as early as AD 1035. These research results provide baseline data that can be compared to model data on future glacial change.



**Figure 3.5** Collecting wood at site LL8.



**Figure 3.6** Site LL9, looking southeast towards the main lobe of the Llewellyn Glacier.

## 4. Present glacier area and volume

### 4.1 Context

As of 2010, there were 367 individual glaciers within the upper Yukon River basin, with a combined area of roughly 1,000 km<sup>2</sup> and an estimated total volume of about 187 km<sup>3</sup> of ice (NCE 2014). The Wheaton, Fantail, Willison and Llewellyn glaciers are representative of the glacial conditions within the study basin (Figure 4.1). The Fantail, along with two smaller nearby glaciers, was surveyed by NCE in 2014 to help determine the regional volume-area scaling relationship (NCE 2014); the Wheaton Glacier was also surveyed during that study (NCE 2014) to help further constrain the volume-area relationship, because it's situated in a different subbasin, and because it has been moderately well studied in the past (see NCE 2014). The Willison and Llewellyn glaciers have the greatest glacier surface area, volume and glacial runoff in the basin. The past changes in surface area and volume of Llewellyn glacier were studied by NCE (2014). The Willison Glacier, the second largest glacier after Llewellyn, was not thoroughly discussed by NCE (NCE 2014). Prior to that study, no field surveys had been carried out for the Llewellyn and Willison glaciers.

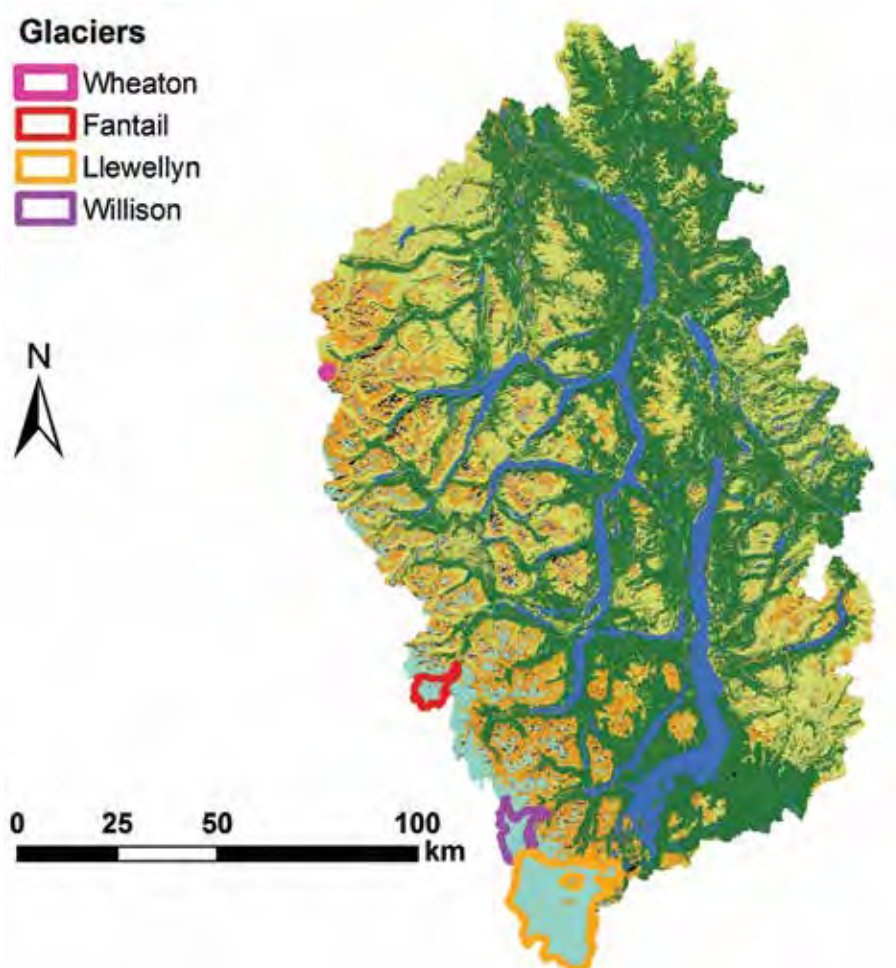


**Figure 4.1** Map of the Upper Yukon River basin showing the locations of the Wheaton, Fantail, Willison and Llewellyn glaciers, including modelled subbasins.

The Llewellyn Glacier is a particularly significant contributor to glacial runoff. It represents nearly half the total surface area of all the glaciers in the basin and more than 70% of the total ice volume (NCE 2014). The glacier has the largest ablation-zone surface area in the region and its terminus extends to a relatively low elevation, which increases the intensity and duration of its melt season. Ice mass loss from this glacier has been significantly greater than that of other glaciers in the basin over the last few decades (NCE 2014), which may indicate that the glacier is especially sensitive to climate change.

Quantifying the ice volume stored in the glaciers of the upper Yukon River basin and characterizing glacier mass balance are important in order to understand river discharge and simulate CRHM, and to examine glacier responses to ongoing climate change. Since the Llewellyn Glacier makes a major contribution to river discharge and has a strong potential responsiveness to changing climate, accurate characterization of it is important.

In this study, field-based ice thickness surveys were performed for the Fantail and Llewellyn glaciers using ground-penetrating radar (GPR). In addition, snow and ice melt rates were determined for the Llewellyn Glacier using ablation wires installed at various elevations. Although the Fantail Glacier has previously been surveyed by NCE (2014), additional GPR locations were surveyed in this study to fill data gaps. The Willison Glacier was not surveyed for this study; however, the GPR results for the Llewellyn Glacier were extrapolated to estimate its ice thickness.

## **4.2 Ground-penetrating radar (GPR)**

From April 22 to May 2, 2014, field-based surveys of ice thickness were carried out for the Fantail and Llewellyn glaciers to estimate current glacier volume and the region's area-volume scaling characteristics. The survey transects across the glacier surfaces were selected to fill data gaps (in the case of the Fantail Glacier), and to best represent their longitudinal and/or cross-sectional profiles given constraints on glacier travel due to ice surface conditions (e.g., crevasses and steep slopes), weather conditions and time. The transect totaled 58.3 km for the Llewellyn Glacier (Figure 4.2) and 20.9 km for the Fantail Glacier (Figure 4.3). The field team was supported by helicopter and flown from Atlin, BC, to reach the survey locations and transport equipment and gear.

Ice thickness values were determined using Yukon College's Blue System Integration, Ltd. (BSI) 5 MHz ground-penetrating radar (GPR) system, towed behind a snow machine. Simultaneous GPS survey provided information on position and surface elevation. The impulse transmitter was built by Icefield Tools (Whitehorse, YT) based on the design of Narod and Clarke, 1994 (Specifications: 1-200 Mhz bandwidth, 24kW peak power, 1.6 kV into 50 Ohms, rise time <2 ns, repetition rate 512 Hz). The 20 m transmitting antenna was a tuned-impedance dipole. A half-dipole (10 m) receiving antenna was connected to a Pico Model 4227 12-bit analog-to-digital converter (sampling rate: 250MS/s), which sent digitized waveforms to an Intel Atom-based 1.6 GHz embedded processing controller for storage. Since each recorded return waveform was a "stacked" average of 100 individual returns, the signal-to-noise ratio was improved by a factor of 10.

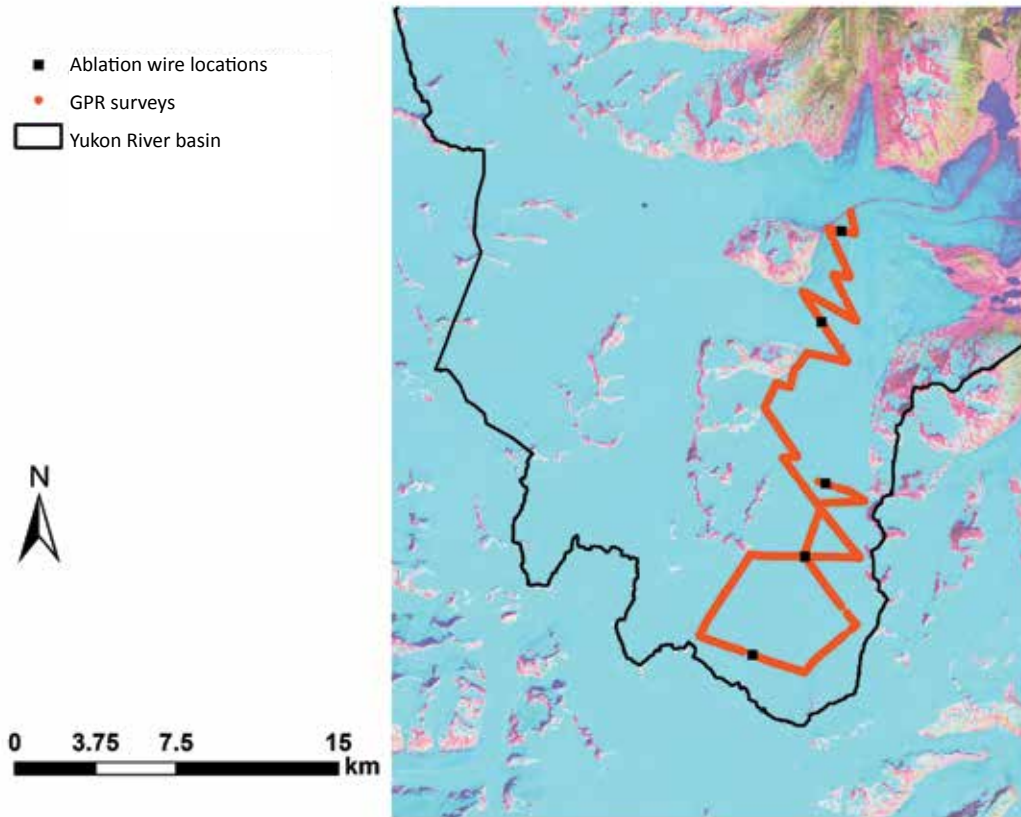


**Figure 4.2** Locations of GPR over Landsat 5 imagery for the Llewellyn Glacier

A Garmin GPS 18x receiver was used to record the location and corresponding ice-surface elevation of each stacked waveform. Using a WAAS (Wide Area Augmentation System), accuracy for these receivers is improved to approximately 3 m.

The radar survey data were processed using BSI's IceRadarAnalyzer software (version 3.1 and 4.0; Figure 4.4) from the time difference  $\Delta t = t_{2\text{-way}} - t_{\text{air}}$ , where  $t_{\text{air}}$  is the arrival of the direct airwave and  $t_{2\text{-way}}$  is the two-way travel time of the wave reflected off the bed. Assuming that the reflection is located at a point midway between the two antennae's centres, the ice thickness  $d$  is related to the time difference as (Equation 4.1):

$$d = \left\{ \left[ \frac{v_{\text{ice}}}{2} \left( \Delta t + \frac{a}{v_{\text{air}}} \right) \right]^2 - a^2 \right\}^{1/2} \quad (4.1)$$

Where  $a = 30$  m is the centre-to-centre antenna distance,  $v_{\text{air}} = 300$  m/ $\mu$ s is the wave propagation speed in air, and  $v_{\text{ice}} = 168$  m/ $\mu$ s is the wave propagation speed in ice. The airwave and bed reflection have a characteristic positive-negative-positive signature in the radar waveform and  $t_{\text{air}}$  and  $t_{2\text{-way}}$  were selected as the rising limb of the first positive excursion in the waveform (see Hubbard and Glasser 2005). Although in many of the radar waveforms the bed reflection is clear and distinct, in others it is weak and/or obscured by noise. In these cases, the bed waveform was band-pass filtered (to eliminate noise) and an exponential gain was applied (to counteract the attenuation of the signal with increasing band depth). Only those returns for which 1) a distinct bed return could be identified and 2) a good GPS location could be obtained, were used to determine ice thickness values.

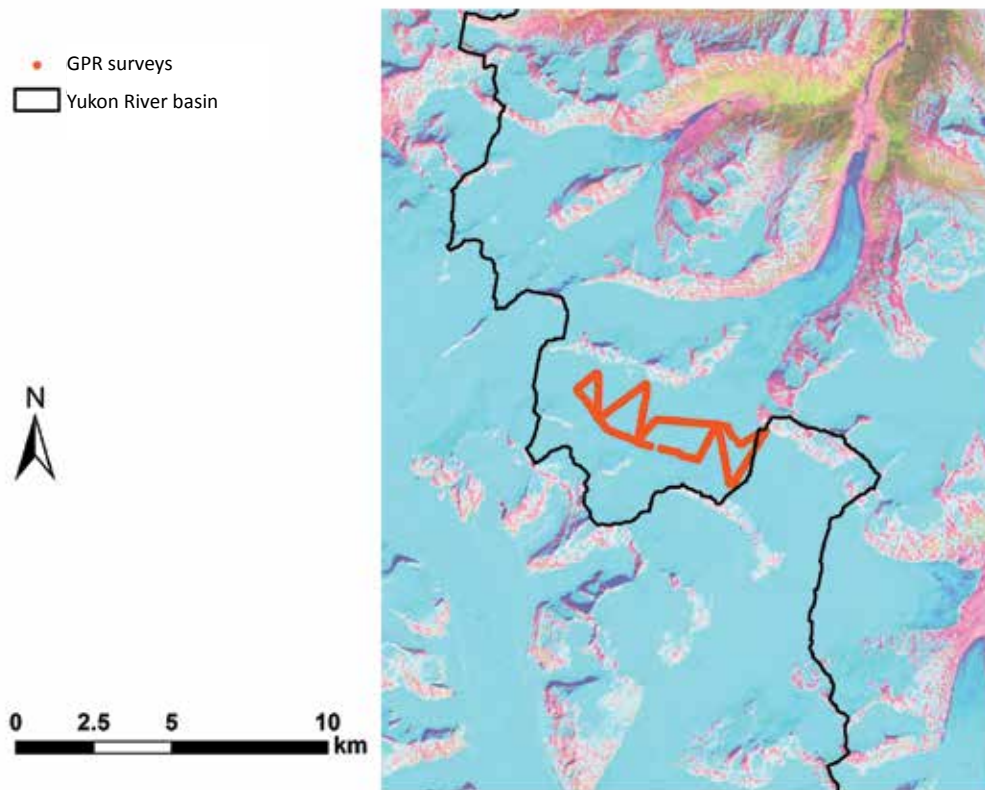


**Figure 4.3** Locations of GPR over Landsat 5 imagery for the Fantail Glacier

Ice thickness values could be discerned where returns in the radar traces were sufficiently strong. Although the glacier thickness could be determined in shallow regions (including near the glacier margins and where several tributary glaciers flow into the main glacier trunk), it was not possible to resolve the ice thickness in the deeper portions of the main glacier trunks. Since the ice was temperate and was thicker in its deeper portions, adequate signal returns were not acquired in these areas.

Ice thickness values that were able to be resolved were extrapolated to the entire study basin. This was done using a method based on surface slope and basal shear stress relationships, similar to GlabTop (Glacier Bed Topography) software; see Linsbauer et al. 2012. Field-measured data for the Wheaton and Fantail glaciers obtained from NCE (2014), in addition to field survey data collected for the Fantail and Llewellyn glaciers in this study, were extrapolated across the entire study region to estimate ice thickness, as follows:

1. to generate cross-sectional profiles in areas where GPR signals could not be resolved, the team used the interpolation technique of Pattyn and Van Huele (1998), which assumes a power law relationship between ice depth and the fractional distance across the glacier;
2. flow lines were determined using open source Geographic Resources Analysis Support System (GRASS) software, after which ice thickness was estimated using the basal shear stress equation (Equation 4.2);

$$h = \frac{\tau}{\rho g \sin\theta} \quad (4.2)$$

where  $h$  is the ice thickness (m),  $\tau$  is the basal shear stress (kPa),  $g$  is the gravity acceleration (9.8 m/s<sup>2</sup>),  $\rho$  is the ice density (900 kg/m<sup>3</sup>) and  $\theta$  is the slope (°). A basal shear stress ( $\tau$ ) of 150 kPa was used (Haerberli and Hoelzle 1995).

3. The differences between the estimated ice thickness at flow lines obtained from step 2 and the GPR observation were corrected as follows; a) the slope, intercept and correlation coefficient of the linear regression between the ice thickness at flow lines estimated from Step 2 and those obtained from observation data were computed; and b) the slope and intercept parameters were used to correct ice thickness at flow lines where field measured ice thickness was not available.
4. The estimated and observed ice thickness values (see steps 2 and 3) were then extrapolated across the entire study basin using a Kriging method in GIS to generate a model of the glacier's bed elevation. With the exception of cases where glaciers flow into or out of the model domain (e.g., ice flowing into the Llewellyn Glacier across the U.S. border), all other glacier margins were assumed to have zero ice thickness. The total volume was then determined as the product of the glacier surface area and the average thickness.

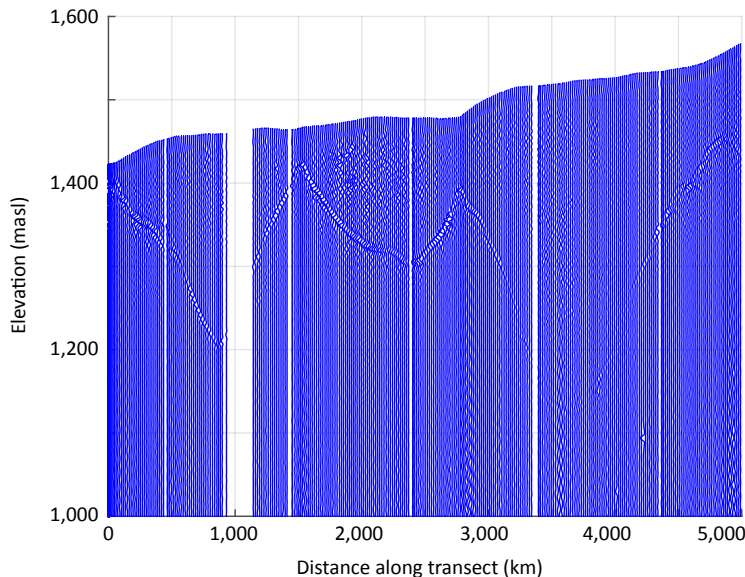


**Figure 4.4** Filtered and amplified ground-penetrating radar (GPR) traces, showing ice thickness values along one portion of the Llewellyn Glacier transects.

Note: Surface elevations (top of blue traces) were determined by GPS survey; ice depths were determined from the difference in time  $\Delta t$  between the air wave arrival (not visible in these filtered traces) to the inferred bed return, here expressed as the V-shaped dipping feature visible over much of the transect. Note that the strength of the bed return diminishes as depths increase, due to attenuation and scattering; returns were not observed in regions where ice thickness values exceeded ~400 m. Gaps in the data indicate poor GPS signal strength.

Volume estimates obtained in this study were validated by comparing measured glacier volume — i.e., from this study and NCE (2014) — with estimates based on samples of glaciers from across the world (Chen and Ohmura 1990). Based on both physical considerations and empirical results

(Chen and Ohmura 1990; Bar et al. 1997), many studies have shown that glacier volume can be related to surface area through a power law relationship of the following form (Equation 4.3):

$$V = c_0 A^{c_1} \quad (4.3)$$

where  $V$  is glacier volume ( $10^6 \text{ m}^3$ , equivalent to  $0.001 \text{ km}^3$ ),  $A$  is glacier surface area ( $10^6 \text{ m}^2$  or  $1.0 \text{ km}^2$ ) and  $C_0$  and  $C_1$  are scaling coefficients. V-A coefficients of  $C_0=28.5$  and  $C_1=1.36$  were applied, based on global estimates (Chen and Ohmura 1990). The  $C_0$  and  $C_1$  values, estimated from the V-A relationship of the glaciers in the Fantail and Wheaton basins, were 31.9 and 1.38, respectively (NCE 2014). Estimates from this study of adding the Llewellyn and Willison glaciers to the V-A relationship estimated by NCE (2014) were 37.1 and 1.31, respectively. The values from both studies appear to align reasonably well with the relationship outlined in Chen and Ohmura (1990); see Figure 4.5.

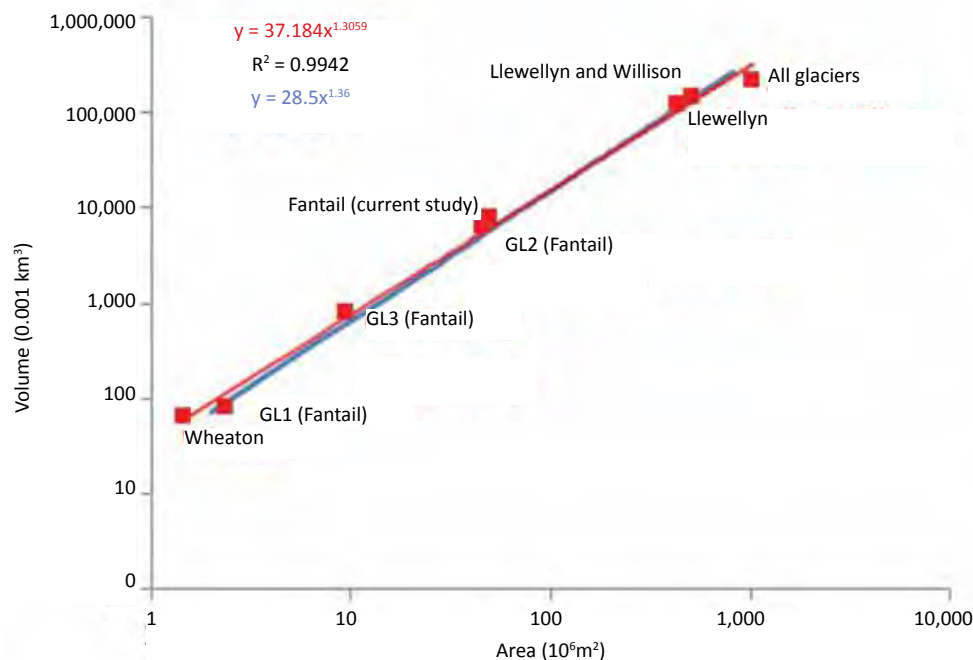


**Figure 4.5** Comparison of glacier surface volume and area measurements, with a plot of the V-A relationship

Notes: V-A relationship is derived from the global set of glaciers in the study of Chen and Ohmura (1990); the Wheaton and GL1, GL2, and GL3 glacier data were obtained from NCE (2014).

There is high confidence in the ice thickness estimates in locations where survey measurements were obtained, but less certainty in the deeper and non-surveyed areas. A maximum ice thickness of 500 m was estimated for all glaciers within the upper Yukon River basin, with an average ice thickness of 200 m, and a glacier surface area of about  $1,030 \text{ km}^2$  and ice volume of  $210 \text{ km}^3$  (Table 4.1). This is slightly larger than the amounts estimated by the 2014 NCE study (i.e.,  $1,000 \text{ km}^2$  and  $187 \text{ km}^3$ , respectively) since the current study included new GPR observation results conducted at the Llewellyn and Fantail glaciers and used 2013 data from Global Land Ice Measurements from Space (GLIMS) for estimating glacier coverage. Other differences might result from GIS data processing,

such as merging, clipping, intersecting, and dissolving files/data. The maximum ice thickness of the Llewellyn and Willison glaciers was estimated at 500 m in the middle portions of the glaciers, with an average thickness of 274 m (Figure 4.6).

**Table 4.1** Summary results of estimated glacier surface area, ice thickness and volume

Glacier	Glacier surface area (km <sup>2</sup> )	Average estimated ice thickness (m)	Maximum estimated ice thickness (m)	Estimated ice volume (km <sup>3</sup> )
Fantail *	50	157	500	8
Llewellyn	432	280	500	121
Llewellyn and Willison	513	274	500	141
All glaciers within the upper Yukon River basin **	1,028	203	500	210

\* Results for the Fantail Glacier were estimated using both the NCE (2014) data and the results of this study.

\*\*This includes the Fantail, Llewellyn and Willison glaciers, as well as the Wheaton Glacier and other small glaciers.

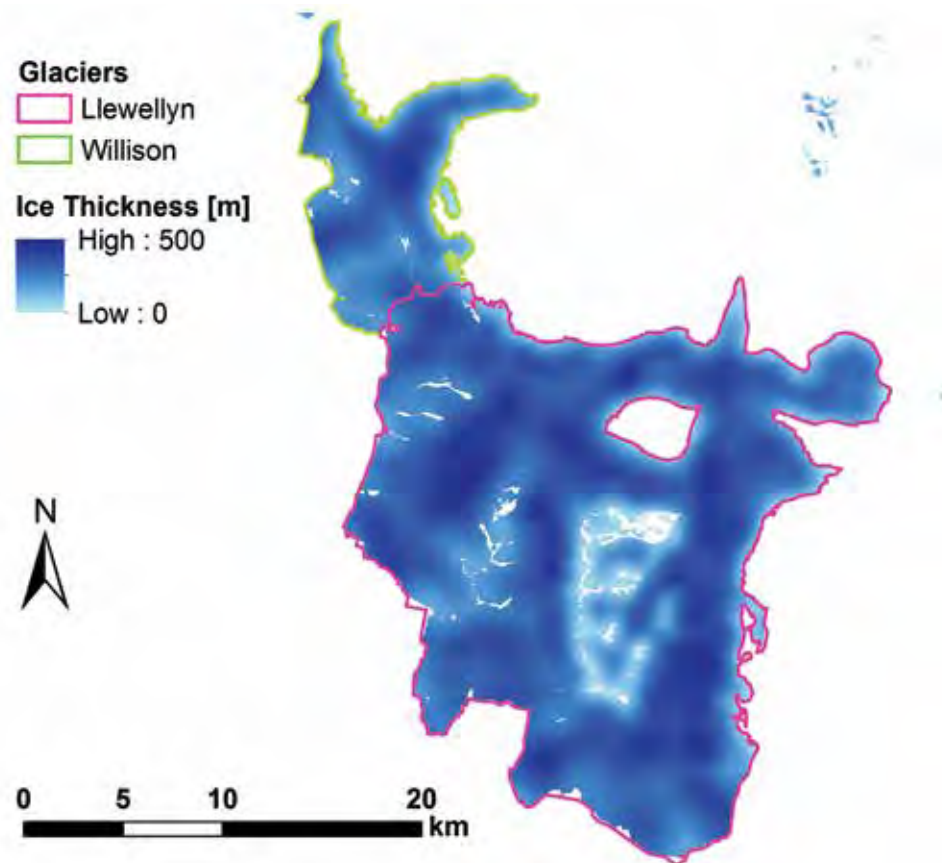


**Figure 4.6** Estimated ice thickness (m) of the Llewellyn and Willison glaciers.

Note: Ice thickness determined using GPR survey data and an analytical approach based on surface slope and basal shear stress relationships.

The Fantail Glacier had lower overall ice thickness (Figure 4.7), as represented through an average ice thickness of 157 m (Table 4.1). In addition, the Fantail Glacier covers a significantly smaller surface area (50 km<sup>2</sup>) than the Llewellyn and Willison Glaciers (513 km<sup>2</sup>). Thus it has a lower estimated ice volume of 8 km<sup>3</sup>, in comparison to 141 km<sup>3</sup> for the Llewellyn and Willison glaciers.

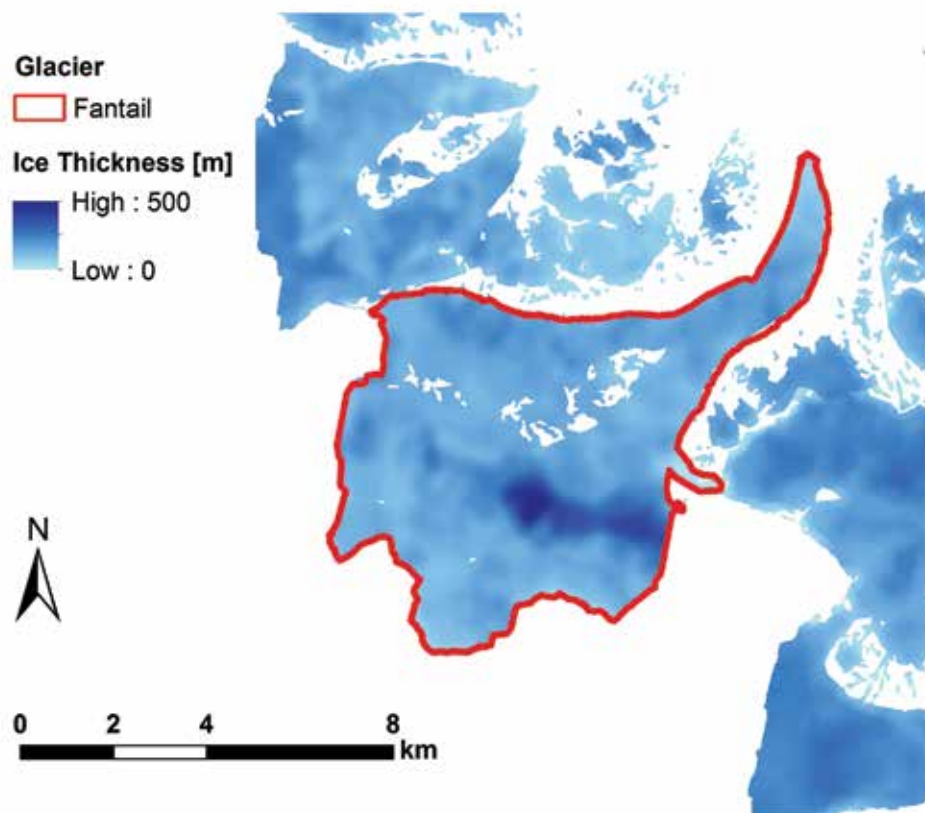


**Figure 4.7** Estimated ice thickness (m) of the Fantail Glacier.

Note: Ice thickness determined using GPR survey data and an analytical approach based on surface slope and basal shear stress relationships.

### 4.3 Ablation wires

Ablation wires were installed at five locations along the Llewellyn Glacier on April 28, 2014, to determine the local melt rate factors for snow and ice. These factors determine the equivalent meltwater layer thickness that is produced for each positive degree-day (see Shea et al. 2009). Wires were installed at elevations ranging from 1,200 m to 1,820 m, and were installed in holes bored ~13 m into the glacier using a Heucke steam drill. The initial exposed wire lengths were measured on installation and remeasured on July 31, 2014; a subset of these wires was remeasured again on August 10, 2014 (Table 4.2). The method used to determine the rate of snowmelt and ice melt and positive degree-day factors from these measurements, and the use of these factors for verifying CHRM meltwater production and mass balance characteristics, is discussed in Section 5.4.4.

**Table 4.2** Ablation wire measurements in each location, 2014

Ablation wire no.	Latitude (°N)	Longitude (°W)	Elevation (masl)	Exposed wire lengths (m)		
				Apr 28	Jul 31	Aug 10
1	58.8935	134.1132	1,820	2.20	3.87	n/a
2	58.9373	134.0848	1,693	2.12	4.04	n/a
3	58.9686	134.0782	1,614	1.69	4.28	4.62
4	59.0343	134.1028	1,349	1.91	4.38	4.78
5	59.0727	134.0989	1,200	2.60	6.46	6.68

#### 4.4 Conclusions

The focus of the glacier-based field investigation was the Llewellyn and Willison glaciers, the largest glaciers of the upper Yukon River basin. The investigation included a ground-penetrating radar (GPR) survey, which was used to determine ice surface elevation and thickness values along a number of longitudinal and transverse profiles. It also included ablation-wire observations that measured the melt rates of snow and ice. The average ice thickness of all glaciers within the upper Yukon River basin was estimated at 200 m, with total glacier surface area and volume of 1,000 km<sup>2</sup> and 210 km<sup>3</sup>, respectively. In the Llewellyn and Willison glaciers, the estimate of ice volume is approximately 141 km<sup>3</sup>, with an average ice thickness of 274 m and surface area of 513 km<sup>2</sup>. The ice melt/snowmelt rates vary by elevation. At 1,820 m (the higher third of the glaciers), melt rates were 1.78 cm/day (approximately 55 cm/month). At 1,200 m (the lower third of the glaciers), melt rates were 4.11 cm/day (approximately 125 cm/month).

These field investigations helped the study team achieve four goals:

- better quantify the present volume of ice stored in the Llewellyn and Willison glaciers and other smaller glaciers within the upper Yukon River basin;
- complement similar field observations conducted on smaller glaciers by NCE and funded by YEC (NCE 2014) so that various sizes and locations of glaciers within the study basin can be well represented;
- verify the hydrological model (CHRM) meltwater production and glacier mass balance characteristics using field observations (see Section 5); and
- better understand the contribution of the Llewellyn and Willison glaciers to regional hydrology and their potential responsiveness to a changing climate (see Section 6).

Overall, these scientific investigations bring substantial benefits to the study and thus to YEC, to address hydrological/glaciological and climate change issues facing the region.

## 5. Developing and applying the Cold Regions Hydrological Model

### 5.1 Model description

Physically-based distributed hydrological models are valuable tools to increase understanding of hydrological responses to climate inputs (e.g., precipitation, air temperature and wind speed) and climate changes. Physical hydrological models use mass and energy balance equations and physical parameters to represent the hydrological processes in a basin. As a result, they generally represent hydrological processes in a basin more accurately than simpler models (e.g., conceptual and lumped models) that rely on model calibration and curve fitting exercises (e.g., Beven 1985, 2001; Beven and O’Connell 1982). The Cold Regions Hydrological Model (CRHM), which was selected and applied for this study, is a flexible and primarily physically based model (Pomeroy et al. 2007).

Several physically based distributed models are available for use in cold regions, including the Distributed Hydrology Soil Vegetation Model (Wigmosta et al. 1994), *Modélisation Environnementale Communautaire*, or MEC - Surface and Hydrology, known as MESH (Pietroniro et al. 2007; Soulis et al. 2000), and Variable Infiltration Capacity (Liang et al. 1994). As noted by Beven (2001), their dependence on calibration/validation schemes can increase uncertainty about model parameters. These models also use the same hydrological model structure in each grid cell for the entire model domain, which may make them inappropriate for heterogeneous basins such as that of the upper Yukon River. CRHM operates with minimal calibration and computes mass balances through hydrological response units (HRUs), which allows it to configure the spatial variability of the study basin’s physical attributes and drainage conditions (Pomeroy et al. 2007). As an additional benefit it provides a flexible, object-oriented modeling system, where various process algorithms (stored in modules) can be selected from an internal library and linked to generate a model that is specific to user needs.

CRHM modules represent physically-based cold region hydrological processes, including direct and diffuse radiation to slopes, long-wave radiation in complex terrain, intercepted snow, blowing snow, sub-canopy turbulent and radiative transfer, sublimation, energy balance snowmelt, infiltration to frozen and unfrozen soils, rainfall interception, evapotranspiration, subsurface flow, depressional storage fill and spill, saturation excess overland flow and routing of surface, subsurface and stream-flow (Pomeroy et al. 2007). There are too many options for modules and their parameters, inputs and outputs to list in this report, but detailed descriptions of each module can be found in the original CRHM manual ([www.usask.ca/hydrology/oldsite/crhm/crhm\\_hp2006.pdf](http://www.usask.ca/hydrology/oldsite/crhm/crhm_hp2006.pdf)). CRHM has been widely applied in cold regions across Canada (including British Columbia, Yukon, Alberta and Northwest Territories), and other parts of the world, including Tibet, Patagonia, the Pyrenees and the Alps; see Ellis and Pomeroy 2007; Dornes et al. 2008; Ellis et al. 2010; López-Moreno et al. 2012; Fang et al. 2013; Zhou et al. 2014. This project applied the model to simulate the dominant hydrological processes of the upper Yukon River basin.

### 5.2 Meteorological and hydrometric data

#### 5.2.1 Station installation and data collection

One of the key limitations identified in NCE’s report on projected future changes in glaciers (NCE 2014) was a significant lack of robust spatial and temporal meteorological data for the study basin, particularly in the high-elevation headwater regions. As a result, for this study NCE installed five automated meteorological stations to address these gaps in observational data (Figure 5.1) and to both drive and constrain the hydrological model. The stations were installed during 2012–14 at

locations that were selected to represent a range of climatic regions, elevations, and spatial air temperature lapse rates. These locations were also selected to complement existing federal, provincial and territorial meteorological stations in the region. Since the major part of runoff was ultimately derived from high elevations, most of the stations were placed at these elevations. See the Yukon Research Metadata Catalogue (<http://envirodata.yukoncollege.yk.ca>) for detailed metadata regarding the five stations.

The stations at Fantail Lake basin, on the leeward side of B.C.'s coastal mountains (see Figure 5.1), were installed in 2012 and represent a drier continental climate zone. The Lower Fantail station (A1) was installed at a low elevation in the forest/wetland complex of a river valley. The Upper Fantail station (A2) was installed on a subalpine ridge line above a glacier valley terminus (see Table 5.1).

The Llewellyn stations were installed adjacent to the Llewellyn Glacier (in Atlin/Téix'gi Aan Tlein Provincial Park, B.C.) in 2013 and represent near-maritime conditions characterized by relatively high snowfall. The Lower Llewellyn station (A3) was installed near the glacier terminus; the Upper Llewellyn station (A4) was installed for the duration of the study on the southeast-facing flank of a large nunatak (i.e., a mass of rock surrounded by glacier ice).

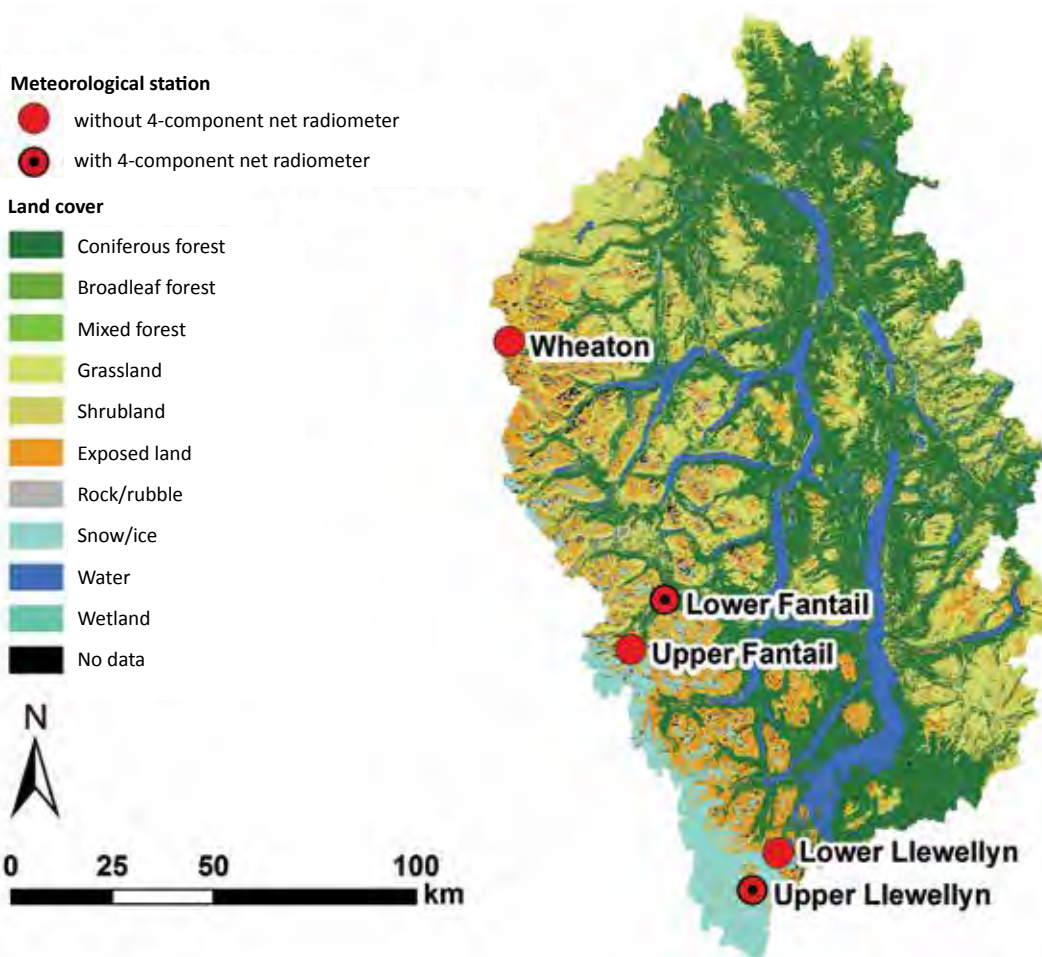


**Figure 5.1** Locations of the five meteorological stations, including the two four-component net radiometers, within the upper Yukon River basin (overlaid on land cover distribution).

The Upper Llewellyn station (A4) was placed in order to investigate energy balance processes in the near-glacier environment as a proxy for glacier mass balance. It was useful for process-based study, but its exposure to high winds made it a poor choice for long-term monitoring of snowpack. As a result, this station has now been removed. The Wheaton station (A5) was installed in 2014 and represents the continental climate of southern Yukon. It is adjacent to the Wheaton Glacier, at the headwaters of the Wheaton River, a tributary of the Yukon River. See Table 5.1 for details of stations.

**Table 5.1** Details of the five meteorological stations installed by NCE from 2012–14: installation date, location, elevation, area description and meteorological components measured.

Name	Installation date	Location (°)	Elevation (masl)	Area description	Component measured
Lower Fantail (A1)	Sept. 21, 2012 (SWE and MET), Aug. 28, 2014 (4–CNR)	59.6135°N, 134.7077°W	700	River valley bottom; rock island in a wetland	SWE, MET (no soil temp.*), 4–CNR
Upper Fantail (A2)	Aug. 31, 2012	59.4929°N, 134.8156°W	1,188	Mountain ridge; terrace; adjacent to a cirque glacier	SWE and MET
Lower Llewellyn (A3)	Aug. 31, 2013	59.1054°N, 134.0380°W	940	Red Mountain; gently sloping bench on lower slopes of east-facing mountain slope; near glacier terminus	SWE and MET
Upper Llewellyn (A4)	Aug. 28, 2013 (SWE and MET), May 19, 2014 (4–CNR)	59.0161°N, 134.1209°W	1,436	Nunatak; bench on lower part of east-facing mountain slope above glacier. Below accumulation zone.	SWE, MET (no soil temp.*), 4–CNR
Wheaton (A5)	Sept. 3, 2014	60.1097°N, 135.5879°W	1,265	Ridge crest in larger mountain valley. Subalpine fir and shrubs. Site partially sheltered by surrounding trees.	SWE and MET

Notes: SWE= snow water equivalent, MET = meteorological (air temperature, soil temperature, relative humidity, barometric pressure, wind speed and direction, rainfall, and average net radiation) and 4–CNR= four-component net radiometer (incoming and outgoing long- and short-wave radiation). \*Soil temp. could not be measured at stations installed on a rocky surface.

Each of the stations measured air temperature, soil temperature, relative humidity, barometric pressure, wind speed and direction, net radiation, rainfall, snow depth and snow water equivalent (SWE) on hourly, sub-daily (every six hours) and daily timescales (Figure 5.2). Individual net radiometers were installed at all meteorological stations, but they measured only the balance of incoming minus outgoing total (short-wave plus long-wave) radiation and were not adequate for validating glacier models. In 2014, four-component net radiometers were retrofitted at two stations: Lower Fantail (A1) and Upper Llewellyn (A4). This provided independent measurements of outgoing long-wave (LWo), incoming long-wave (LWi), outgoing short-wave (SWo), and incoming short-wave (SWi) radiation. The location of the net radiometers was determined using correlation analysis among radiation-transport variables (i.e., albedo, water vapour, air temperature, elevation, land cover, and aspects). These were obtained from data assimilation retrieval products such as Environment Canada’s Global Environmental Multiscale Model (GEM) and atmospheric re-analysis data products such as North American Regional Reanalysis (NARR).

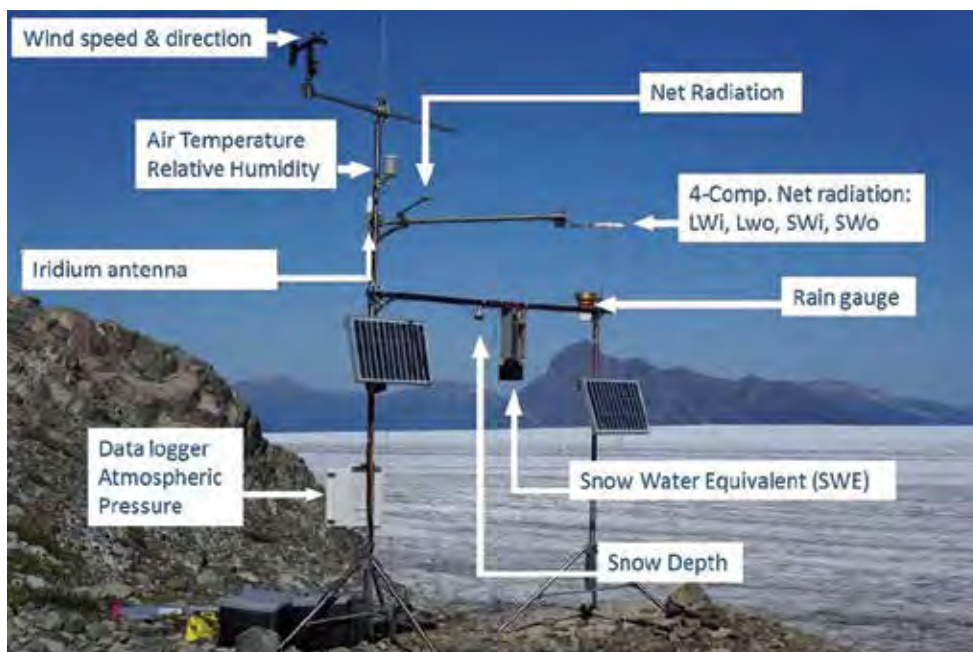


**Figure 5.2** The Upper Llewellyn meteorological station installed by NCE, showing all instrumentation, including a four-component net radiometer.

Meteorological data were automatically transmitted via Iridium satellite communication from the stations to the Campbell Scientific server on a weekly basis. Data are shown in Table 5.2. Automated data retrieval software was developed by the NCE team to facilitate a convenient, user-friendly data format that allowed for easy download and creation of graphs and tables (refer to the Data Retrieval Software Manual; NCE 2016).

**Table 5.2** Meteorological components measured and names of measurement instruments.

Component measured	Instrument name
Wind speed and direction	R.M. Young Wind Monitor Alpine Version, Model 05103AP
Snow depth	Sonic Ranger 50KHz, Model SR50A
Rainfall	Texas Electronics Tipping Bucket Rain Gauge 8-inch-diameter funnel, Model TE525WS
Net solar radiation	Kipp and Zonen Net Radiometer, Model NR Lite2
Barometric pressure	Vaisal PTB110 Barometric Pressure Sensor 500mb, Model CS106
Air temperature and relative humidity	Rotronics Relative Humidity and Air Temperature Probe, Model HC-S3-XT
Snow water equivalent (SWE)	Snow Water Equivalent Sensor, Model CS725
Soil temperature	Soil Temperature Thermistor Probe, Model 109
Incoming and outgoing long- and short-wave radiation	Kipp and Zonen Four-Component Net Radiometer, Model CNR4

Note: A CR1000-55 data logger equipped with a measurement and control module with 4MB RAM was used to record the data.

### 5.2.2 The existing network

Data gathered from the five SWE/Met stations installed by NCE were complemented by existing meteorological stations to calibrate, constrain and operate CRHM (Figure 5.3a). The stations collected various meteorological data, including air temperature, relative humidity, wind speed and precipitation. These data were later used to force CRHM. Data were acquired through Environment Canada, Government of Yukon, Yukon Geological Survey, University of Ottawa, and Yukon Avalanche Association, among others (see Table 5.3). In addition, four gauged hydrometric stations with robust data records and manually sampled SWE survey data (Figure 5.3b, Table 5.3), measured during spring (either three or four times a year) by the Yukon Department of Environment's Water Resources Branch, were used to evaluate CRHM performance.

**Table 5.3** Meteorological, hydrometric and SWE stations

Station ID number						Station name	Data source
Tm	WS	RH	Pcp	SWE	Q		
1	1	1	n/a	n/a	n/a	Lower Fantail	Yukon Energy Corporation and Yukon College
2	2	2	n/a	n/a	n/a	Upper Fantail	
3	3	3	n/a	n/a	n/a	Lower Llewellyn	
4	4	4	n/a	n/a	n/a	Upper Llewellyn	
5	5	5	n/a	n/a	n/a	Whitehorse A	Environment Canada
6	6	6	n/a	n/a	n/a	Whitehorse Auto	
7	7	7	n/a	n/a	n/a	Carcross	Yukon Avalanche Association (YAA)
8	8	8	n/a	n/a	n/a	Jakes Corner	
n/a	n/a	9	n/a	n/a	n/a	Mount Racine	
9	9	10	n/a	n/a	n/a	Mount Sima	
10	10	11	n/a	n/a	n/a	YAAAND	
11	11	12	n/a	n/a	n/a	YAAFRA	
12	12	13	n/a	n/a	n/a	YAASUM	
13	n/a	n/a	n/a	n/a	n/a	Tagish	
14	13	14	n/a	n/a	n/a	Alpine Wolf Creek	Government of Yukon (Department of Environment, Water Resources Branch)
15	14	15	n/a	n/a	n/a	Buckbrush Taiga Wolf Creek	
16	15	16	n/a	n/a	n/a	Forest Wolf Creek	
17	n/a	n/a	n/a	n/a	n/a	Cowley Creek	Yukon Geological Survey
18	16	17	n/a	n/a	n/a	Chilkoot Pass	National Park Service (U.S.)
19	17	18	n/a	n/a	n/a	Sheep Camp	
20	n/a	n/a	n/a	n/a	n/a	Skagway Captain	SNOTEL
21	18	19	n/a	n/a	n/a	Atlin School	University of Ottawa (Geography Dept.)
22	19	20	n/a	n/a	n/a	Atlin Monarch Mt1	

**Table 5.3** (continued)

n/a	n/a	n/a	1	n/a	n/a	Atlin	Environment Canada
n/a	n/a	n/a	2	n/a	n/a	Graham Inlet	
n/a	n/a	n/a	3	n/a	n/a	Annie Lake Robinson	
n/a	n/a	n/a	4	n/a	n/a	Carcross	
n/a	n/a	n/a	5	n/a	n/a	Potter Creek Wahl	
n/a	n/a	n/a	6	n/a	n/a	Whitehorse A	
n/a	n/a	n/a	7	n/a	n/a	Whitehorse Auto	
n/a	n/a	n/a	8	n/a	n/a	Whitehorse Riverdale	
n/a	n/a	n/a	9	n/a	n/a	Fraser Camp	
n/a	n/a	n/a	n/a	1	n/a	Atlin	Government of Yukon (Water Resources Branch, Department of Environment)
n/a	n/a	n/a	n/a	2	n/a	Log Cabin	
n/a	n/a	n/a	n/a	3	n/a	Montana Mountain	
n/a	n/a	n/a	n/a	4	n/a	Tagish	
n/a	n/a	n/a	n/a	5	n/a	Whitehorse Airport	
n/a	n/a	n/a	n/a	n/a	1	Yukon River at Whitehorse	Environment Canada (Water Survey of Canada)
n/a	n/a	n/a	n/a	n/a	2	Atlin River near Atlin	
n/a	n/a	n/a	n/a	n/a	3	Wheaton River near Carcross	
n/a	n/a	n/a	n/a	n/a	4	Tutshi River at outlet of Tutshi Lake	

Note: See also Figure 5.3. ID numbers correspond to the various measured parameters and data source, where Tm= air temperature, WS = wind speed, RH= relative humidity, Pcp= precipitation, SWE= snow water equivalent and Q= flow.

### 5.2.3 GEM-LAM and grid correction

To further improve the quality of the spatiotemporal meteorological data (Figure 5.3a), model calibration and operation also used archived meteorological data from the Canadian limited-area model version of the Global Environment Multiscale configuration (GEM-LAM) produced by Environment Canada. GEM-LAM is a high-resolution grid model that represents local conditions, physical processes and organization of weather systems at all scales.

Two sets of grids from the GEM-LAM model were applied to fill the gaps in temporal data and generate spatially continuous data for the entire study basin. Precipitation data were determined by Canadian Precipitation Analysis, or CaPA (Mahfouf et al. 2007), and data for air temperature, wind speed, long- and short-wave radiation, specific humidity and air pressure were determined by Regional Deterministic Prediction System, or RDPS (Coté et al. 1998a and b; Yeh et al. 2002). The CaPA and RDPS data grids covered the study basin with a spatial resolution of approximately 5 km (east/west) and 10 km (north/south) and a total of 386 grid points (Figure 5.4).

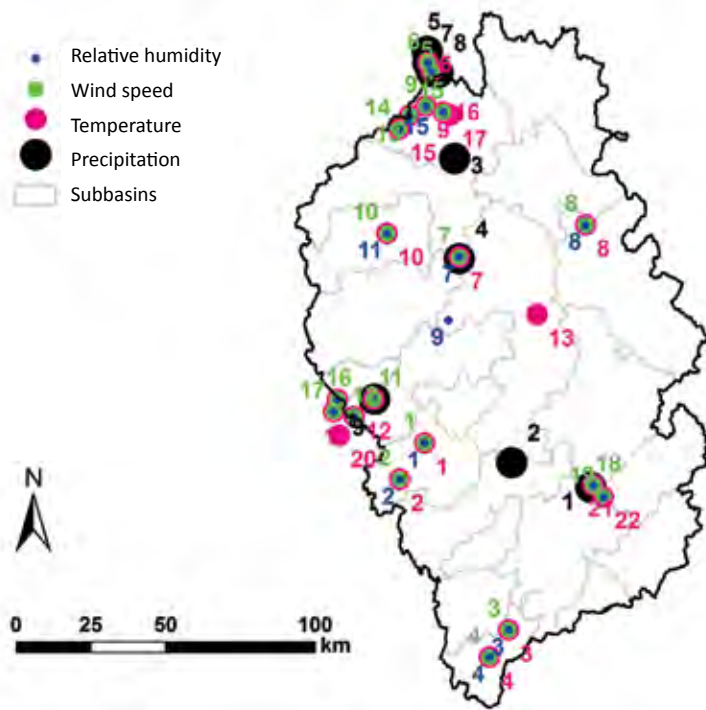


**Figure 5.3a** Sampling locations for meteorological stations.  
 Note: numbers correspond to station locations (see Table 5.3).

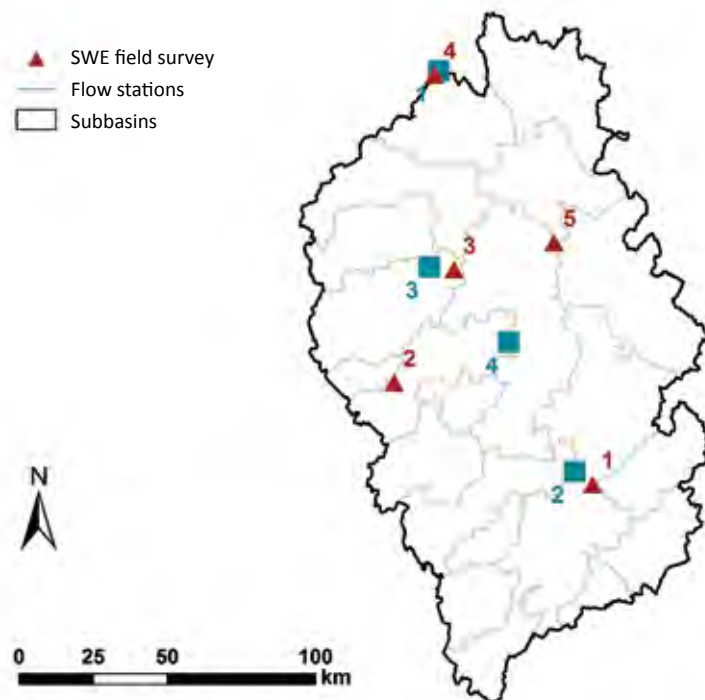


**Figure 5.3b** Sampling locations for hydrometric and SWE stations.  
 Note: numbers correspond to the station location (see Table 5.3).

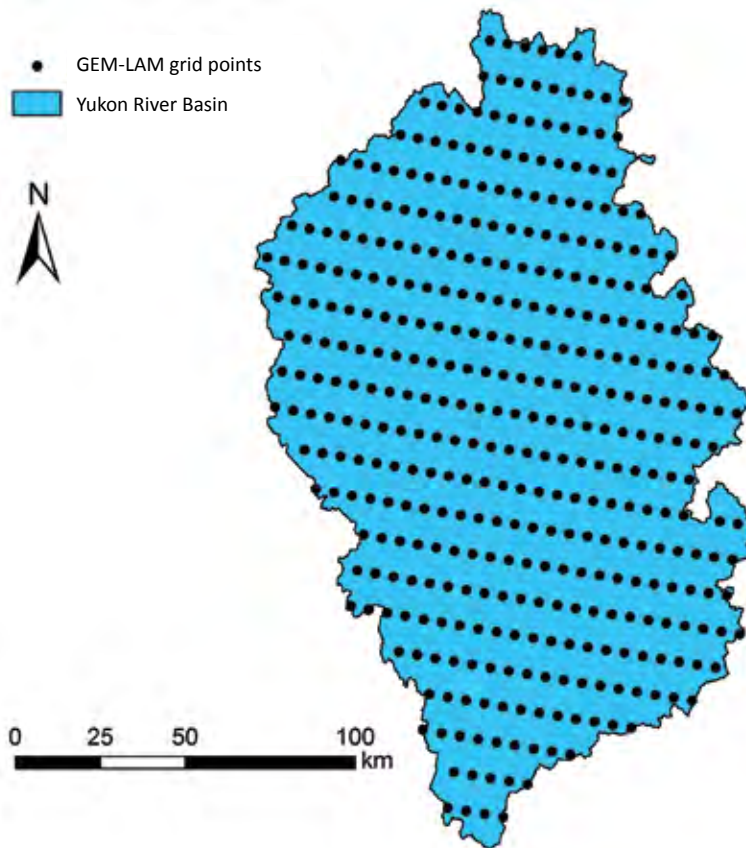


**Figure 5.4** Spatial distribution of GEM-LAM grid points.

Since some of the GEM-LAM data varied from the observed meteorological data, the RDPS and CaPA data were corrected prior to simulation in CRHM. The RDPS data were initially corrected with the observed data by the following three steps:

1. applying a linear regression method, for which correlation coefficients were 0.94 for temperature (from 22 stations), 0.82 for wind speed (from 19 stations) and 0.53 for relative humidity (from 20 stations);
2. interpolating the linear regression parameters (i.e., intercept and slope values) to the grid points using the Inverse Distance Weight method, or IDW (Shepard 1968), where the values at unknown points are calculated with a weighted average based on the values at the known points (closer points are weighted higher than points that are farther away); and
3. correcting the raw RDPS data at each grid point using the linear regression parameters to generate corrected meteorological data.

Since the correlation values between the observed meteorological data and CaPA data were very low ( $< 0.1$ ), the CaPA precipitation data were corrected using a different method, which involved:

1. computing the ratio values of the mean annual precipitation between the observed and raw CaPA data (at the closest CaPA grid point to the meteorological observation station);
2. interpolating the ratio values to the entire study region using the IDW approach; and
3. correcting the precipitation values at each grid point by multiplying the raw CaPA data by the interpolated ratio values from step 2.

## 5.3 Model set-up and parameter definition

### 5.3.1 Delineating the basin

Determining the study basin's physical attributes is important for characterization of land cover and drainage conditions, which in turn allows for the delineation of subbasins and hydrological response units (HRUs). The Environmental Systems Research Institute's ArcGIS 10.1 software (ESRI 2011) was used to analyze the digital elevation model (DEM), hydrometry, soils and land cover data in order to determine the basin's physical attributes. Data on elevation (Figure 5.5) and land cover (Figure 5.1) were collected from GeoBase ([www.geobase.ca](http://www.geobase.ca)), which has a grid resolution of 20 km. Soil data were generated from the Harmonized World Soil Database Version 1.2 (Nachtergaele et al. 2012). The spatial resolution of the soil data was rather coarse and no detailed data were available for soil depths.

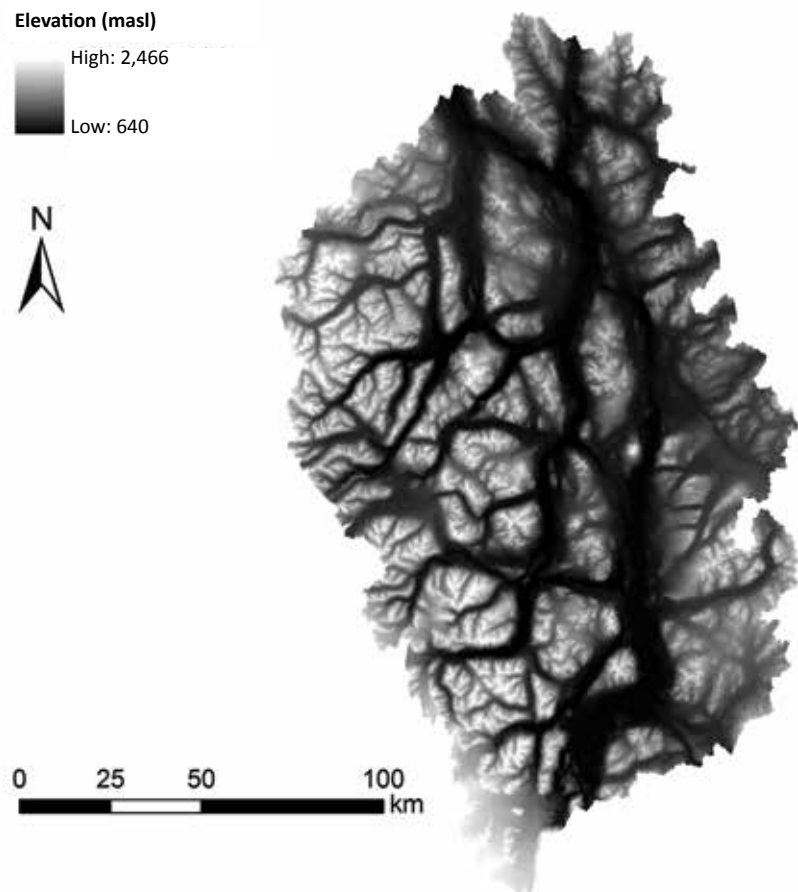


**Figure 5.5** Spatial distribution of the Digital Elevation Model (DEM).

DEM data and Archydro software (ESRI 2011) were used to delineate the study basin into twenty subbasins (Figure 5.6), and to generate the routing sequence between the modeled subbasins and HRUs (Figure 5.7a and b). Each subbasin was divided into HRU classes based on land cover (Tables 5.4 and 5.5), including ice/glacier, rock, exposed land, grassland, shrubland, coniferous forest, broad-leaf forest, mixed forest, open water, and wetland.

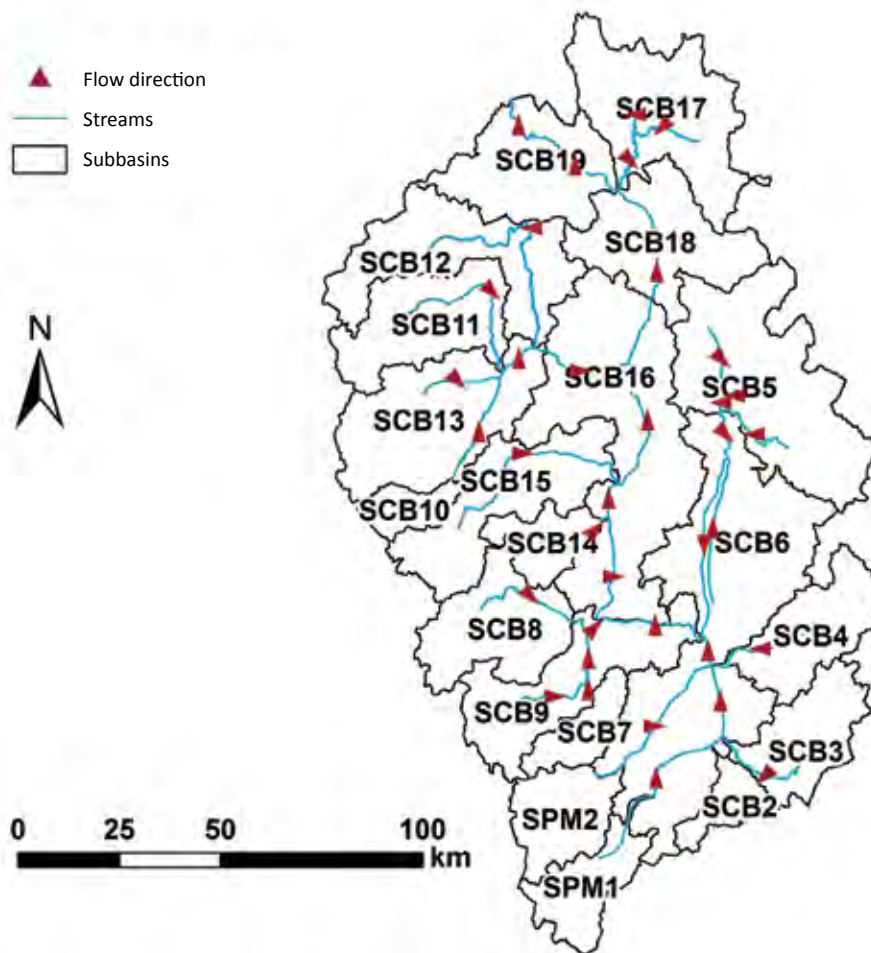


**Figure 5.6** Subbasin delineations and flow direction.

Each ice/glacier unit was further divided into nine elevation bands (Figure 5.8), in order to characterize changing environmental conditions. The elevation bands were based on DEM data and were defined as 2,000–2,466 m; 1,750–2,000 m; 1,539–1,750 m; 1,398–1,539 m; 1,263–1,398 m; 1,129–1,263 m; 996–1,129 m; 865–996 m; and 640–865 m. The grassland and rock HRUs were further subdivided by aspects (computed from the DEM data in ArcGIS) to represent north (0–180°), south (180–360°) and flat (0°) aspects. The National Hydro Network, accessed through Natural Resources Canada, was used to approximate the small and main river channel HRUs.

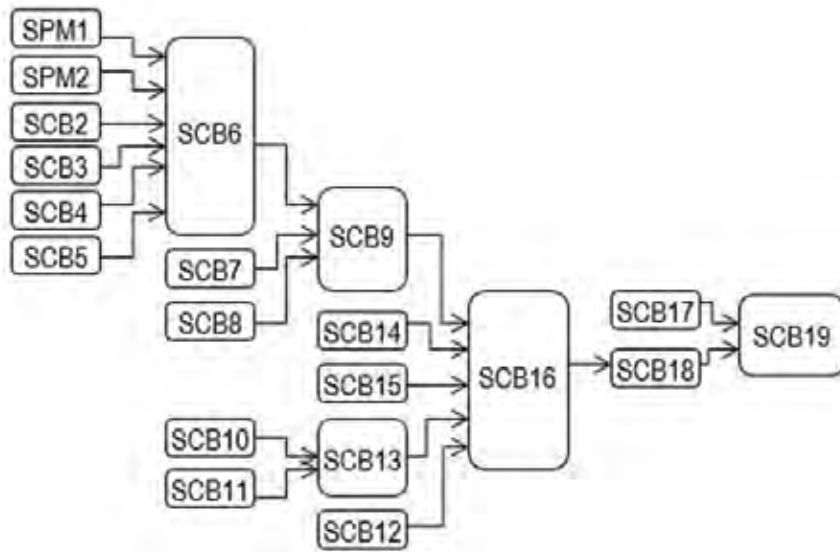


Figure 5.7a Direction of flow for the modeled subbasins.

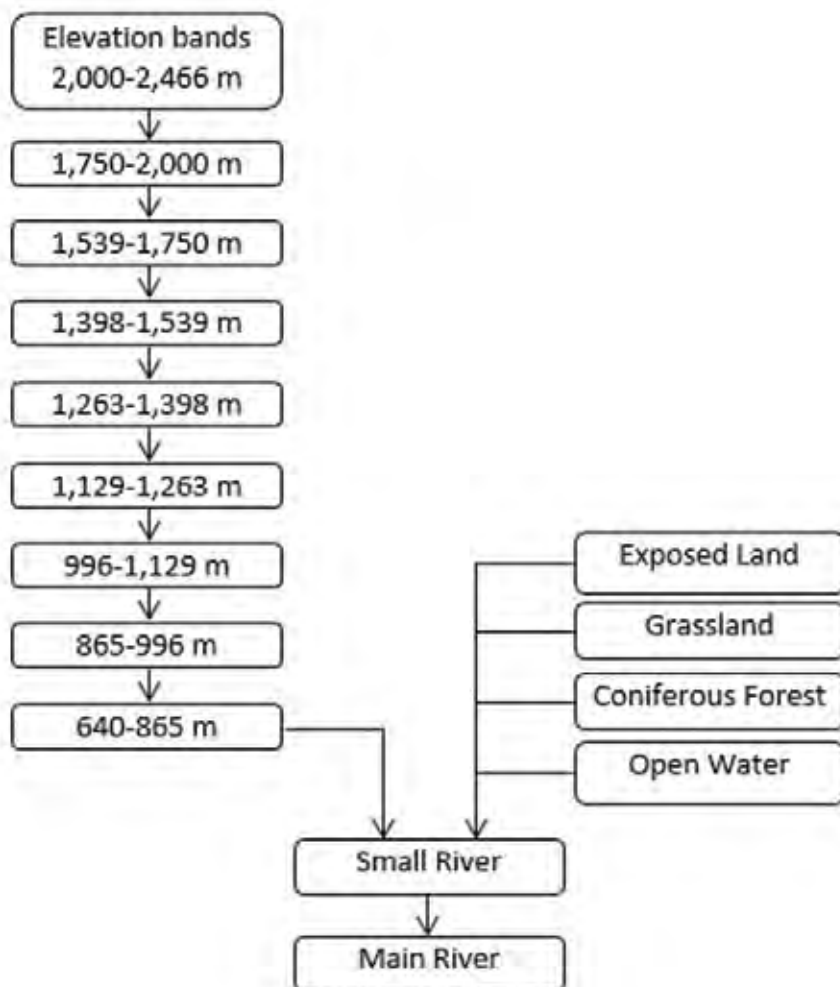


Figure 5.7b An example of flow direction for modeled HRUs in subbasin SPM1.

**Table 5.4** CRHM basin details: group and subbasin names, subbasin area, model structure and associated HRUs and land-cover classification.

Group name	Subbasin		Model structure*	HRU numbers and associated land-cover classification**
	Name	Area (km <sup>2</sup> )		
A	SPM1	526.5	G	(1)LC2; (2)LC3; (3)LC4; (4)LC5; (5)LC6; (6)LC7; (7)LC8; (8)LC9; (9)LC10; (10)LC15; (11)LC17; (12)LC21; (13)LC1; (14)LC24; (15)LC25
B	SPM2	434.2	G	(1)LC2; (2)LC3; (3)LC4; (4)LC5; (5)LC6; (6)LC7; (7)LC8; (8)LC9; (9)LC15; (10)LC17; (11)LC21; (12)LC1; (13)LC24; (14)LC25
C	SCB2	246.3	NG	(1)LC15; (2)LC17; (3)LC16; (4)LC21; (5)LC23; (6)LC1; (7)LC24
D	SCB3	645	NG	(1)LC15; (2)LC17; (3)LC16; (4)LC21; (5)LC23; (6)LC1; (7)LC24
E	SCB4	683.4	NG	(1)LC15; (2)LC17; (3)LC16; (4)LC21; (5)LC23; (6)LC1; (7)LC24
F	SCB5	1639	NG	(1)LC15; (2)LC17; (3)LC16; (4)LC21; (5)LC23; (6)LC1; (7)LC24
G	SCB6	2715	NG	(1)LC3; (2)LC4; (3)LC5; (4)LC11; (5)LC15; (6)LC17; (7)LC16; (8)LC21; (9)LC22; (10)LC23; (11)LC23; (12)LC1; (13)LC24
H	SCB7	314.4	NG	(1)LC2; (2)LC3; (3)LC4; (4)LC5; (5)LC6; (6)LC15; (7)LC17; (8)LC16; (9)LC21; (10)LC23; (11)LC1; (12)LC24; (13)LC25
I	SCB8	816.7	G	(1)LC2; (2)LC3; (3)LC4; (4)LC5; (5)LC6; (6)LC7; (7)LC8; (8)LC9; (9)LC13; (10)LC14; (11)LC15; (12)LC19; (13)LC20; (14)LC16; (15)LC21; (16)LC22; (17)LC23; (18)LC1; (19)LC24; (20)LC25
J	SCB9	979.9	G	(1)LC2; (2)LC3; (3)LC4; (4)LC5; (5)LC6; (6)LC7; (7)LC8; (8)LC13; (9)LC14; (10)LC15; (11)LC19; (12)LC20; (13)LC16; (14)LC21; (15)LC22; (16)LC23; (17)LC1; (18)LC24; (19)LC25
K	SCB10	220.7	G	(1)LC3; (2)LC4; (3)LC5; (4)LC6; (5)LC7; (6)LC8; (7)LC13; (8)LC14; (9)LC15; (10)LC19; (11)LC20; (12)LC16; (13)LC21; (14)LC22; (15)LC1; (16)LC24; (17)LC25
L	SCB11	863	G	(1)LC2; (2)LC3; (3)LC4; (4)LC13; (5)LC14; (6)LC15; (7)LC19; (8)LC20; (9)LC16; (10)LC21; (11)LC22; (12)LC23; (13)LC1; (14)LC24; (15)LC25
M	SCB12	1143	G	(1)LC2; (2)LC3; (3)LC13; (4)LC14; (5)LC15; (6)LC19; (7)LC20; (8)LC16; (9)LC21; (10)LC22; (11)LC23; (12)LC1; (13)LC24; (14)LC25
N	SCB13	1252	G	(1)LC2; (2)LC3; (3)LC4; (4)LC5; (5)LC6; (6)LC7; (7)LC13; (8)LC14; (9)LC15; (10)LC19; (11)LC20; (12)LC16; (13)LC21; (14)LC22; (15)LC23; (16)LC1; (17)LC24; (18)LC25
O	SCB14	339.5	G	(1)LC2; (2)LC3; (3)LC4; (4)LC11; (5)LC15; (6)LC17; (7)LC16; (8)LC21; (9)LC22; (10)LC23; (11)LC23; (12)LC1; (13)LC24; (14)LC25
P	SCB15	1005	G	(1)LC2; (2)LC3; (3)LC4; (4)LC5; (5)LC6; (6)LC13; (7)LC14; (8)LC15; (9)LC19; (10)LC20; (11)LC16; (12)LC21; (13)LC22; (14)LC23; (15)LC1; (16)LC24; (17)LC25
Q	SCB16	2159	G	(1)LC3; (2)LC4; (3)LC11; (4)LC15; (5)LC17; (6)LC16; (7)LC21; (8)LC22; (9)LC23; (10)LC23; (11)LC1; (12)LC24; (13)LC25

**Table 5.4** (continued)

R	SCB17	1251	NG	(1)LC15; (2)LC19; (3)LC20; (4)LC16; (5)LC21; (6)LC22; (7)LC23; (8)LC23; (9)LC1; (10)LC24; (11)LC25
S	SCB18	991.9	NG	(1)LC15; (2)LC19; (3)LC20; (4)LC16; (5)LC21; (6)LC22; (7)LC23; (8)LC23; (9)LC1; (10)LC24; (11)LC25
T	SCB19	955.3	NG	(1)LC15; (2)LC19; (3)LC20; (4)LC16; (5)LC21; (6)LC22; (7)LC23; (8)LC1; (9)LC24; (10)LC25
U	River flow estimates in each subbasin	—	—	(1) SPM1; (2)SPM2; (3)SCB2; (4)SCB3; (5)SCB4; (6)SCB5; (7)SCB6; (8)SCB7; (9)SCB8; (10)SCB9; (11)SCB10; (12)SCB11; (13)SCB12; (14)SCB13; (15)SCB14; (16)SCB15; (17)SCB16; (18)SCB17; (19)SCB18; (20)SCB19

Note: \*Model structure G used for glacierized and NG used for non-glacierized areas.

\*\*Refer to Table 5.5 for details on HRUs and classification names.

**Table 5.5** Land cover (LC) numbers and their associated classifications.

LC no.	LC classification	LC no.	LC classification
LC1	Open water	LC14	Rock/rubble flat-facing
LC2	Ice/glacier (elevation band: 2,000–2,466 m)	LC15	Exposed land
LC3	Ice/glacier (elevation band: 1,750–2,000 m)	LC16	Shrubland
LC4	Ice/glacier (elevation band: 1,539–1,750 m)	LC17	Grassland
LC5	Ice/glacier (elevation band: 1,398–1,539 m)	LC18	Grassland north-facing
LC6	Ice/glacier (elevation band: 1,263–1,398 m)	LC19	Grassland south-facing
LC7	Ice/glacier (elevation band: 1,129–1,263 m)	LC20	Grassland flat-facing
LC8	Ice/glacier (elevation band: 996–1,129 m)	LC21	Coniferous forest
LC9	Ice/glacier (elevation band: 865–996 m)	LC22	Broadleaf forest
LC10	Ice/glacier (elevation band: 640–865 m)	LC23	Mixed forest
LC11	Rock/rubble	LC24	Small channel
LC12	Rock/rubble north-facing	LC25	Main channel
LC13	Rock/rubble south-facing		

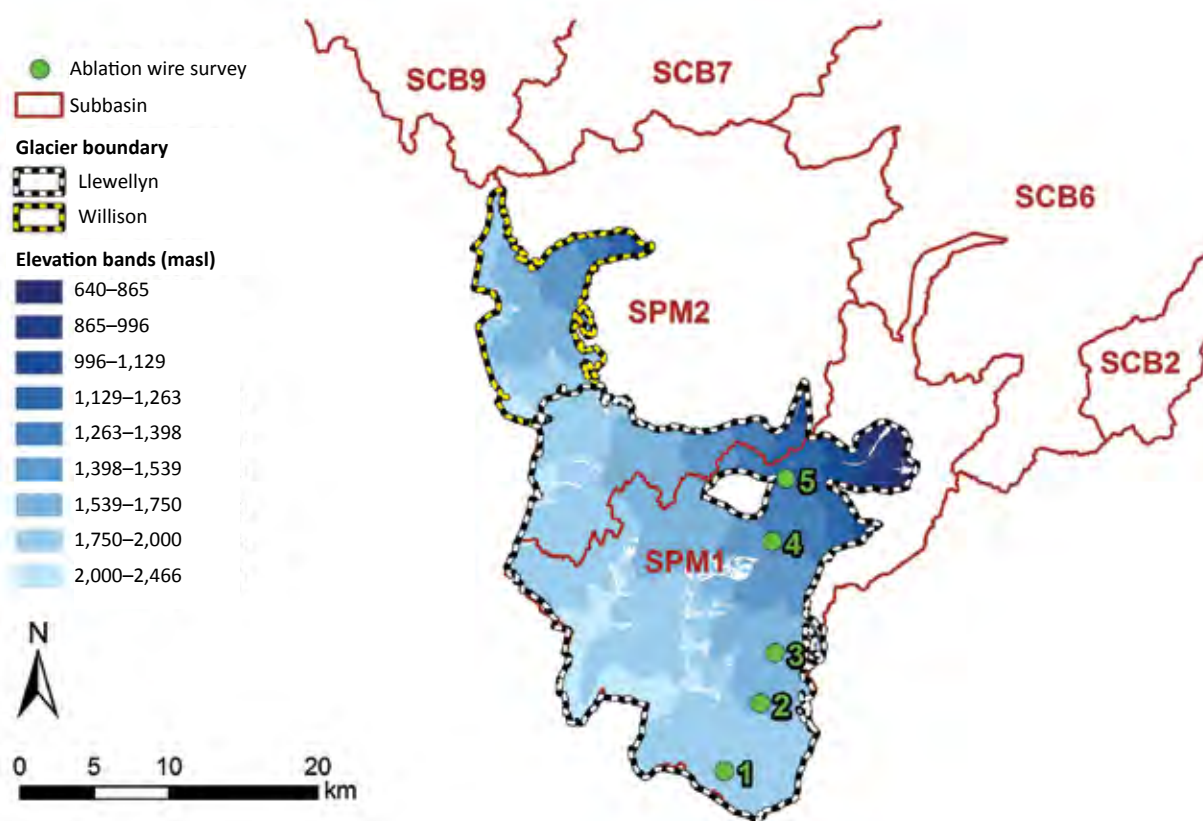


**Figure 5.8** Elevation bands of the Llewellyn (dashed black-white lines) and Willison (dashed black-yellow lines) glaciers used in CRHM; green dots are the locations of the ablation wires; and red lines are the subbasin boundaries.

### 5.3.2 Determining model structure

Two model structures were assembled and applied to the subbasins in the model. They consist of a series of modules selected by the user to represent relevant hydrological processes. Development of the model structure was informed by the results from earlier CRHM modeling experiments performed on Wolf Creek (Pomeroy et al. 2010; Rasouli et al. 2014), a tributary of the upper Yukon River located within the study basin. The modules of each structure differed depending on the presence or absence of a glacier in the subbasin.

The non-glacierized model structure (NG) was applied to the majority of the study basin, since the basin primarily consists of non-glacierized areas. The non-glacierized model structure consisted of 14 different modules that represent the physical processes in non-glacierized areas (Figure 5.9). The glacierized model structure (G) was applied only to the glacierized areas; it also consisted of 14 different modules that represent the physical processes in glacierized areas (Figure 5.10). Similar modules were applied for both model structures; however, the glacierized structure contained the `winter_meltflag`, `Glacier2` and `z_s` and `_rho` modules to differentiate seasonal melts and calculate glacier mass balance and snow cover thickness, respectively (Table 5.6). These modules were not included in the non-glacierized model structure. The `FrozenAyers`, `LongVt` and `SnobalCRHM` modules were included exclusively in the non-glacierized model structure to estimate soil infiltration and calculate incoming long- and short-wave radiation and snowmelt, respectively (Table 5.6).

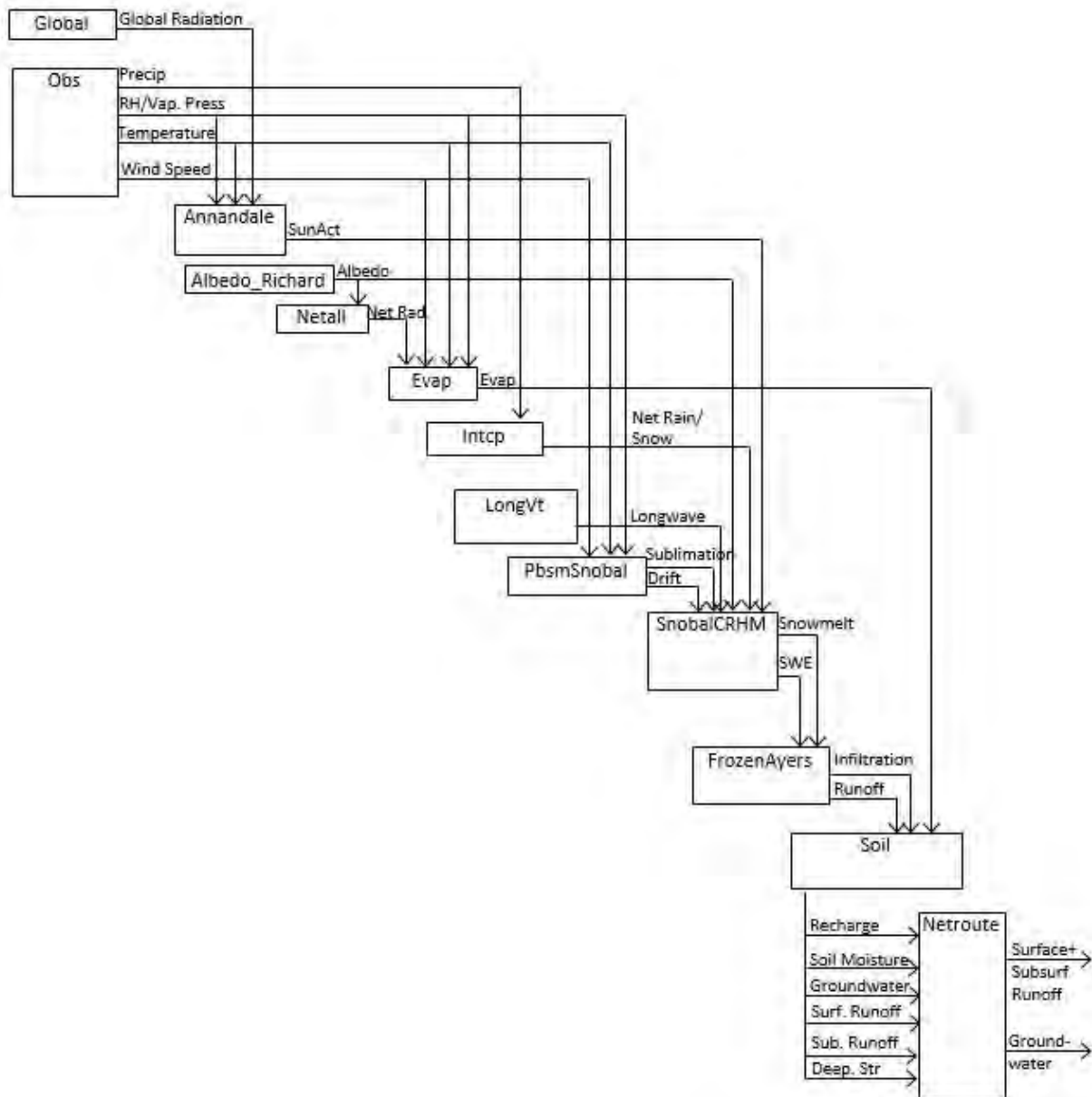


Figure 5.9 CRHM structure for non-glacierized areas (model NG).

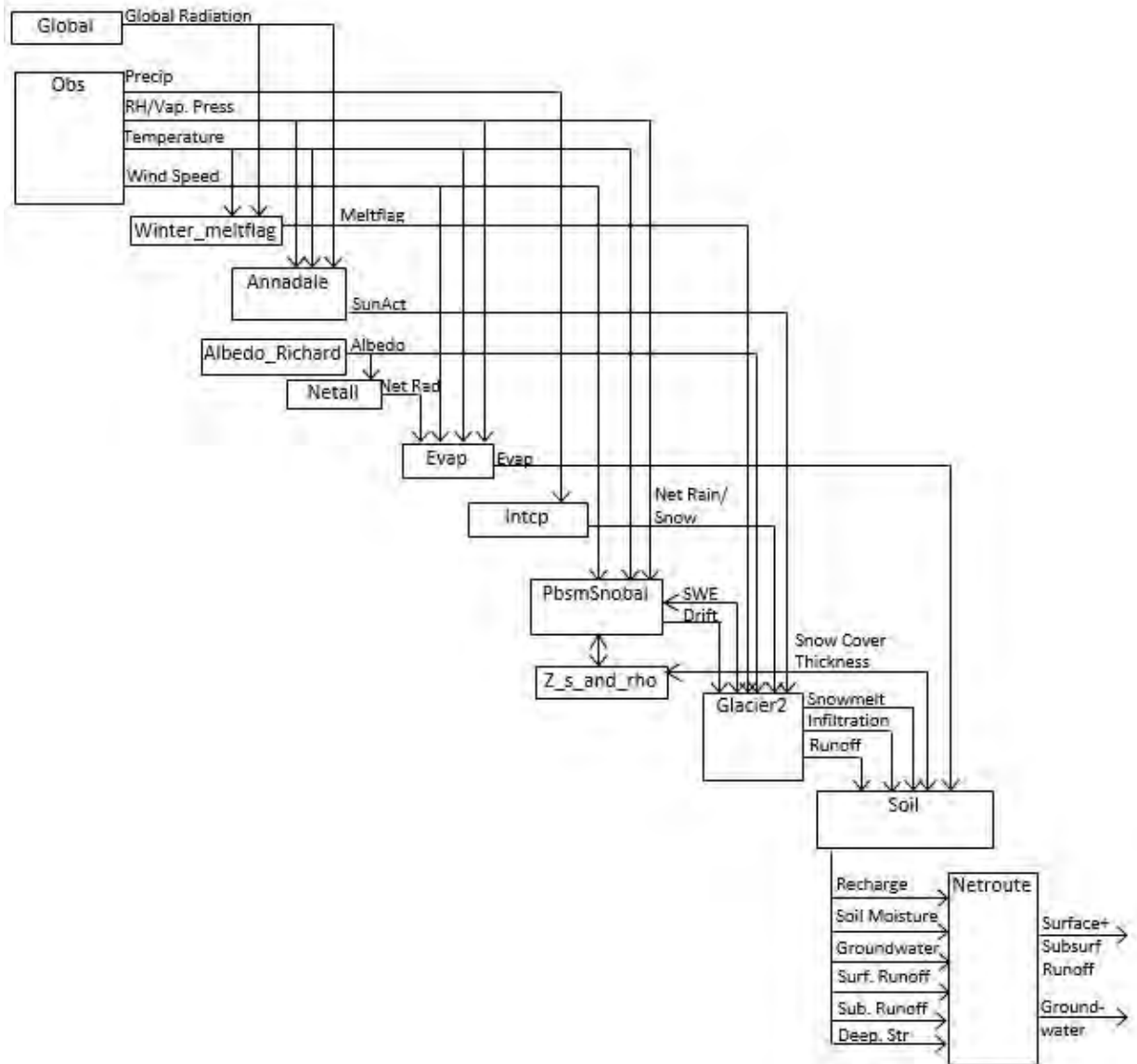


Figure 5.10 CRHM structure for glacierized areas (model G).

**Table 5.6** Module names and definitions for non-glacierized (NG) and glacierized (G) model structures.

Module name	In NG	In G	Module definition
Albedo_Richard	yes	yes	computes snow cover albedo during summer and winter, and for the beginning and duration of the melt period (Essery 1997)
Annandale	yes	yes	estimates sunshine hours from minimum and maximum daily temperature (Annandale et al. 2002)
Basin	yes	yes	outlines the basic physical attributes of the basin study area, such as basin area, HRU area, latitude, elevation, ground slope (GSL) and aspect angle (ASL)
Evap	yes	yes	computes daily evapotranspiration (Granger and Gray 1989; Granger and Pomeroy 1997) using interval values from after snowmelt to fall snow cover, depending on positive net radiation, wind speed, and temperature solved in an energy balance equation
FrozenAyers	yes	no	estimates frozen soil infiltration using Zhao and Gray (1999) and unfrozen soil infiltration using Ayers (1959)
Glacier2	no	yes	calculates glacier net losses or gains (ice, firn, snowmelt, etc.) using energy and mass balance equations and assuming that glaciers are static ice masses that melt in place and decrease in volume over time, with no lateral movement of the frozen mass
Global	yes	yes	calculates theoretical interval short-wave radiation, direct and diffuse solar radiation, and maximum sunshine hours based on latitude, elevation and slope and aspect, following Garnier and Ohmura (1970)
Intcp	yes	yes	computes summer and winter interception (i.e., net rain and snow)
LongVt	yes	no	calculates incoming long-wave radiation using terrain view factor and short-wave radiation (Sicart et al. 2006)
Netall	yes	yes	computes the net all-wave radiation from sunshine hours, temperature and humidity (Granger and Gray 1990)
noetroute	yes	yes	estimates route runoff based on lag and route timing parameters (Clark 1945)
Obs	yes	yes	computes temperature, precipitation, relative humidity, evaporation and wind speed data from the observation input files for each HRU, with temperature lapse rate, area, elevation, and wind-induced under-catch parameters — this model uses an hourly time step interval for air temperature, wind speed and relative humidity, and a daily time step interval for precipitation
PbsmSnobal	yes	yes	calculates snow transport and sublimation, including drift — the model has been extended to accommodate the transport of snow from HRUs with lesser to greater roughness, according to the fractions specified in the distribution parameter (Pomeroy and Li 2000)
Snobal-CRHM	yes	no	computes snowmelt using the energy balance of snow properties, measurement heights and depths, and energy exchanges (Gray and Landine 1987)

**Table 5.6** (continued)

Soil	yes	yes	estimates soil moisture, depressional storage, and surface/subsurface and groundwater flows throughout the year (Leavesley et al. 1983; Pomeroy et al. 2007; Dornes et al. 2008; Fang et al. 2010 and 2013) —the top soil layer receives infiltration from depressional storage, snowmelt and rainfall, while the bottom layer receives percolation from lower-layer infiltration or directly from the surface through macropores; the hydraulic conductivity in the top soil layer is computed using Darcy's equation and parameters for it are calculated using Brooks and Corey's (1964) relationship
Winter_meltflag	no	yes	differentiates the major spring melt from the fall and late spring snow melts
Z_s and_rho	no	yes	computes average snow cover density and total snow cover thickness

### 5.3.3 Glacier mass balance

Winter and summer glacier mass balances were based on the timing and magnitude of snowmelt/ice melt, according to Østrem and Brugman (1991) and Stahl and Moore (2006). The summer mass balance —  $bs(t, h)$ , for a given year ( $t$ ) at each HRU ( $h$ ) — was calculated for the complete flow of snow melt off the glacier (Equation 5.1):

$$bs(t, h) = - \left[ \max[SWE(t, h)] + \sum M_{ice}(t, h) \right] \quad \text{if } \min[SWE(t, h)] = 0 \quad (5.1)$$

It was also calculated for the incomplete flow of snow melt off the glacier (Equation 5.2):

$$bs(t, h) = \min[SWE(t, h)] - \max[SWE(t, h)] \quad \text{if } \min[SWE(t, h)] > 0 \quad (5.2)$$

For both equations, SWE is snow water equivalent (m) and  $\sum M_{ice}(t, h)$  is the cumulative ice melt for the year until the beginning of continuous snow cover at each glacier HRU (m).

The winter mass balance —  $bw(t, h)$  — was computed as follows (Equation 5.3):

$$bw(t, h) = \max[SWE(t, h)] \quad (5.3)$$

The net glacier mass balance —  $bn(t, h)$  — for a given year at each HRU is the sum of the summer and winter mass balance for each glacier HRU, per Equation 5.4:

$$bn(t, h) = bw(t, h) + bs(t, h) \quad (5.4)$$

The total glacier mass balance —  $MB(t, h)$  — for each HRU in a given year was calculated per Equation 5.5:

$$MB(t, h) = \sum (A(h).bn(t, h)) \quad (5.5)$$

where  $A(h)$  is the area of each glacier HRU.

### 5.3.4 Estimating model parameters

Model parameters are the coefficients assigned in module equations to compute model outputs. They were estimated from studies of the Wolf Creek basin (Pomeroy et al. 2010; Rasouli et al. 2014), field observations, default values commonly used in hydrology that are available in CRHM (i.e., hydraulic conductivity of different soil types) and literature review. Parameters that strongly effect flow variability and snowmelt/ice melt are listed in Table 5.7.

**Table 5.7** Calibrated and non-calibrated CRHM parameters used in this study that strongly influence flow variability and snowmelt/ice melt.

Model parameter	Description	Unit	Range of values	C or NC
a1	Albedo decay time constant for cold snow	s	1.08E7	NC
a2	Albedo decay time constant for melting snow	s	7.2E5	NC
Albedo_Bare	Initial albedo for bare ground	NA	0.05 – 0.2	NC
Albedo_Snow	Initial albedo for snow cover	NA	0.8	NC
amax	Maximum albedo for fresh snow	NA	0.84	NC
amin	Minimum albedo for aged snow	NA	0.5	NC
A_S	Stalk diameter	m	0.003-0.8	NC
distrib	Distribution fraction	NA	1-10	NC
fetch	Fetch distance	m	300-1000	NC
F_Qg	Fraction to ground flux	NA	0.05	NC
gwKstorage	groundwater storage constant	d	0-100	C
gwLag	groundwater lag delay	h	0-500	C
gw_K	Daily ground water drainage from groundwater reservoir	mm/d	0-50	C
Ht	Vegetation height	m	0.001-0.7	NC
iceLag	Ice melt lag delay	h	0-200	C
icestorage	Ice melt storage constant	d	0-100	C
ice_Albedo	Initial glacier ice albedo	NA	0.2	NC
ice_to_infil_K	Daily ratio of ice melt to infiltration	NA	0-1	C
krs	Location index (interior or coastal)	NA	0.16-0.19	NC
Kstorage	Aggregated storage constant	d	0-80	C
Lag	Aggregated lag delay	h	0-50	C
lapse_rate	Temperature lapse rate	°C/100m	0.65	NC
lower_ssr_K	Daily subsurface drainage from soil column	mm/d	0–100	C
N_S	Vegetation number density	1/m <sup>2</sup>	1–10	NC
rain_to_infil_K	Daily fraction of rainfall to infiltration	NA	0-1	C

**Table 5.7** (continued)

rechr_ssr_K	Daily subsurface drainage from recharge	mm/d	0-50	C
rs	Stomatal resistance	d/m	0	NC
runKstorage	Runoff storage constant	d	0-80	C
runLag	Runoff lag delay	h	0-150	C
smin	Minimum snowfall to refresh snow albedo	mm/h	10	NC
soil_withdrawal	Water withdrawal function for soil type (sand/loam/clay/organic)	NA	1-2	NC
ssrKstorage	Subsurface runoff storage constant	d	0-100	C
ssrLag	Subsurface runoff lag delay	h	0-200	C
SWEAA	Annual mean accumulation of glacier SWE	mm/yr	0.3	NC
SWElag	Snowmelt lag delay	h	0-100	C
SWEstorage	Snowmelt storage constant	d	0-200	C
SWE_to_infil_K	Daily fraction of snow melt to infiltration	NA	0-1	C
TKMA	Annual mean temperature of glacier	°C	-20	NC
Zwind	Wind measurement height	m	2	NC

Note: C = calibrated ; NC = non-calibrated

Parameters that were not measured by any previous studies were calibrated. These included routing and lag parameters for soil, river and glaciers, and river channels and glaciers between subbasins and HRUs, as well as surface depressional storage parameters and subsurface drainage factors. Due to limited information about subsurface flow over thawing frozen soils, subsurface drainage factors were calibrated from observed streamflow. These calibrated parameters were optimized using the dynamically dimensioned search (DDS) approach (Tolson and Shoemaker 2007) available in the OSTRICH software toolkit (Matott 2007). The DDS approach finds optimum solutions from a set number of model evaluation runs:

- DDS performs a global search of the parameter set;
  - the approach seeks optimum local solutions as a function of iteration number and the user-specified maximum number of function evaluations; and
  - DDS optimizes the parameters within the set of possible model parameter ranges.
- The transition from global to local search is performed dynamically by reducing the size of the dimensions of the tuning model parameters.

## 5.4 Model evaluation and results

### 5.4.1 Model evaluation

This section evaluates CRHM, particularly modeled flow, SWE variation, glacier mass balance and glacier discharge in comparison to observation data, satellite imagery, DETIM, and results from previous studies (such as unpublished data from the Juneau Icefield Research Program).

CRHM was used to simulate hydrology from May 1, 2006 to December 31, 2013. The period between May 1 and December 31, 2006 was used to warm up the model; model evaluation was performed using data that extended from January 1, 2007 to December 31, 2013. Three calibration-validation

schemes were performed to evaluate the sensitivity of the calibrated parameters on modeled flow performances::

- the model was run for 2006–10 for calibration and 2010–13 for validation;
- the model was run for 2010–13 for calibration and 2006–10 for validation; and
- the entire 2006–13 data period was used to obtain the optimized model parameters.

The calibration-validation schemes were evaluated on the basis of the Nash-Sutcliffe Efficiency, or NSE (Equation 5.6; Nash and Sutcliffe 1970):

$$NSE = 1 - \left( \frac{\sum_{t=1}^N (Q_{obs} - Q_{sim})^2}{\sum_{t=1}^N (Q_{obs} - \overline{Q_{obs}})^2} \right) \quad (5.6)$$

They were also evaluated on the basis of root-mean-square error, or RMSE (Equation 5.7; Hyndman and Koehler 2006):

$$RMSE = \sqrt{\frac{1}{N} \left( \sum_{t=1}^N (Q_{obs} - Q_{sim})^2 \right)} \quad (5.7)$$

In equations 5.6 and 5.7  $Q_{obs}$  and  $Q_{sim}$  are the observed and simulated values of either flows or SWEs, respectively, and  $\overline{Q_{obs}}$  is the average of  $Q_{obs}$  values over  $N$  number of data points of the study period.

No major differences were observed between the NSE and RMSE values associated with the three calibration-validation schemes (Table 5.8); thus, there were no significant differences in flow model performance among the three schemes. For this reason, and since the third option provided the longest time period, the results of the third option were used for the analysis discussed in Section 5.4.

Non-glacierized areas within a subbasin were evaluated based on NSE and RMSE: the modeled flow performances were evaluated using NSE and RMSE criteria and the modeled SWE performances were evaluated using RMSE criteria. Glacierized areas within a subbasin were evaluated through rates of snowmelt/ice melt and surface elevation changes and by comparing glacier mass balance based on satellite imagery and the Distributed Temperature Index Model, or DETIM (Hock and Tilm-Reijmer 2013). The main reason to compare DETIM, CRHM and satellite imagery was to observe the relative location of a glacier's Equilibrium Line Altitude (ELA).

DETIM was applied to estimate summer and winter glacier mass balance and thus to observe the relative location of ELA. DETIM was formulated based on the premise of a high correlation between air temperature and melt (Hock 2003; Hock and Tilm-Reijmer 2013). The simplest variant of DETIM was used in this study; it is the degree-day approach, which requires minimal input data. Other variants that require additional data, such as clear-sky direct radiation and global radiation, were not available for the entire study period (2006–13), which means that further data processing would be required for the other variants of DETIM to be applied. Even though the degree-day approach is simple, it can effectively capture glacier mass balance through correlating air temperature and melt (Hock 2003).

**Table 5.8** Nash-Sutcliffe Efficiency (NSE) and root-mean-square error (RMSE) values for the three calibration-validation schemes and four hydrometric stations.

Calibration-validation scheme	Subbasin		NSE		RMSE (m <sup>3</sup> /s)	
	No.	Name	Cal	Val	Cal	Val
2006–10 used for calibration and 2010–13 used for validation	SCB11	Wheaton River	0.82	0.73	4.6	5.5
	SCB15	Tutshi River	0.94	0.78	4.0	8.6
	SCB6	Atlin River	0.91	0.84	24.5	32.8
	SCB19	Yukon River at Whitehorse	0.90	0.77	44.7	69.5
2010–13 used for calibration and 2006–10 used for validation	SCB11	Wheaton River	0.61	0.80	6.7	4.7
	SCB15	Tutshi River	0.83	0.88	7.0	6.4
	SCB6	Atlin River	0.91	0.86	24.0	30.6
	SCB19	Yukon River at Whitehorse	0.87	0.80	50.1	64.6
2006–13 used for calibration (no validation scheme was performed)	SCB11	Wheaton River	0.74	N/A	5.4	N/A
	SCB15	Tutshi River	0.88		6.2	
	SCB6	Atlin River	0.90		26.0	
	SCB19	Yukon River at Whitehorse	0.87		51.9	

The most important formulation to calculate the simple degree-day approach used in DETIM is computing the daily melt ( $M$ ) of ice and snow, which is a function of positive degree-day factors (DDFs) of ice and snow, as described in Equation 5.8:

$$M = \frac{DDF_s}{DDF_i} T_d \quad (5.8)$$

where  $T_d$  is daily mean air temperature (expressed in degrees above 0°C; temperatures below 0°C are assigned values of 0, and  $DDF_s$  and  $DDF_i$  are DDFs of snow and ice, respectively).

In this study, the DDF of snow was estimated from ablation wire observations and determined using those days during the observation period when the mean daily temperature was above 0°C (temperatures were measured at the Upper Llewellyn meteorological station). The estimated DDF snow parameter, estimated from the ablation wires installed in the accumulation zone (i.e., ablation wire 1; see Table 5.9), was approximately 3.5 mm water equivalent (w.e.)/°C/day. Unfortunately, not enough observation data was available, particularly at the lower elevations, to estimate the DDF of ice. The DDF ice parameter was taken from Braithwaite (1995), which lists the DDFs for various glaciers, including those in arctic Canada; it was 5.5 mm w.e./°C/day). This value is similar to the average DDF of ice estimated from the ablation wires in the ablation zone (ablation wires 3, 4 and 5; Table 5.9) for July 31–August 10 (all snow was assumed to have melted during this period).

Other data required to run the DETIM were lapse rate, DEM, aspects, slope and initial snow cover. The lapse rate value used in the simulation was 6.5°C/km, based on data obtained from the Upper and Lower Llewellyn meteorological stations. Since the simulation started in August the initial snow cover was assumed to be zero for the entire study area. The same DEM, aspect and slope angle data used to simulate CRHM were applied to DETIM.

### 5.4.2 Flow variation

A comparison of modeled versus observed flows from the four hydrometric stations indicates that CRHM was able to accurately capture observed flows in the four gauged locations, including seasonal variations of higher summer flows and lower winter flows (Figure 5.11a–d). Slightly less accurate model performance during 2012–13 can be attributed to the installation of new meteorological stations, along with the closure of some existing stations that had provided robust long-term data.

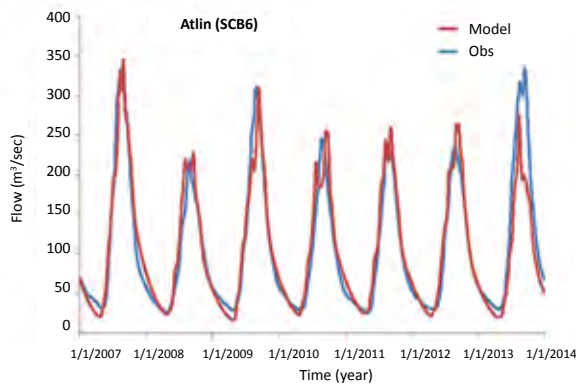


**Figure 5.11a** Atlin River (SCB6): modeled versus observed flow, 2007–13.

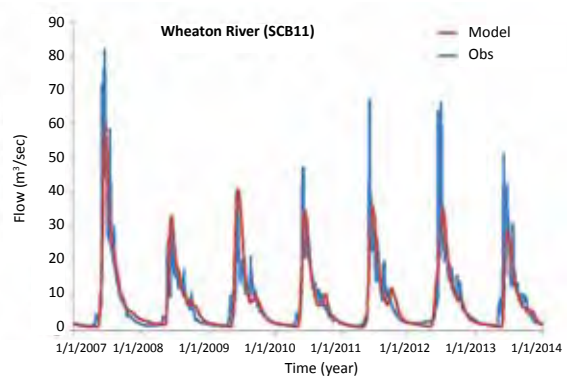


**Figure 5.11b** Wheaton River (SCB11): modeled versus observed flow, 2007–13.

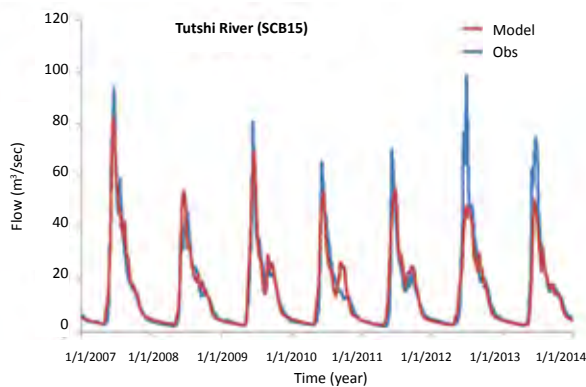


**Figure 5.11c** Tutshi River (SCB15): modeled versus observed flow, 2007–13.

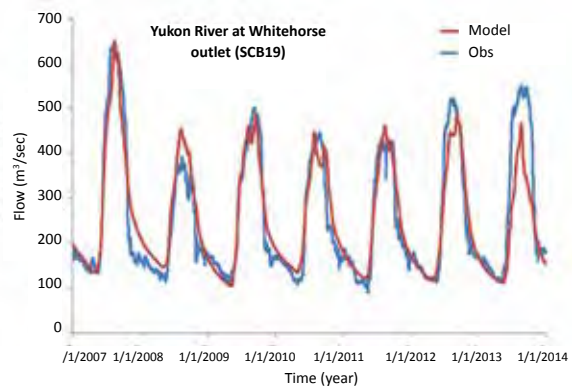


**Figure 5.11d** Yukon River at Whitehorse outlet (SCB19): modeled versus observed flow, 2007–13.

Climate variability related to topography and land cover among the subbasin locations was found to strongly influence flow. Faster flow-recession curves were produced in the western subbasins, Wheaton (SCB11) and Tutshi (SCB15), than in the other gauged subbasins; e.g., Atlin River (SCB6) and Yukon River at Whitehorse (SCB19); see Figure 5.11a–d. This can be attributed to higher elevation, steeper slopes (Figure 5.12), a smaller number of water/lake areas, and generally higher precipitation (Figure 5.13) and SWE, which are a result of shorter vegetation land cover (see Section 5.4.3).

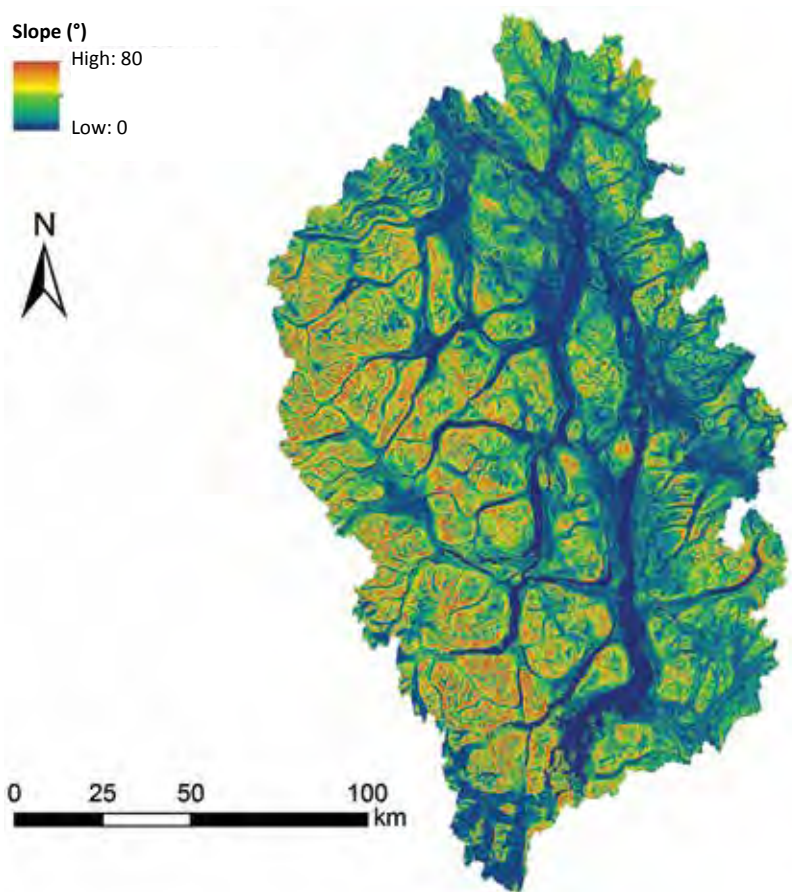


**Figure 5.12** Slope (in degrees) for the upper Yukon River basin.

Flow outputs were estimated by CRHM for each subbasin, and were further analyzed to compare subbasin runoff and therefore compare the amount of water discharging from each subbasin. Runoff was calculated by dividing the estimated flow for each subbasin by the subbasin area. Similar to flow, subbasin runoff was influenced by climate, topography and land cover.

Runoff varies spatially and seasonally (Figure 5.14). Western regions generally contribute larger runoff than other regions, particularly during summer (Figures 5.14a–d). Western regions are dominated by glacierized areas and higher elevations (Figure 5.5) and steeper slopes (Figure 5.12), in combination with higher precipitation (Figure 5.13) causing greater snowmelt/ice melt and thus summer runoff. For example, runoff from the Llewellyn (SPM1) and Willison (SPM2) glaciers to the SPM1 and SPM2 outlets was approximately four times higher in the summer than the spring (Figure 5.14a–b). This indicates the strong influence of snowmelt/ice melt from the Llewellyn and Willison glaciers on basin runoff during the summer.

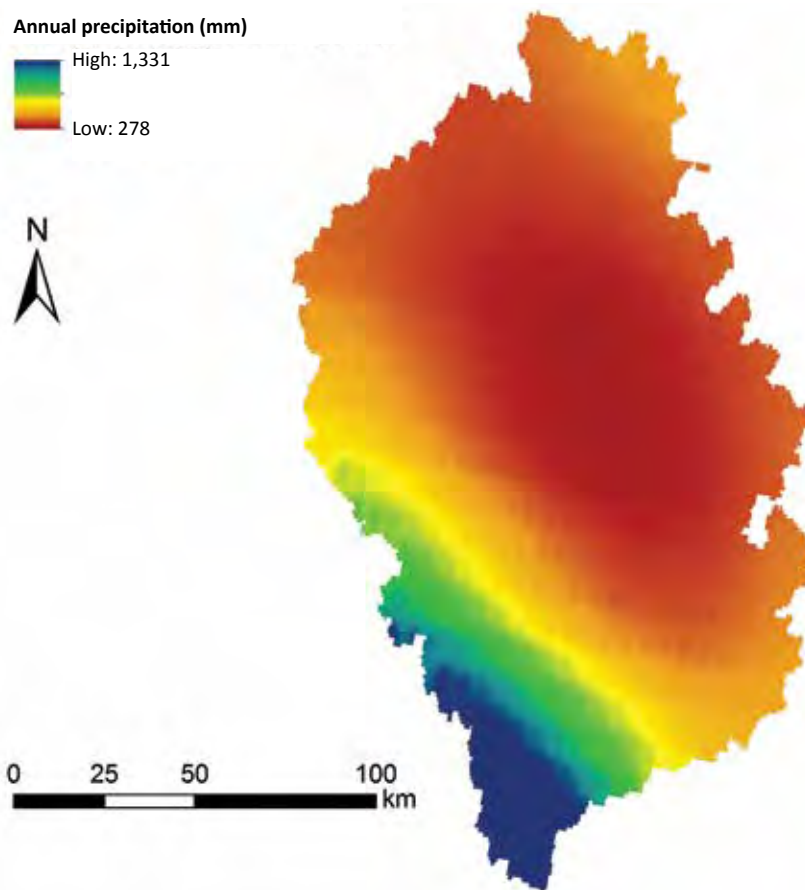


**Figure 5.13** Corrected annual precipitation (mm) for the upper Yukon River basin, 2006–13.

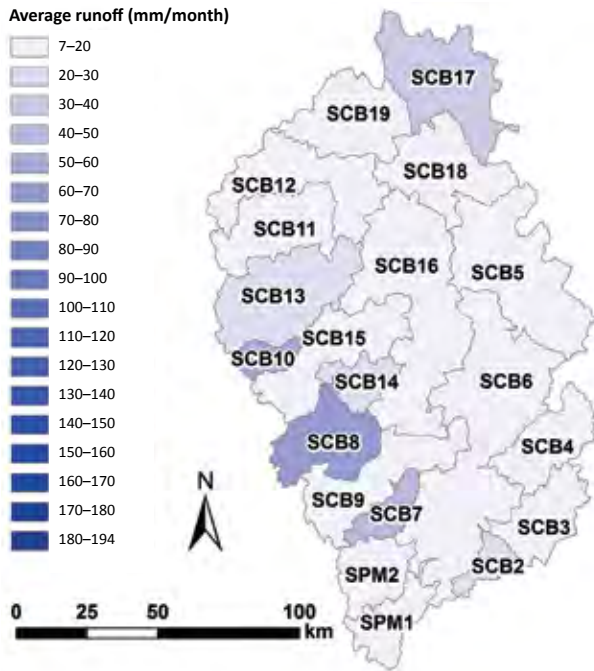


**Figure 5.14a** Spatial distribution of average runoff (mm/month) for March, April and May for the upper Yukon River basin, averaged over 2007–13.

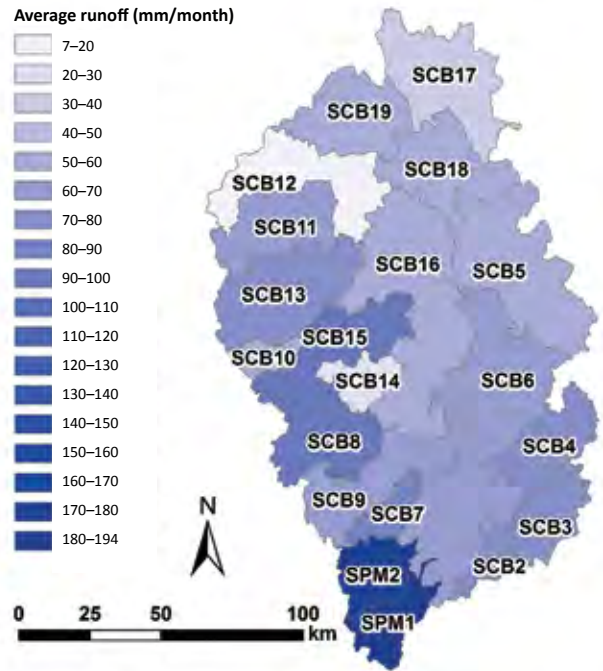


**Figure 5.14b** Spatial distribution of average runoff (mm/month) for June, July and August for the upper Yukon River basin, averaged over 2007–13.

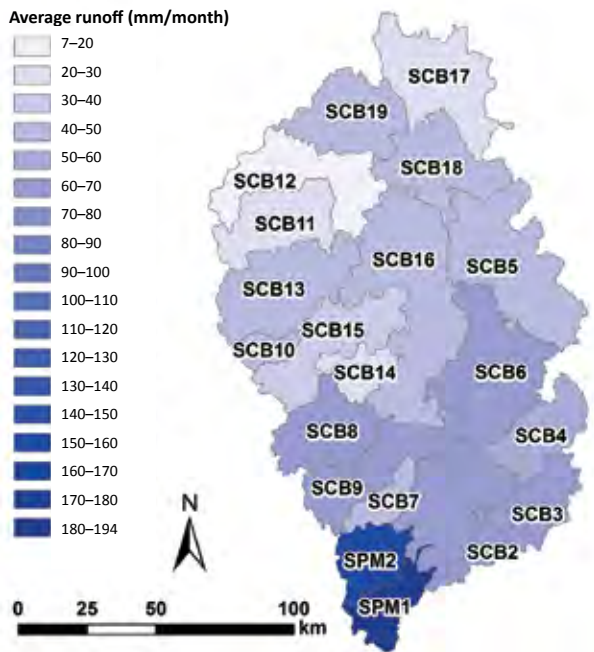


**Figure 5.14c** Spatial distribution of average monthly values of all seasons (mm/month) for the upper Yukon River basin, averaged over 2007–13.

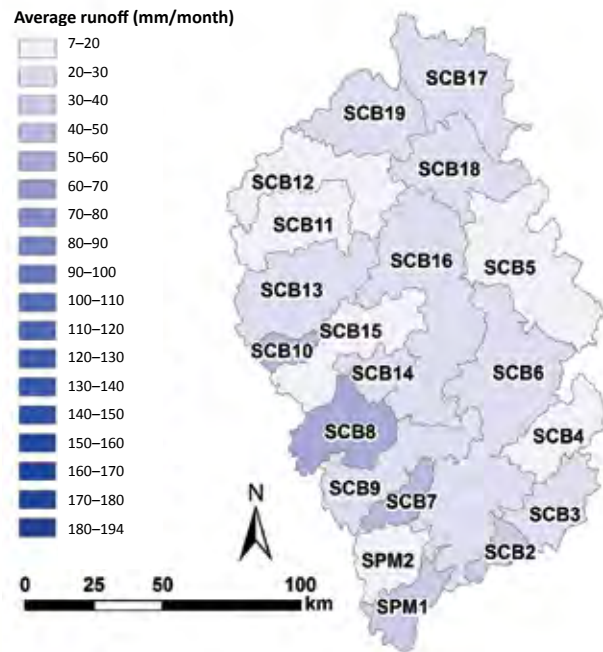


**Figure 5.14d** Spatial distribution of average monthly values for December, January and February (mm/month) for the upper Yukon River basin, averaged over 2007–13.

Note: For Figure 5.14a, b, c and d, runoff was calculated by dividing the flow at each subbasin by the subbasin area.

### 5.4.3 SWE variation

The SWE variations of CRHM model outputs were validated with snow surveys for the 2007–13 period. RMSE values across the five SWE survey locations (Figure 5.3b) ranged from 39 to 102 mm, which means that the model captured peak SWE values at the five locations relatively accurately (Figure 5.15a–e). Since land-cover characteristics (i.e., shrubland) were similar among the surveyed SWE locations, broad climatic setting (related to latitude and proximity to the Pacific Ocean) and local microclimatic influences (such as aspect, slope, topography and prevailing wind direction) are believed to control snow processes at these locations.

Peak SWE values generally occurred at the beginning/middle of April. Higher peak SWE values were found at Log Cabin, the most westerly survey location (Table 5.3). In general, snow began to accumulate in late September at the Log Cabin location and didn't melt until mid-June. In contrast, snow accumulation at the other four locations began at the beginning of October and melted by the end of May. Higher SWE values and a longer period of snow accumulation in the western portion of the subbasin are attributed to higher precipitation (Figure 5.13) and colder temperatures due to higher elevations (Figure 5.5).

Modeled SWE variability across the entire basin was strongly influenced by land cover. Throughout the basin, the exposed land and short vegetation of the western regions (dominated by exposed land, ice and grassland cover) experienced higher average annual SWE than the relatively tall vegetation of the central/eastern regions, which are dominated by shrubland and coniferous forest (Figure 5.16a–d). Similarly, areas within each subbasin that are covered by shorter vegetation generally produced higher SWE values than those covered by taller vegetation.

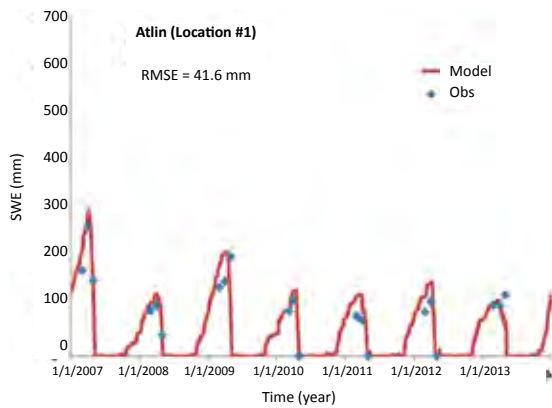


**Figure 5.15a** Atlin: Modeled versus observed SWE, 2007–13.

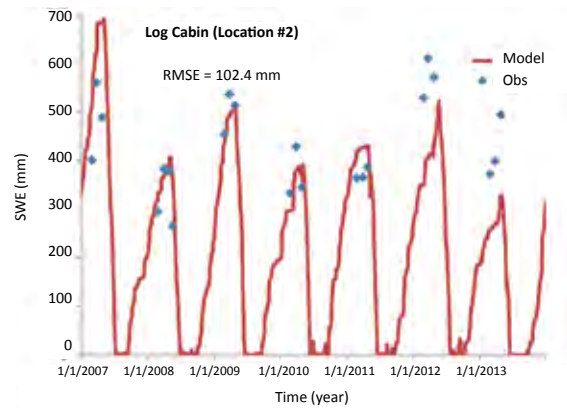


**Figure 5.15b** Log Cabin: modeled versus observed SWE, 2007–13.

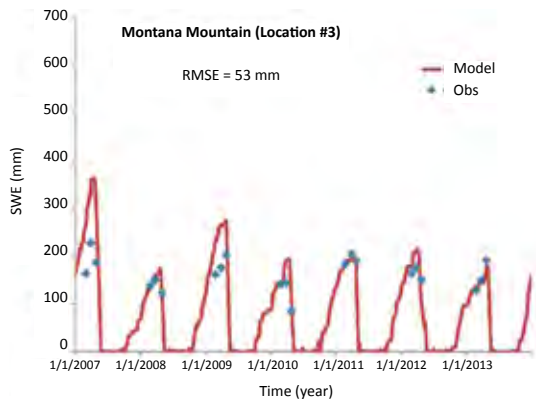


**Figure 5.15c** Montana Mountain: modeled versus observed SWE, 2007–13.

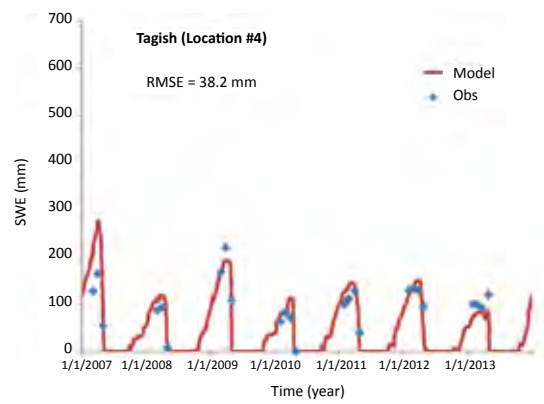


**Figure 5.15d** Tagish: modeled versus observed SWE, 2007–13.

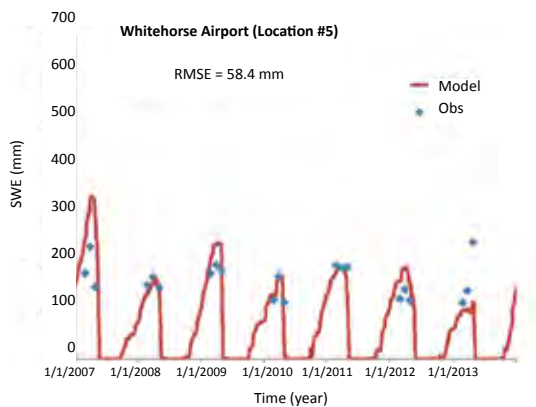


**Figure 5.15e** Whitehorse Airport: modeled versus observed SWE, 2007–13.

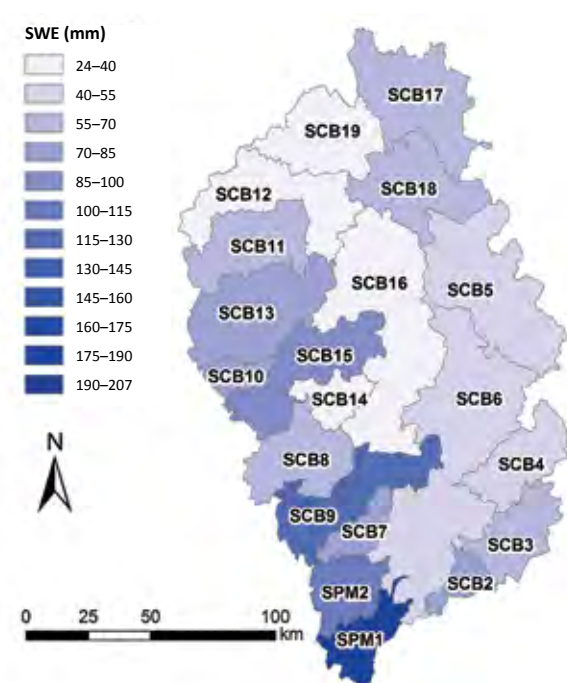


**Figure 5.16a** SWE variability (mm) in each subbasin for coniferous forest, averaged over 2007–13.

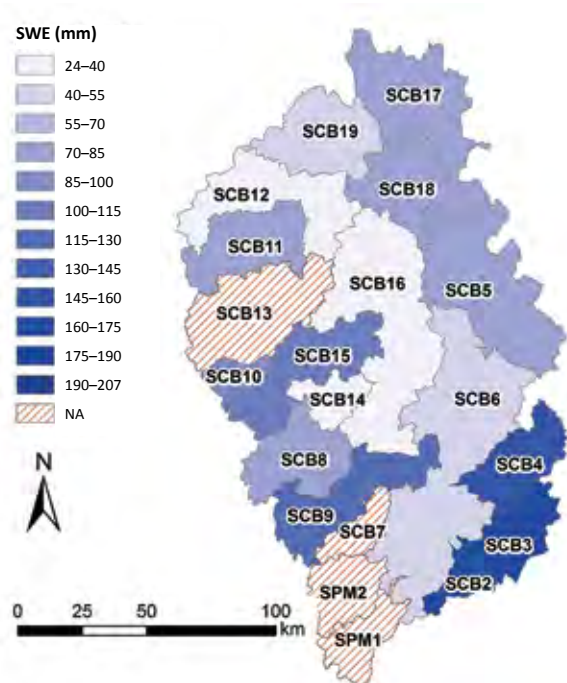


**Figure 5.16b** SWE variability (mm) in each subbasin for shrubland, averaged over 2007–13.

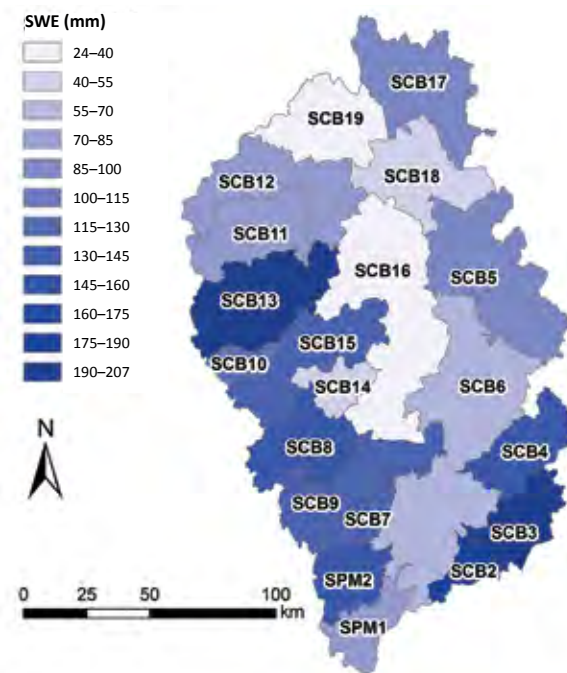


**Figure 5.16c** SWE variability (mm) in each subbasin for exposed land, averaged over 2007–13.

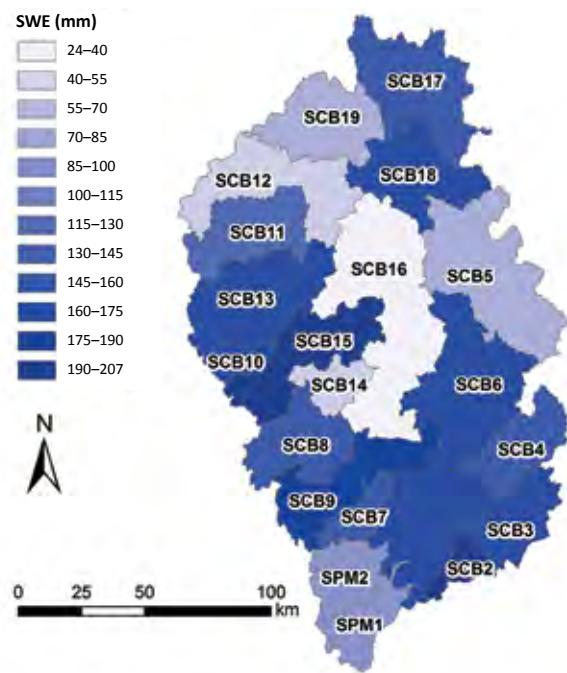


**Figure 5.16d** SWE variability (mm) in each subbasin for grassland, averaged over 2007–13.

#### 5.4.4 Glacier mass balance

In analyzing glacier mass balance, the study focused on the Llewellyn and Willison glaciers, the two largest glaciers in the study basin. The glaciers were divided into nine elevation bands (Figure 5.8) to better characterize elevational gradients in accumulation and ablation and to allow determination of the the equilibrium line altitude (ELA) that separates them. Glacier mass balance was evaluated by comparing the ELA line determined from satellite imagery to the ELA determined from CRHM and DETIM. Similar glacier mass balance results were produced by CRHM and DETIM (Figure 5.17a–c).

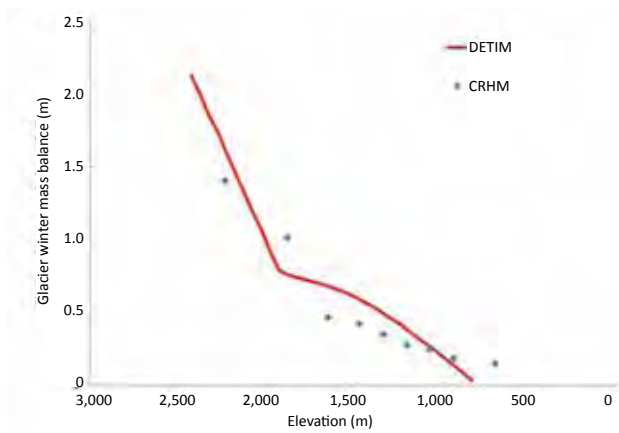


**Figure 5.17a** Comparison of winter glacier mass balance: DETIM and CRHM, Llewellyn Glacier, averaged over 2007–13.

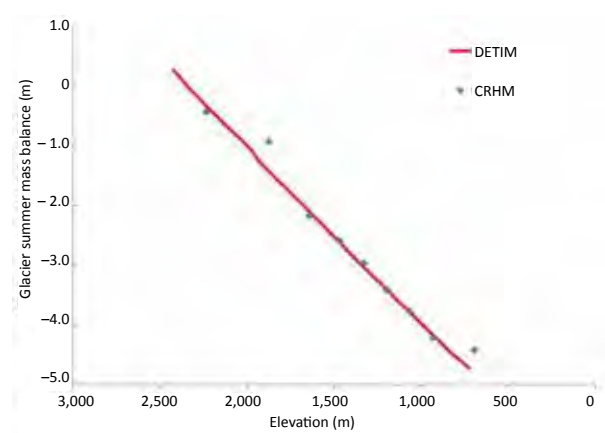


**Figure 5.17b** Comparison of summer glacier mass balance: DETIM and CRHM, Llewellyn Glacier, averaged over 2007–13.

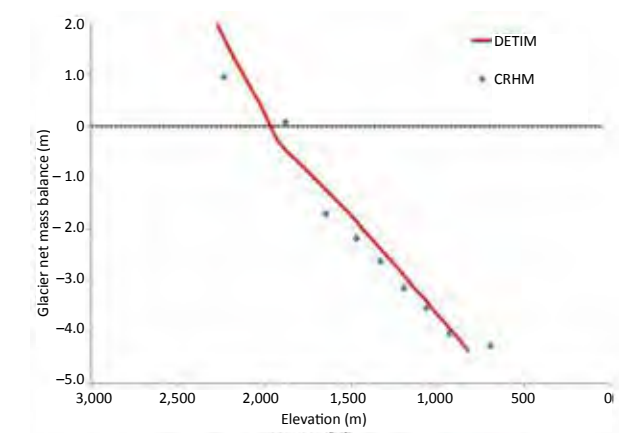


**Figure 5.17c** Comparison of net glacier mass balance: DETIM and CRHM, Llewellyn Glacier, averaged over 2007–13.

Evaluation of the two models indicated that the two highest elevation bands (1,750–2,000 m and 2,000–2,466 m) were in the glacier accumulation zone; i.e., they gained more mass in winter than they lost in summer (Figure 5.17). In contrast, the elevation bands lower than 1,750 m were within the glacier ablation zone; thus, they lost more mass in summer than they gained in winter. This means that the model's ELA is estimated to be approximately 1,750 m. A similar ELA, in the range of 1,600–1,700 m, was determined from satellite imagery. The satellite imagery ELA was discerned by inspecting colour at known elevation contours: the transition between light and dark blue indicated the ELA (Figure 5.18).

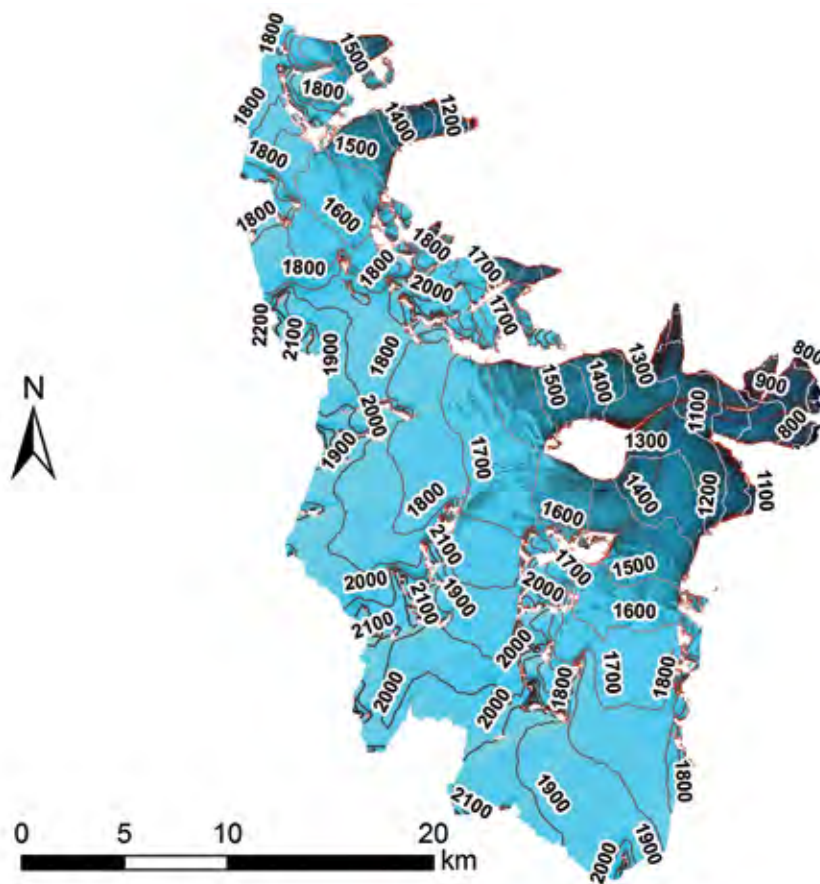


**Figure 5.18** Landsat satellite imagery of the Llewellyn and Willison glaciers, June 27, 2006.

Note: Numbers on map indicate elevation contours.

Visual inspection of satellite imagery and comparison of CRHM and DETIM outputs produced similar ELAs, which suggests that, to first-order, CRHM captured glacier mass balance relatively well. The similar patterns of seasonal glacier mass balances (Figure 5.19a–c) validated the selection of model structure and model parameters used, particularly for the Llewellyn Glacier.

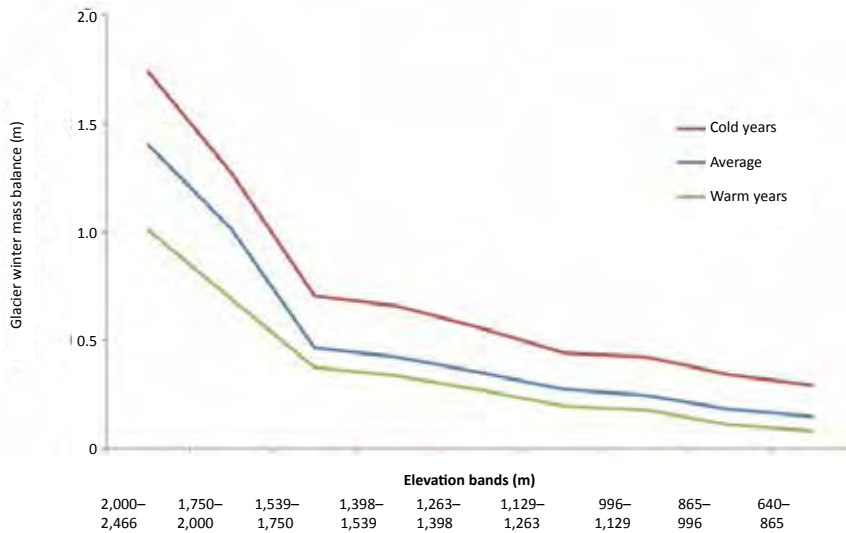


**Figure 5.19a** Comparison of winter glacier mass balance for cold, average and warm years for nine elevation bands, Llewellyn Glacier, averaged over 2007–13.

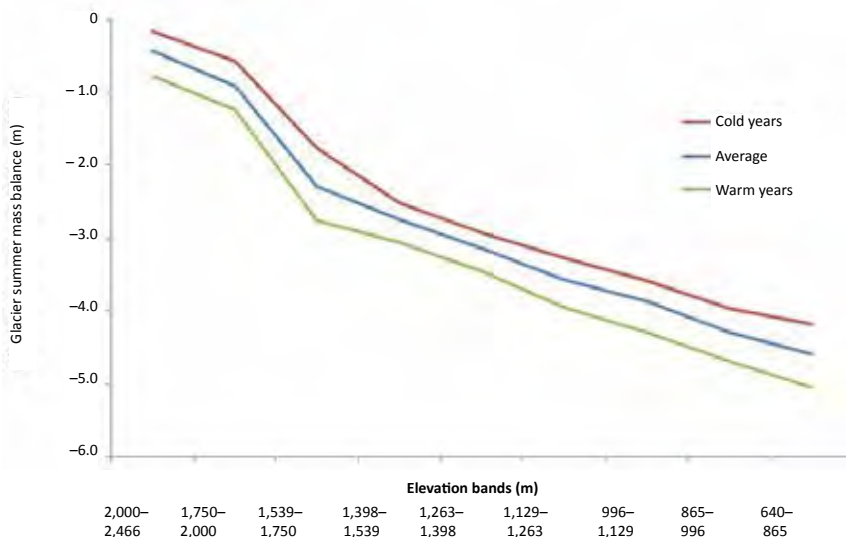


**Figure 5.19b** Comparison of summer glacier mass balance for cold, average and warm years for nine elevation bands, Llewellyn Glacier, averaged over 2007–13.

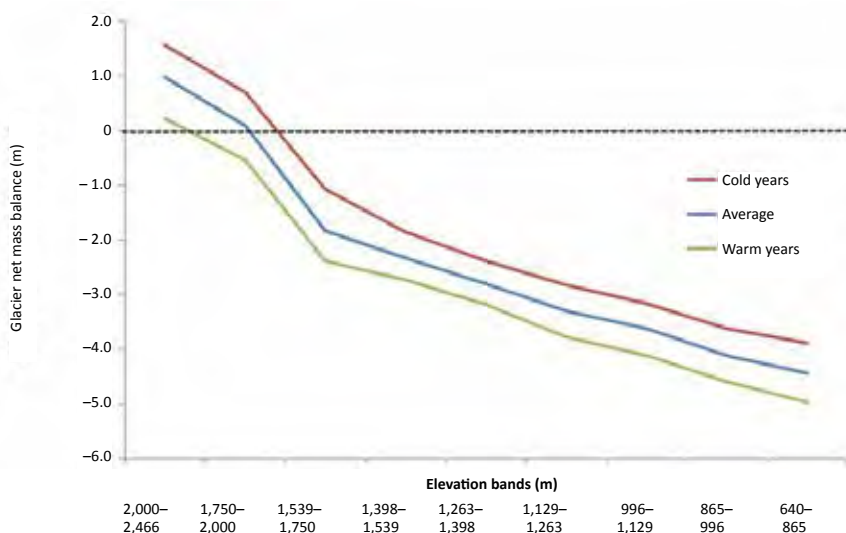


**Figure 5.19c** Comparison of net glacier mass balance for cold, average and warm years for nine elevation bands, Llewellyn Glacier, averaged over 2007–13.

The satellite imagery data were not further analyzed (i.e., only visual inspection was performed) due to limited time, personnel, budget and software availability. There are three potential reasons for the slight discrepancy between the model ELA and the ELA determined from satellite imagery:

- the satellite image may have been obtained prior to the end of summer melt;
- end-of-melt snowline may vary year to year; and
- the vertical resolution of the elevational bands used in the CRHM structure are relatively coarse (i.e., CRHM segregates areas at similar elevations within a given subbasin into the same HRU group, even if they are separated by significant topographical features).

Glacier ELA varied for the simulated hydrology period (2007–13), depending on the average annual temperature (i.e., colder or warmer than average temperature; Figure 5.19). As expected, glacier net mass balance decreased in warmer years. During the warmer years only the highest elevation band (2,000–2,466 m) was in the accumulation zone, and the ELA increased to 2,000 m. During the colder years the ELA did not change from that in average temperature years (1,750 m), but overall glacier net mass balance increased. Since winter glacier mass balances were more variable at higher elevations between the coldest and warmest modeled years (Figure 5.19), peak SWE values vary more in accumulation zones than in ablation zones. In contrast, summer mass balances were most variable at lower elevations between the coldest and warmest modeled years; thus, variability in summer melt is due to snowpack and snow melt processes, rather than by winter SWE.

Surface elevation loss was captured reasonably well by CRHM, with a modeled loss of 13 m (modeled from 2007–13) and an observed loss of 11.5 m (measured from 2001–13; unpublished data, Juneau Icefield Research Program). Additional information regarding the validity of CRHM's glacier mass balance values can be gained from the ablation wire measurements performed on the Llewellyn Glacier.

The modeled snowmelt/ice melt rates slightly underestimated the rates determined by the ablation wire observations (Table 5.9). However, both the modeled and observed rates demonstrated a trend of increasing snowmelt/ice melt from higher to lower elevation bands within the ablation zone (only the ablation zone was considered since snowmelt/ice melt does not occur in the accumulation zone).

The discrepancies can be attributed to two factors:

- the model estimates melt over a large distributed area within a specified HRU and elevation band, while the melt from the ablation wire surveys is estimated only at the site of the wires; and
- the field observations were collected only for 2014, whereas the snowmelt/ice melt for the model was averaged over the model simulation period of 2007–13.

**Table 5.9** Comparison of the rate of summer snowmelt/ice melt by elevation for ablation wire surveys and modeled outputs.

No.	Ablation wire observation						Modeled output		
	Location	Point elevation	Rate of snowmelt/ice melt (cm/day)		Positive DDFs (mm/°C/day)*		Elevation band	Average rate of snowmelt/ice melt (cm/day)	
			Apr 28–Jul 31, 2014	Jul 31–Aug 10, 2014	Snow	Ice		Apr 28–Jul 31, 2007–13	Jul 31–Aug 10, 2007–13
1	58.8935 °N, 134.1132 °W	1,820 m	1.78	—	3.5	—	1,750–2,000 m	0.75	—
2	58.9373 °N, 134.0848 °W	1,693 m	2.04	—	—	—	1,539–1,750 m	1.84	—
3	58.9686 °N, 134.0782 °W	1,614 m	2.76	3.40	—	5.7	1,539–1,750 m	1.84	2.54
4	59.0343 °N, 134.1028 °W	1,349 m	2.63	4.00	—	6.7	1,263–1,398 m	2.38	2.59
5	59.0727 °N, 134.0989 °W	1,200 m	4.11	2.20	—	3.7	1,129–1,263 m	2.62	2.62

Notes: \* estimated values used for DETIM model parameters; DDFs = Degree Day Factors

Elevation influenced the timing of ice melt. In the lowest elevation band of the ablation zone, ice melt started earlier — at the middle of April. In the highest elevation band of the ablation zone, ice melt began later — at the end of June (see Table 5.10). In the ablation zone, the amount of ice melt was between two and three times greater than the amount of snowmelt (Table 5.10), indicating a larger contribution of ice melt than snowmelt to glacial discharge.

**Table 5.10** Modeled timing of the start of ice melt and ratio of ice melt to snowmelt peak, ablation zone of the Llewellyn and Willison glaciers, averaged for 2006–13.

Elevation band (masl)	Date of start of ice melt	Average ratio of ice melt peak to snowmelt peak
1,539–1,750	June 22	1.89
1,398–1,539	June 6	1.92
1,263–1,398	May 26	2.07
1,129–1,263	May 11	2.20
996–1,129	May 4	2.35
865–996	April 23	2.86
640–865	April 11	3.12

## 5.5 Understanding and interpreting model uncertainties

Every modeling approach is subject to uncertainties. CRHM is a physically-based distributed hydrological model that quantitatively describes hydrology using mass and energy balance equations and physical parameters. By using the principles of physics and thermodynamics, the model is grounded in well understood and well accepted scientific theory. However, the complexity of natural systems and our ability to measure and understand them present challenges to even the best physically-based model. The quality of modeled outputs is determined by many factors, including the quality of input data, parameters and mathematical description of physical processes (i.e., equations).

Input data can include a variety of measured hydrometeorological data. For this model, inputs included land-cover, elevation, soil and meteorological data. Some of these data (e.g., on surface elevation) are fairly well constrained; other data are not as well constrained due to the large area of the basin, high spatial and temporal variability, and limited amount of foundational work that has been done in the region. For example, the soil data for the basin are available only in coarse resolution, and there are few locations where high-quality meteorological data have been monitored over the long term. Other inputs are highly variable in both space and time, such as land cover, which is highly spatially variable and is slowly evolving as forests age and as higher elevations become more suitable for shrub and tree growth.

For this project, almost a year was spent collecting, reviewing and quality checking the various data sources, but it is important to recognize that the measured data necessarily include a degree of error and represent conditions local to the point of measurement. This was an important motivation for the installation of new monitoring stations, but these only begin to address the sparsity of the meteorological network in the region. The true value of stations such as those installed during the project will increase the longer they are left in place, because longer time series help improve certainty about the expected conditions in a location.

For a spatially distributed model such as CRHM, data measured at specific points in the basin must be interpolated to cover the whole area. Interpolation can be done using well understood thermodynamic rules (such as calculating environmental lapse rates for air temperature), or statistical methods such as inverse distance weighting. Regardless of the interpolation approach used, values for areas between data points are always an estimate. Micro-scale variation can be “missed” by the interpolation scheme even if there is a dense observational network. This potential to miss spatial variability through interpolation is even greater where there are few points with direct measurement of conditions. An excellent example is the spatial variability of precipitation: it is not uncommon for a storm to hit one part of Whitehorse, but completely miss another part.

In this implementation of the CRHM, there are also a number of cases where mathematical descriptions are used to describe physical processes that are very difficult to measure – particularly for an area the size of the upper Yukon River basin. For example, evapotranspiration is very hard to quantify. There are no evapotranspiration data for the study area that would be suitable for use in the model, so they need to be estimated one of several available empirical relationships. The best relationship to use in a particular location can be selected by considering the climatological region and the input data available, but there is no one method that will universally provide the best

results. The project used the Granger method (Granger and Gray 1989) because the data were available to support it. This method is supported by past research work in Wolf Creek basin (Rasouli et al. 2014).

For these reasons, some degree of misfit between the hydrological model and the actual hydrological system is unavoidable. Overtuning the model (e.g., by choosing parameter values that provide a nominally better fit but diverge from reasonable values) can result in apparent improvements in model performance, but at the cost of lower reliability when conditions and/or forcings differ from those used during the calibration and validation phases. All methods and input data for this study have been carefully chosen and evaluated to provide modeled outputs. Based on the metrics used to evaluate model fit, this implementation of CRHM for the upper Yukon River basin appears to accurately recreate observed streamflow, glacier mass balance, and SWE. In fact, the implementation of CRHM in the 19,600-km<sup>2</sup> upper Yukon River basin performs as well as that in studies of the much smaller Wolf Creek (179-km<sup>2</sup>) and Binggou (30.3-km<sup>2</sup>) basins by Rasouli et al. (2014) and Zhou et al. (2014), respectively.

## 5.6 Conclusions

This section discusses the simulation of glacial-hydrology processes in the upper Yukon River basin using CHRM. The main aims were to 1) improve understanding of river flow, snow variation and glacier mass balance in the basin; and 2) validate CRHM for future simulations (discussed in Section 6). The model was able to simulate SWE — as determined by snow surveys, flow observation, glacier mass balance and ablation-wire surveys — with relatively high accuracy. The fit between model and observed flows (determined using NSE) at the Whitehorse outlet is 0.88. It indicates that 88% of the observed flow variability can be captured by the model. In other subbasin outlets within the basin, NSEs vary from 0.74 to 0.90. As a comparison, Zhou et al. (2014), using CRHM, found NSE values as high as 0.76 and 0.55 in the mountainous Bingou and Zuomaokong basins (both in China), respectively.

Analysis found that snowpack SWE, river flow and glacier mass balance were strongly affected by a complex combination of climatological, topographic and land-cover characteristics in the basin. Some key findings are as follows:

- the western portions of the basin are characterized by higher elevations and greater precipitation and SWE values, with land cover dominated by short vegetation and exposed land. In contrast, the central and eastern portions are generally lower in elevation, with lower precipitation and SWE values, and with land cover dominated by tall vegetation;
- climate varies spatially and seasonally and strongly modulates the magnitude and timing of snow accumulation, snowmelt and ice melt, depending on land cover and topography; and
- climate and topography strongly influence the proportion of melt from snow and melt from ice and the magnitude and timing of ice melt, as shown particularly for the Llewellyn and Willison glaciers.

Western regions generally contribute larger runoff than other regions, particularly during summer. Runoff from the Llewellyn (SPM1) and Willison (SPM2) glaciers to the SPM1 and SPM2 outlets was approximately four times higher in the summer than the spring. On the Llewellyn and Willison glaciers, the ELA (Equilibrium Line Altitude) was determined to be 1,750 m. Below this elevation, ice melt dominated; the onset and magnitude of melt varied with elevation.

## 6. Climate scenario analysis

Evidence shows that climate has a strong impact on hydrological conditions in arctic and subarctic regions. Warming temperatures have a powerful effect on the timing of snow melting and thawing, changing the extent and duration of snow cover, causing glaciers to thin and retreat, and modifying seasonal river flow (NCE 2014; Berthier et al. 2010; Brabets and Walvoord 2009; Déry et al. 2009; Moore et al. 2009; Prowse and Furgal 2009; Fleming and Clarke 2003; Serreze et al. 2000; Whitfield and Cannon 2000, Prowse et al. 2006; Porparto and Ridolfi 1998). This impact is expected to occur at a greater rate in arctic and subarctic regions than in most other parts of the world, with potentially significant hydrological impacts in these areas (Solomon et al. 2007; Hinzman et al. 2005; Woo et al. 1992).

Glacier melt makes a large contribution to river flow in areas dominated by snow and glaciers in the southern Yukon Territory (NCE 2014). Since climate change could have a significant impact on future hydrological conditions in the upper Yukon River basin, it is critical that the range of likely changes to the timing and magnitude of flow of the Yukon River through Whitehorse be examined to ensure that Yukon's hydro-electric power generation needs continue to be met.

This section estimates projected changes in climate and flow using CRHM and investigates climate-related factors and conditions that affect hydrological conditions in the basin. As discussed in earlier sections, this study applied CRHM, which has a full set of physically based modules representing cold hydrological processes (Pomeroy et al. 2007). Previous modeling by NCE used a simple conceptual hydrological approach, HBV-EC (*Hydrologiska Byråns Vattenbalansavdelning*-Environment Canada), which did not account for complex hydrological processes dominated by snow and glaciers, such as long-wave radiation in complex terrain, blowing snow, sublimation, and infiltration to frozen and unfrozen soils (NCE 2014).

### 6.1 Climate data

For this study, future climate scenarios were derived using two different general circulation models (GCMs): Geophysical Fluid Dynamics Laboratory, Princeton University (GFDL) and *Institut Pierre Simon Laplace*, based in France (IPSL). Both models were run using two of the Intergovernmental Panel on Climate Change (IPCC) scenarios: Representative Concentration Pathway (RCP) 4.5 and RCP 8.5; see IPCC 2013. Note that only these two GCMs were applied in this current study due to data availability at finer time steps (i.e., at three-hourly time steps) that are accessible to the general public and also due to time and budget constraints. The GCM outputs were used as input data for CRHM to support evaluation of climate change in the upper Yukon River basin. Prior to being used in CRHM, GCM data were corrected using interpolation, statistical bias correction (Samuel et al. 2012) and disaggregation methods. This approach is a significant improvement on the earlier NCE study into future hydrological changes in this region (NCE 2014), which used a basic approach to projection of future climate.

The RCP scenarios are part of an initiative launched by the international climate research community. The Coupled Model Intercomparison Project (CMIP) is part of the Intergovernmental Panel on Climate Change (IPCC). The latest CMIP was used in support of the panel's fifth assessment report (IPCC 2013). The IPCC adopted four RCP scenarios for their report that represent varying concentrations of emitted greenhouse gases. The scenarios were named after the estimated radiative forcing values in the year 2100 relative to pre-industrial values:

- RCP2.6: a low-forcing scenario;
- RCP4.5: a low-to-moderate-forcing stabilization scenario;
- RCP6.5: a moderate-to-high-forcing stabilization scenario; and
- RCP8.5: a high-forcing scenario.

Not all RCP scenarios were applied in this study due to time constraints. The project team selected an optimistic scenario (RCP4.5) and a worst-case scenario (RCP8.5), with respect to greenhouse gas concentrations. The climatic variables obtained from the two scenarios include near-surface minimum air temperature (GCM standard name: tasmin), maximum air temperature (tasmax), and precipitation flux (*pr*) in daily time steps; and near-surface eastward (*uas*) and northward (*vas*) components of wind, near-surface specific humidity (*huss*), and surface air pressure (*ps*) in three-hour time steps (later disaggregated into hourly time steps; see Section 6.2.1). Although only air temperature, precipitation, relative humidity and wind speed were required for simulation of CRHM, the other variables listed were required to compute relative humidity and wind speed. Precipitation and air temperature were obtained directly from the GCM data.

Wind speed (*wspd*) was computed as follows (Equation 6.1):

$$wspd = \sqrt{uas^2 + vas^2} \quad (6.1)$$

Where *uas* = near-surface eastward wind (m/s) and *vas* = near-surface northward wind (m/s)

Relative humidity was computed as follows (Equation 6.2):

$$RH = 100 \frac{w}{w_s} \approx 0.263pq \left[ \exp\left(\frac{17.67(T - T_0)}{T - 29.65}\right) \right]^{-1} \quad (6.2)$$

Where (Equation 6.2.1, 6.2.2 and 6.2.3)

$$w \equiv \frac{m_v}{m_v + m_d} \approx q \quad (6.2.1)$$

$$w_s \equiv \frac{m_{vs}}{m_d} = \frac{e_s R_d}{R_v(p - e_s)} \approx 0.622 \frac{e_s}{p} \quad (6.2.2)$$

$$e_s(T) = e_s \exp\left[\left(\frac{L_v(T)}{R_v}\right) \left(\frac{1}{T_0} - \frac{1}{T}\right)\right] \approx 611 \exp\left(\frac{17.67(T - T_0)}{T - 29.65}\right) \quad (6.2.3)$$

Where

*q* = specific humidity of the mass mixing ratio of water vapour to total air (dimensionless);  
*m<sub>v</sub>* = specific mass of water vapour (kg); *m<sub>vs</sub>* = specific mass of water vapour at equilibrium (kg);  
*m<sub>d</sub>* = specific mass of dry air (kg); *w* = mass mixing ratio of water vapour to dry air (dimensionless);  
*w<sub>s</sub>* = mass mixing ratio of water vapour to dry air at equilibrium (dimensionless); *e<sub>s</sub>* = saturation vapour pressure (Pa); *e<sub>s</sub>(T)* = saturation vapour pressure at T (Pa); *R<sub>d</sub>* = specific gas constant for dry air (J kg K); *R<sub>v</sub>* = specific gas constant for water vapour (J kg K); *L<sub>v</sub>* = specific enthalpy of vapourization (J kg); *p* = pressure (Pa); *T* = air temperature (K); and *T<sub>0</sub>* = reference air temperature (273.15 K)

## 6.2 Predicting hydrological responses to climate forcing using CRHM

GCM climate data for air temperature, precipitation, relative humidity, and wind speed were corrected using interpolation, bias correction and disaggregation methods before being forced into CRHM in order to estimate future river flow changes. Software to perform the bias correction, interpolation and disaggregation was developed by NCE team using Fortran codes and is part of the CRHM manual (NCE 2016). Time periods and GCM data can be adjusted within the code to fit the needs of the user. To run the software, users must download the correct GCM data, select the appropriate grid points for the study basin, and determine the current and future time periods to be simulated. The software arranges the outputs so that they can be used in CRHM.

Previously validated parameters (see Section 5.3.4) were used to model the 2014–30 and 2031–45 periods. No land-use changes were assumed, with the exception of changes in glacier area. For this reason, simulation of changes in glacier extent and thickness was required to predict future climate outputs.

### 6.2.1 Interpolation, bias correction, and disaggregation methods

Since the raw GCM climate data had a low spatial resolution and varied from the meteorological observation data for 2006–13, the previously corrected GEM-LAM data (see Section 5.2.3) were used to correct the raw GCM climate data for the RCP4.5 and RCP8.5 scenarios. Prior to correction, the GCM data at each GCM grid point were interpolated to GEM-LAM grid points using the Inverse Distance Weight method (Shepard 1968).

Following interpolation, statistical bias correction methods were applied to all four climate variables. Air temperature and precipitation were corrected using a statistical bias correction method developed by Samuel et al. (2012) that is specific to those variables. Since simulation in the CRHM required daily data for precipitation, but hourly data for air temperature, relative humidity and wind speed, a disaggregation method was applied to those variables following statistical bias correction.

The precipitation data of the two climate models were corrected by following three steps:

- The precipitation frequency of each climate model was corrected by truncating the empirical distribution of the raw daily climate model precipitation above a threshold value, so that the mean frequency of rainfall above the threshold matched the observed frequency of mean rainfall;
- A two-parameter gamma distribution was used to fit the truncated daily climate-model and observed precipitation data for each of the 12 calendar months; and
- The cumulative distribution function of the truncated daily climate-model precipitation was mapped to that of the observed data. The distribution of frequency and the intensity of precipitation for the target closest to the grid point of the climate models were corrected to the observation station.

The air temperature data were corrected by following two steps:

- The distribution of maximum and minimum daily air temperature was mapped onto the observed distribution for each of the 12 calendar months based on a normal distribution; and
- The corrected daily maximum and minimum air temperature were disaggregated into hourly average air temperature using a simple combination of the sine curve approach, similar to the method applied by Chen et al. (1993). The disaggregation formula is described in Equation 6.3.

$$T_{hav} = \begin{cases} T_1 - A_1 \left\{ \cos \left( \frac{\pi(t - t_1)}{T'} \right) \right\}, & t \leq t_2 \\ T_2 - A_2 \left\{ \cos \left( \frac{\pi(t + L')}{24 - T'} \right) \right\}, & t > t_2 \end{cases} \quad (6.3)$$

where

$$T_1 = (T_{dmax1} + T_{dmin1})/2$$

$$A_1 = (T_{dmax1} - T_{dmin1})/2$$

$$T_2 = (T_{dmax2} + T_{dmin2})/2$$

$$A_2 = (T_{dmax2} - T_{dmin2})/2$$

$$T' = (t_2 - t_1)$$

$$L' = (24 - T') - t_2, \text{ and}$$

$T_{hav}$  = hourly average air temperature

$T_{dmax1}$  = daily maximum air temperature at day  $d$

$T_{dmin1}$  = daily minimum air temperature at day  $d$

$T_{dmax2}$  = daily maximum air temperature at day  $d+1$

$T_{dmin2}$  = daily minimum air temperature at day  $d+1$

The parameters  $t_1$  and  $t_2$  were calculated from the time of the minimum value at sunrise ( $t_1$ ) and the maximum value at solar noon ( $t_2$ ), both of which were influenced by the latitude and longitude of the study sites and the days of the year.

Wind speed and relative humidity were corrected by following two steps:

- The climate model data were disaggregated into hourly data by assuming a uniform distribution of relative humidity and wind speed data; i.e., measurements were assumed to be the same over the three-hour time period.
- The hourly data were corrected with the observation data using a simple scaling formula, described in Haddeland et al. (2012) as follows (Equation 6.4):

$$V_{fcor} = V_{fgcm} \frac{\bar{V}_{cobs}}{\bar{V}_{cgcm}} \quad (6.4)$$

where  $V_{fcor}$  is the time series of projected future atmospheric variables (wind speed or relative humidity) for any given hour,  $V_{fgcm}$  is the time series of raw data of future climate model atmospheric variables,  $\bar{V}_{cobs}$  is the mean of observed atmospheric variables for any given hour, and  $\bar{V}_{cgcm}$  is the mean of current climate model atmospheric variables.

### 6.2.2 Glacier cover change model: simulating glacier retreat and advance

Future glacier ice volume and surface area were estimated for the glacierized areas in order to determine changes in glacier cover. The glacier ice volume and surface area were resolved using the Glacier Cover Change Model (GCCM; see NCE 2016). The GCCM is a coupled model with CRHM; it reads CRHM outputs, computes changes in glacier surface area and subsequently arranges new area changes by HRUs to be used for the next simulation in CRHM. The model can be used to estimate glacier cover changes at specific time intervals. It was created using ArcGIS software and computer codes written in Fortran, by following four steps:

- Each elevation band for each subbasin in the glacierized areas was divided into 10 groups based on DEM, each group having the same area. Each group was then divided into grid cells with a resolution of 10 m x 10 m. The ice volume of each grid cell was determined using the cell's known ice thickness (this was estimated using the method discussed in Section 4.2);
- CRHM model outputs (ice melt/accumulation) were distributed to each group in such a way that the distribution of the ice volume had smooth changes from one group to another and from one elevation band to another, while maintaining the ice volume estimated by CRHM. This was achieved by computing and optimizing coefficient values for ice-volume estimates for each group using the dynamically dimensioned search approach (Tolson and Shoemaker 2007) available in the OSTRICH software toolkit (Matott 2007);
- The groups at the higher elevations in each elevation band were assumed to have lower ice melt volume than the groups at the lower elevations in that band. If ice melt at the lowest elevation in a band surpassed the current ice volume in that band, the higher elevation band was assumed to lose all its ice. This procedure was repeated for all elevation bands to obtain new ice volume estimates; and
- The above results were then used to obtain the retreat/advance of glacier surface area at each elevation band. Areas newly free of glaciers were considered exposed land, rock or water (depending on their surrounding land-cover characteristics) for subsequent hydrological simulations.

### 6.2.3 Workflow of the coupled CRHM, BCM and GCCM

Figure 6.1 illustrates the modeling steps involved in estimating projected climate, future river flows and glacier surface area and volume; these steps link the BCM, CRHM and GCCM. There are four modeling steps:

- downloading GCM outputs prior to simulation in the CRHM;
- correcting the GCM outputs using the bias correction model (BCM; see Section 6.2.1);
- simulating CRHM, which was validated for the 2006-13 period (discussed in Section 5), using corrected GCM outputs to obtain estimates of river flows and glacier net balance; and
- inputting the glacier net mass balance of CRHM outputs in GCCM to obtain new glacier extents, which can be used to model future time periods in CRHM (see Section 6.2.2).

Section 6.3 presents the results and analysis of future river flow and glacier cover changes using GCM outputs, derived from GFDL and IPSL with RCP4.5 and RCP8.5 scenarios for the periods of 2014-30 and 2031-45. These three models (BCM, CRHM and GCCM) are provided to YEC so that it can run simulations at specific time intervals while applying a range of GCM outputs. Specific instructions on how to run the three models are included in the manual provided as a companion to this report (NCE 2016).

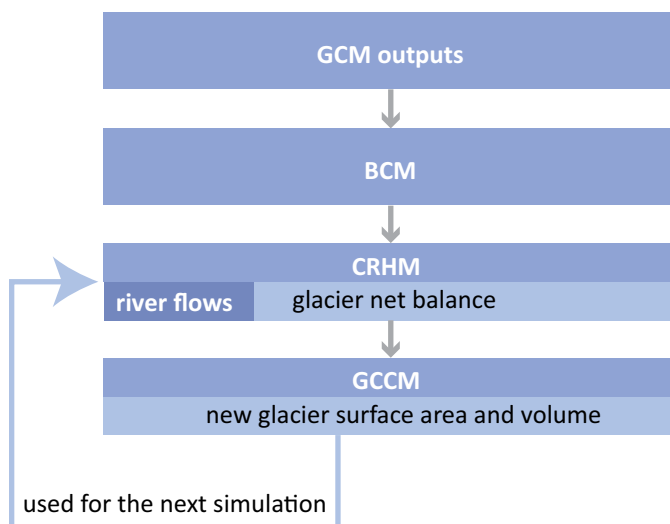


**Figure 6.1** Modeling steps of the BCM, CHRM and GCCM.

### 6.3 Results of climate analysis

The interpolation, bias correction and disaggregation methods corrected the bias of the GCM outputs and reduced their uncertainties prior to using them for hydrological projections. The correction methods reduced the errors of the raw GCM outputs, averaged over 2014–45, by a minimum of 9% (relative humidity) and a maximum of 335% (precipitation); see Table 6.1. There was a large difference between observed and predicted GCM data for precipitation due to its randomness. The difference was also likely caused by a high number of observed dry days, but continuous light rainfall predicted by the GCM (Boberg et al. 2007; Kim et al. 2002).

**Table 6.1** Climate variables and reduction of bias (%) from raw GCM outputs averaged over 2014–45 for two GCM models.

Meteorological component	Reduction in bias (%)	
	GFDL	IPSL
Mean maximum air temperature	63	67
Mean minimum air temperature	92	131
Precipitation	335	274
Relative humidity	17	9
Wind speed	134	122

Note: GFDL = Geophysical Fluid Dynamics Laboratory; IPSL = Institut Pierre Simon Laplace

The differences in projected change vary among GCMs and scenarios; see Table 6.2. Each model operates under different sets of boundary conditions, number of experiments, and duration of simulations (Wilby et al. 2002). In general, the projected changes (future-current conditions) estimate increased maximum and minimum air temperature, precipitation, and relative humidity, while wind speed showed a slight decrease (Table 6.2). Comparing the values between scenarios,

RCP 8.5 estimated higher maximum and minimum temperature on average, but lower precipitation, relative humidity and wind speed than RCP4.5.

**Table 6.2** Differences in future climate variable changes for GCMs and scenarios

Meteorological component	Period	GFDL		IPSL		Average difference	
		RCP4.5	RCP8.5	RCP4.5	RCP8.5	GFDL vs. IPSL*	RCP4.5 vs. RCP8.5**
Maximum air temperature (°C)	2014–30	0.23	1.15	0.83	1.01	-0.61	0.92
	2031–45	1.59	1.37	1.67	1.51	0.14	0.18
Minimum air temperature (°C)	2014–30	-0.08	0.68	1.03	1.07	-1.10	0.76
	2031–45	1.09	0.77	1.93	1.60	-0.39	0.05
Precipitation (mm/month)	2014–30	3.37	2.75	4.28	1.21	-0.91	-0.62
	2031–45	4.62	3.28	7.11	0.94	1.54	-3.07
Relative humidity (%)	2014–30	-0.03	0.21	0.85	-0.20	-0.89	0.25
	2031–45	0.52	0.21	0.25	-0.46	0.41	-1.05
Wind speed (m/s)	2014–30	-0.02	-0.08	0.09	0.02	-0.11	-0.05
	2031–45	-0.09	-0.12	0.05	-0.02	-0.09	-0.07

\* positive values indicate GFDL is larger than IPSL

\*\* positive values indicate RCP8.5 is larger than RCP4.5

### 6.3.1 Potential future climate conditions

#### 6.3.1.1 Temporal variation

The study compared current observations with projected future temporal changes for 2014–30 and 2031–45 for five climate variables: maximum air temperature, minimum air temperature, precipitation, relative humidity and wind speed. The results and analysis presented below use the corrected GCM outputs averaged for the entire study basin. For the sake of simplicity, the raw data are not shown here, since the trend changes between current and future periods are similar for both the corrected and raw GCM outputs.

##### *Maximum air temperature*

Relative to current conditions (2006–13), estimated increases in maximum air temperature were larger and more frequent than estimated decreases in maximum air temperature (Figure 6.2):

- Overall, the increases were higher for the RCP8.5 scenario than for the RCP4.5 scenario. The GFDL model estimated minimal decreases in maximum air temperature and large increases in future maximum air temperature between March and August.
- A large increase in future maximum air temperature was estimated for the IPSL between January and mid-July, with no significant predicted decreases.

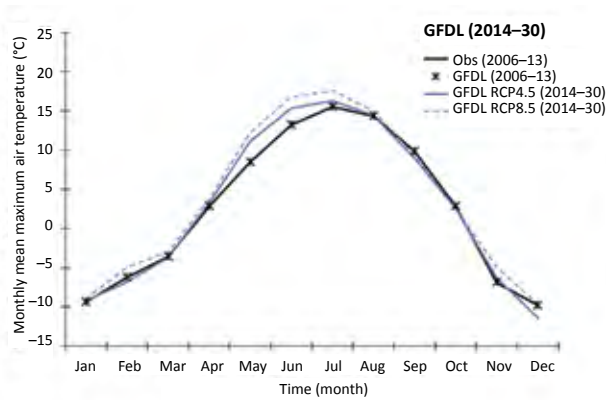


**Figure 6.2a** Estimated temporal changes in maximum air temperature for GFDL 2014–30.

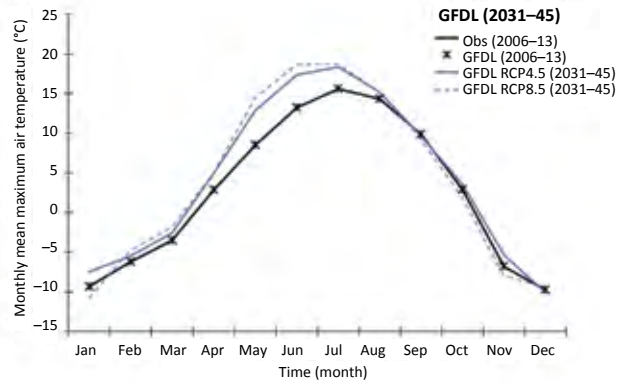


**Figure 6.2b** Estimated temporal changes in maximum air temperature for GFDL 2031–45.

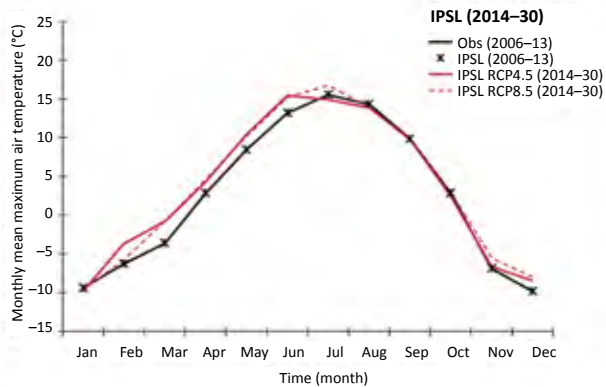


**Figure 6.2c** Estimated temporal changes in maximum air temperature for IPSL 2014–30.

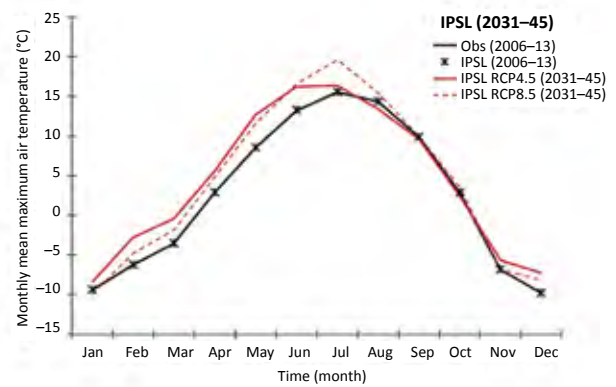


**Figure 6.2d** Estimated temporal changes in maximum air temperature for IPSL 2031–45.

*Minimum air temperature*

Relative to current conditions, estimated increases in minimum air temperature were larger and more frequent than estimated decreases in minimum air temperature (Figure 6.3). Overall, the increases were higher for the RCP8.5 scenario than for the RCP4.5 scenario:

- the GFDL estimated significant increases in minimum air temperature between December and mid-February and from April to August for 2014–30 and significant increases between January and August for 2031–45;
- the GFDL model estimated minimal decreases in minimum air temperature for the winter months for both 2014–30 and 2031–45; and
- the IPSL estimated significant increases between December and August for 2014–31 and between December and September for 2031–45. No significant decreases in minimum air temperature were estimated for the IPSL model.

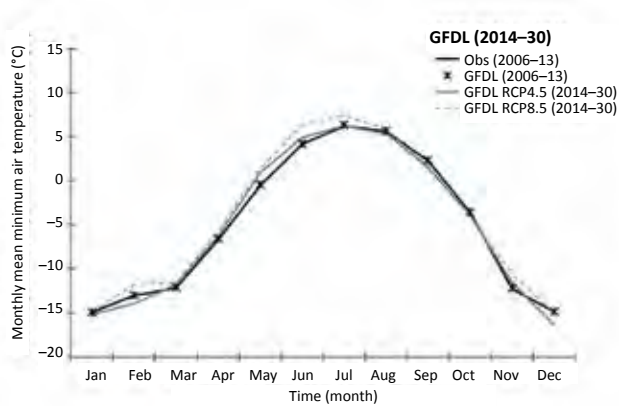


**Figure 6.3a** Estimated temporal changes in minimum air temperature for GFDL 2014–30.

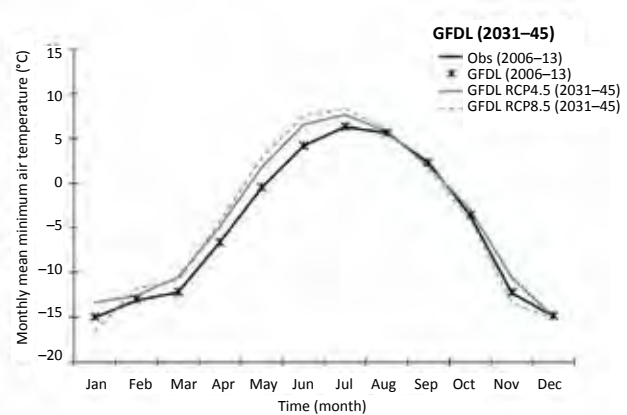


**Figure 6.3b** Estimated temporal changes in minimum air temperature for GFDL 2031–45.

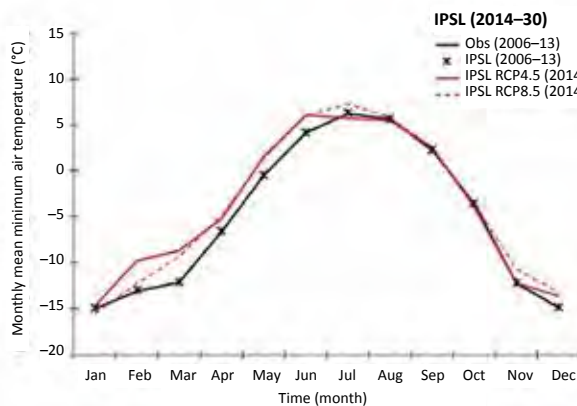


**Figure 6.3c** Estimated temporal changes in minimum air temperature for IPSL 2014–30.

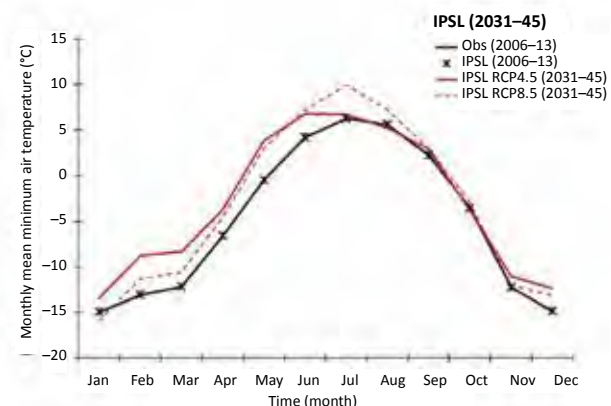


**Figure 6.3d** Estimated temporal changes in minimum air temperature for IPSL 2031–45.

### Precipitation

Relative to current conditions, estimated increases in precipitation were larger and more frequent than estimated decreases in precipitation (Figure 6.4). The most significant increases in precipitation for both the GFDL and IPSL models were estimated from mid-January to mid-March and from mid-June to mid-September:

- the RCP4.5 scenario estimated larger increases in precipitation from mid-January to mid-March than the RCP8.5 scenario did;
- in general, the RCP8.5 scenario estimated larger increases from mid-June to mid-September than the RCP4.5 scenario did, with the exception of the IPSL 4.5 scenario for 2031–45;
- the IPSL 4.5 scenario estimated larger increases in precipitation than the RCP8.5 scenario did from mid-June to mid-September, with the exception of the IPSL for 2031–45; and
- both models estimated minimal decreases in precipitation.

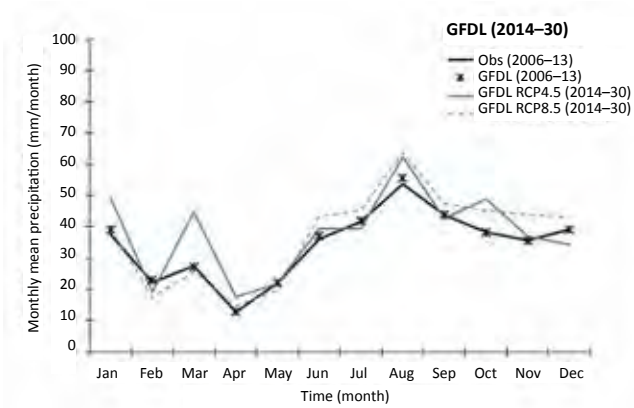


**Figure 6.4a** Estimated temporal changes in precipitation for GFDL 2014–30.

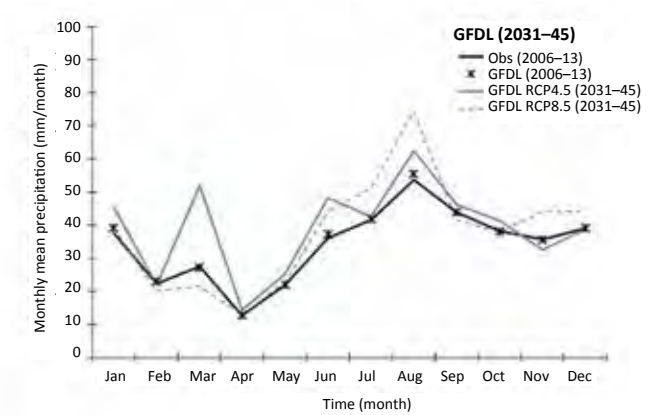


**Figure 6.4b** Estimated temporal changes in precipitation for GFDL 2031–45.

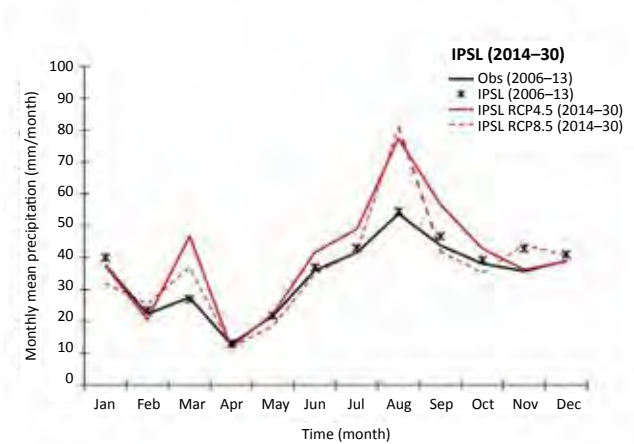


**Figure 6.4c** Estimated temporal changes in precipitation for IPSL 2014–30.

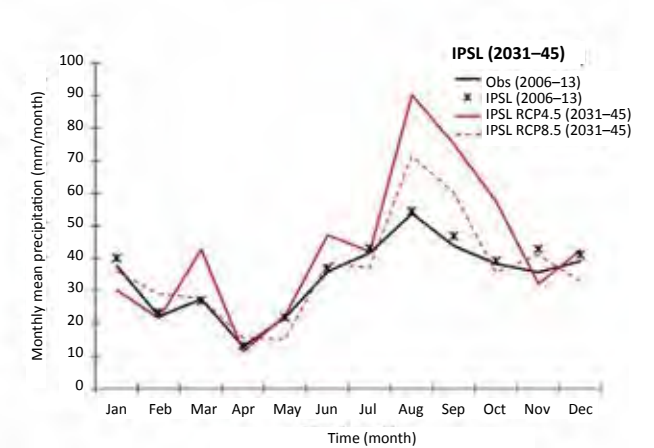


**Figure 6.4d** Estimated temporal changes in precipitation for IPSL 2031–45.

### Relative humidity

Relative humidity both increased and decreased significantly relative to current conditions (Figure 6.5):

- the GFDL estimated significant increases in relative humidity from mid-August to mid-November;
- the GFDL estimated fluctuations in relative humidity both above and below current conditions from December to May; and
- overall, the IPSL model estimated relative humidity fluctuations both above and below current conditions, with significant GFDL decreases in relative humidity between mid-March and mid-June for the RCP8.5 scenario.

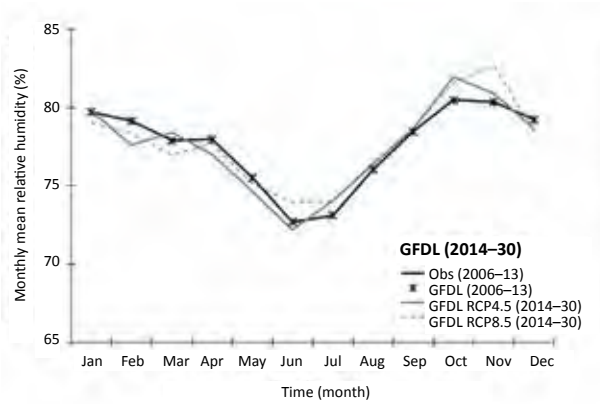


**Figure 6.5a** Estimated temporal changes in relative humidity for GFDL 2014–30.

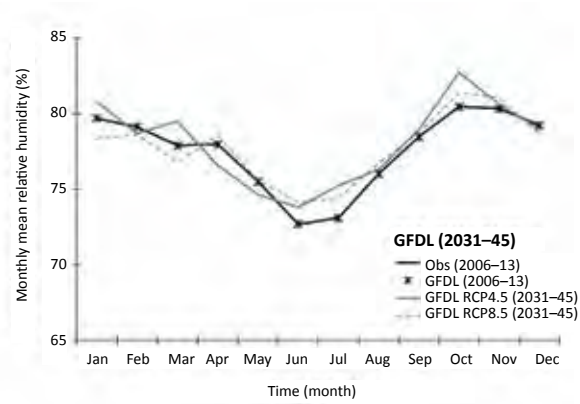


**Figure 6.5b** Estimated temporal changes in relative humidity for GFDL 2031–45.

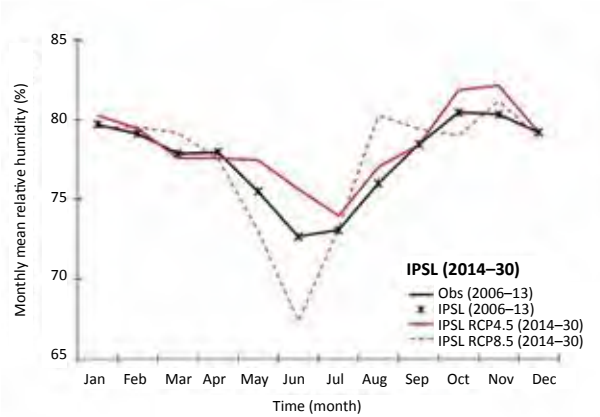


**Figure 6.5c** Estimated temporal changes in relative humidity for IPSL 2014–30.

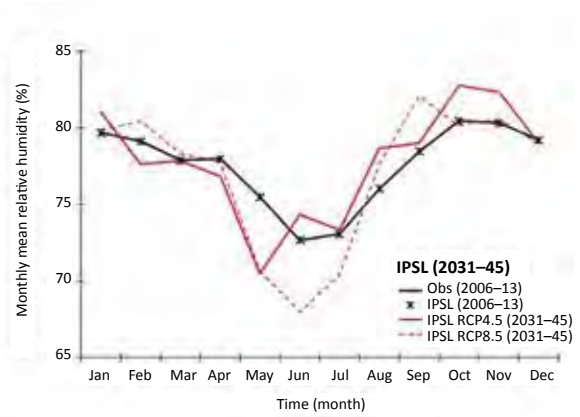


**Figure 6.5d** Estimated temporal changes in relative humidity for IPSL 2031–45.

*Wind speed*

Relative to current conditions, the GFDL model estimated larger and more frequent decreases than increases in wind speed, with larger estimated decreases for the RCP8.5 scenario than for the RCP4.5 scenario (Figure 6.6). In contrast, the IPSL model estimated larger and more frequent increases in wind speed, more so for the RCP4.5 scenario than the RCP8.5 scenario:

- in general, the GFDL estimated significant decreases in wind speed throughout most of the year; and
- estimated wind speed fluctuated both above and below current conditions for the IPSL model, with significant increases predicted from mid-May to October.

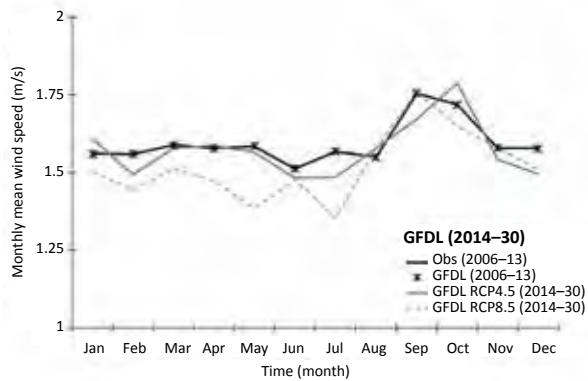


**Figure 6.6a** Estimated temporal changes in wind speed for GFDL 2014–30.

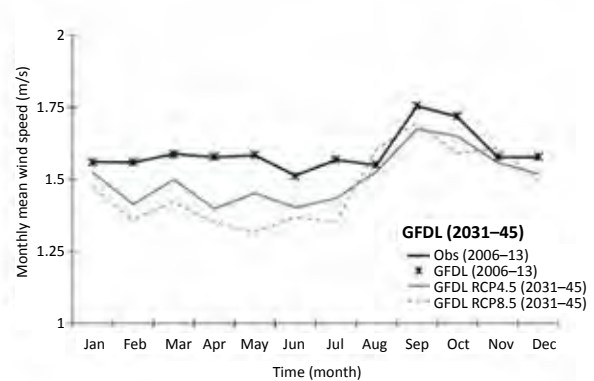


**Figure 6.6b** Estimated temporal changes in wind speed for GFDL 2031–45.

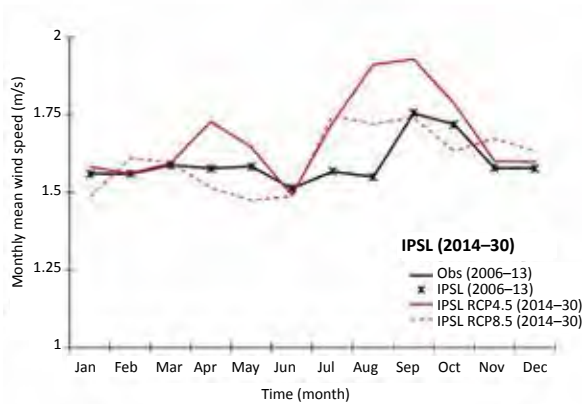


**Figure 6.6c** Estimated temporal changes in wind speed for IPSL 2014–30.

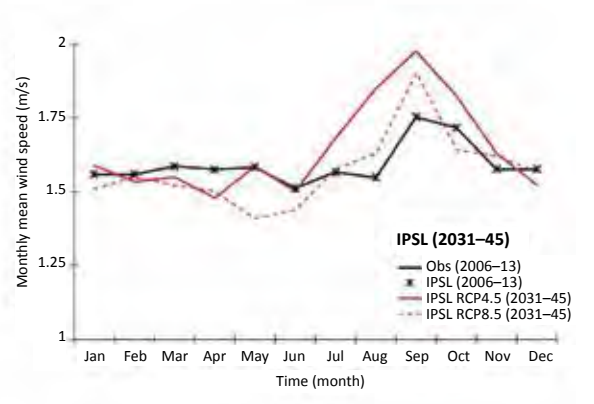


**Figure 6.6d** Estimated temporal changes in wind speed for IPSL 2031–45.

### 6.3.1.2 Spatial variation

The projected future changes (for 2014–30 and 2031–45) of five climate variables — maximum air temperature, minimum air temperature, precipitation, relative humidity and wind speed — were spatially investigated and changes in magnitude were compared. Note that the analysis presented below uses corrected GCM outputs and compares the average values of each climate variable between current and future periods (averaged over the entire period).

#### Maximum air temperature

Both models estimated increases in maximum air temperature in most of the study basin, relative to current conditions (2006–13), with the exception of a decreasing trend for maximum air temperature in the southern portion of the basin for the RCP4.5 scenario of the GFDL in 2014–30 (Figure 6.7a):

- the IPSL estimated larger increases of maximum air temperature in the northern and eastern regions of the basin than in other parts of the basin;
- the GFDL estimated larger increases of maximum air temperature in the northern region than in other parts of the basin; and
- the GFDL projected a wider range of possible changes in maximum air temperature than the IPSL did; the highest increase in maximum air temperature projected by the GFDL was approximately 2.2°C.

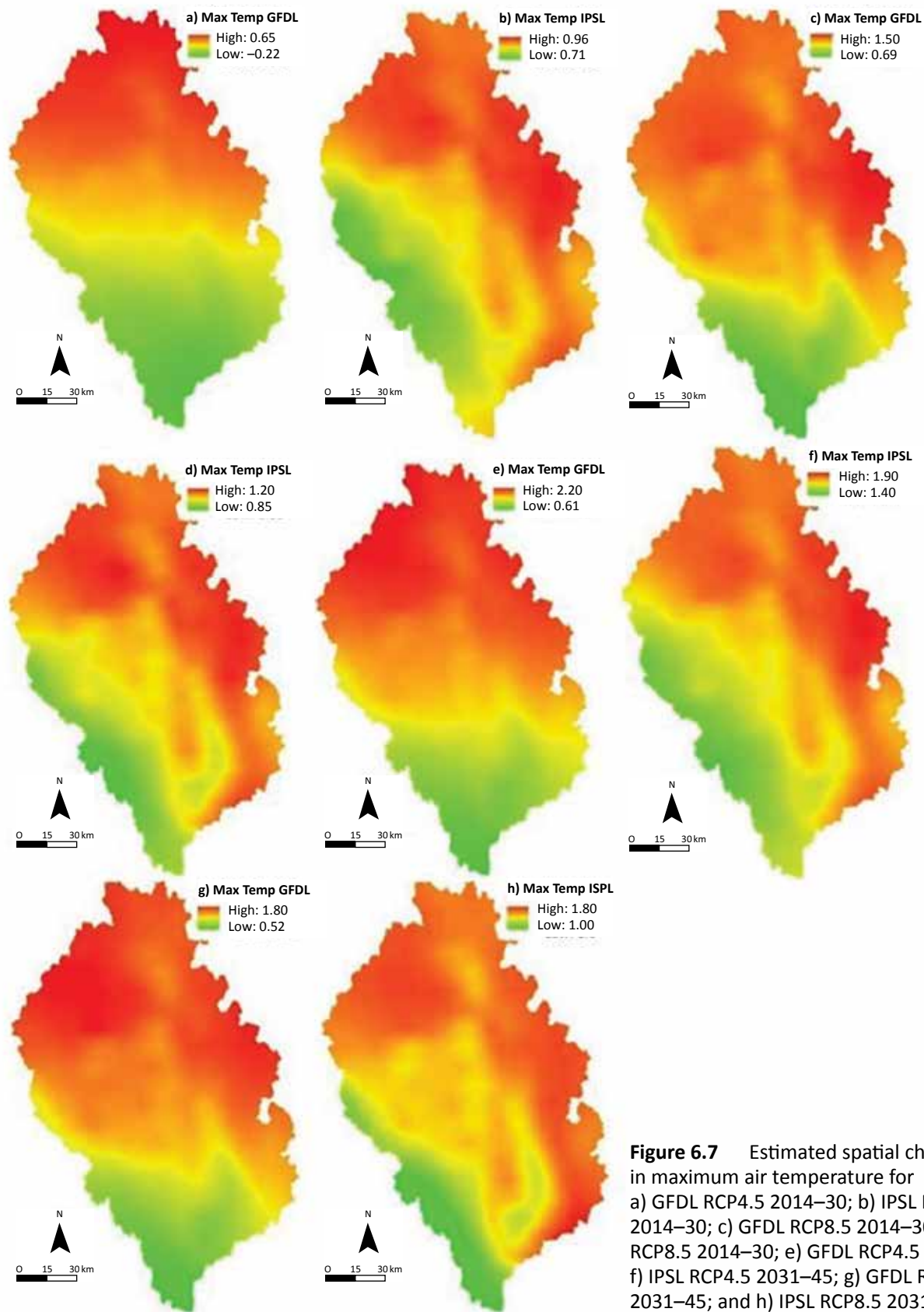


**Figure 6.7** Estimated spatial changes in maximum air temperature for a) GFDL RCP4.5 2014–30; b) IPSL RCP4.5 2014–30; c) GFDL RCP8.5 2014–30; d) IPSL RCP8.5 2014–30; e) GFDL RCP4.5 2031–45; f) IPSL RCP4.5 2031–45; g) GFDL RCP8.5 2031–45; and h) IPSL RCP8.5 2031–45.

#### *Minimum air temperature*

Relative to current conditions, the GFDL estimated increases in minimum air temperature in most of the basin, with the exception of the southwest region (scenario RCP4.5 for 2014–30; Figure 6.8):

- the IPSL estimated larger increases in minimum air temperature in the northern and eastern regions of the basin than in the rest of the basin;
- for the GFDL, increases in minimum air temperature varied spatially across the basin, based on the time period and scenario; and
- the IPSL projected a wider range of possible changes in minimum air temperature: its highest projected increase was 2.2°C.

#### *Precipitation*

Relative to current conditions, precipitation was estimated to increase across the entire basin, with no decrease in precipitation estimated for either time period, scenario or model (Figure 6.9):

- the GFDL estimated higher increases of precipitation as bands across the basin;
- the IPSL increases were concentrated in the western regions; and
- the IPSL projected a wider range of possible changes in precipitation than the GFDL did; its highest projected increase in precipitation was 174 (mm/month).

#### *Relative humidity*

Relative humidity both increased and decreased across the basin relative to current conditions, based on the different time periods, scenarios and models (Figure 6.10):

- the IPSL RCP8.5 scenarios for both 2014–30 and 2031–45 estimated decreases in relative humidity across the entire study basin;
- the GFDL estimated higher increases in relative humidity for the northern and southern regions for both the RCP4.5 and RCP8.5 scenarios;
- for the IPSL RCP4.5 scenario increases varied spatially across the basin; and
- the IPSL projected a wider range of possible changes in relative humidity than the GFDL did; the highest estimated increase in relative humidity was 1%.

#### *Wind speed*

The GFDL model predicted both increases and decreases in wind speed relative to current conditions, estimating wind speed increases in the southern portion of the basin and decreases in the northern portion (Figure 6.11):

- the IPSL estimated small increases in wind speed that varied spatially across the basin in all cases except the RCP8.5 scenario for 2031–45, where wind speed was estimated to decrease across the entire study basin; and
- the GFDL projected a wider range of possible changes in wind speed; its highest estimated increase in wind speed was 0.2 metres/second.

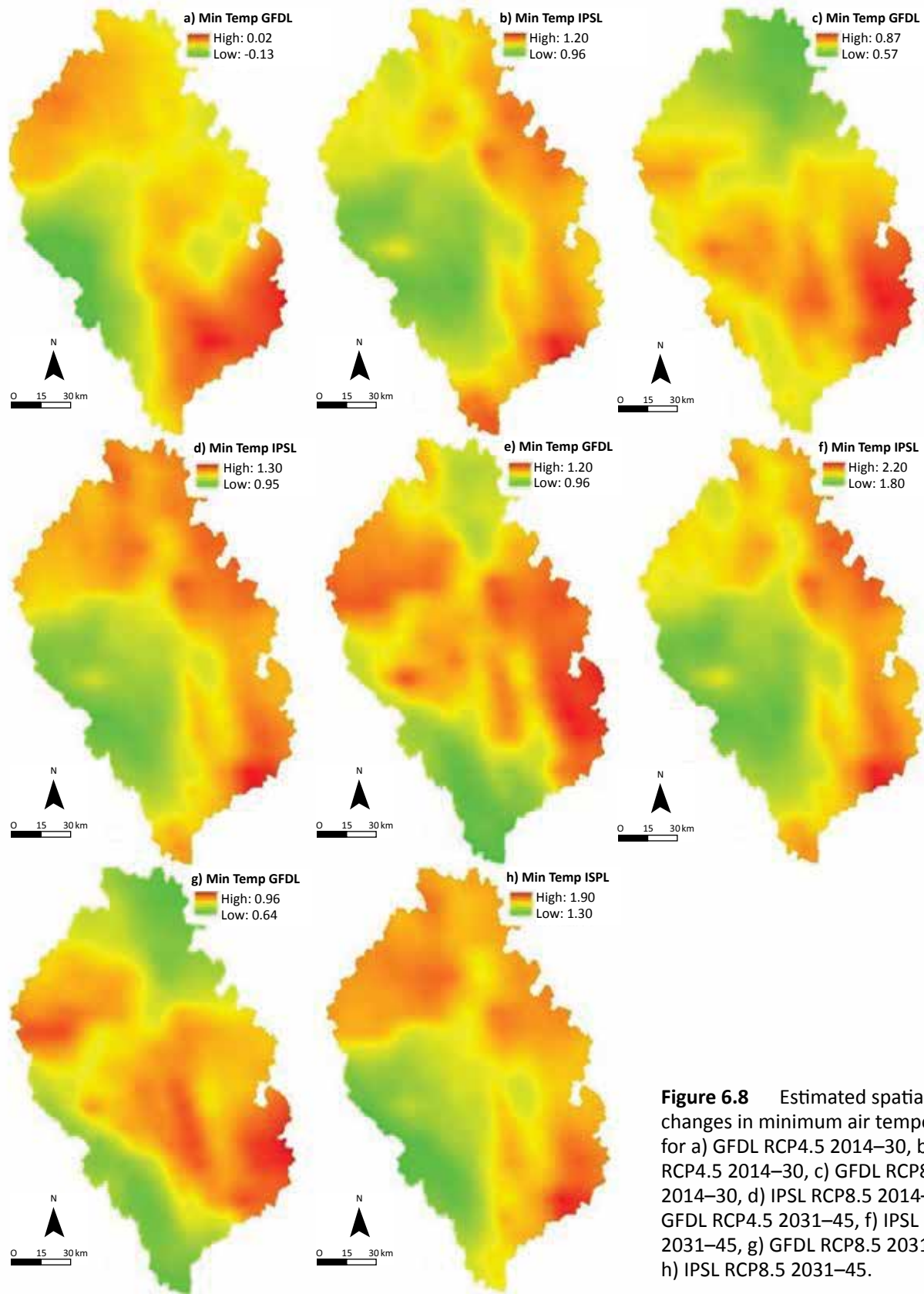


**Figure 6.8** Estimated spatial changes in minimum air temperature for a) GFDL RCP4.5 2014–30, b) IPSL RCP4.5 2014–30, c) GFDL RCP8.5 2014–30, d) IPSL RCP8.5 2014–30, e) GFDL RCP4.5 2031–45, f) IPSL RCP4.5 2031–45, g) GFDL RCP8.5 2031–45 and h) IPSL RCP8.5 2031–45.

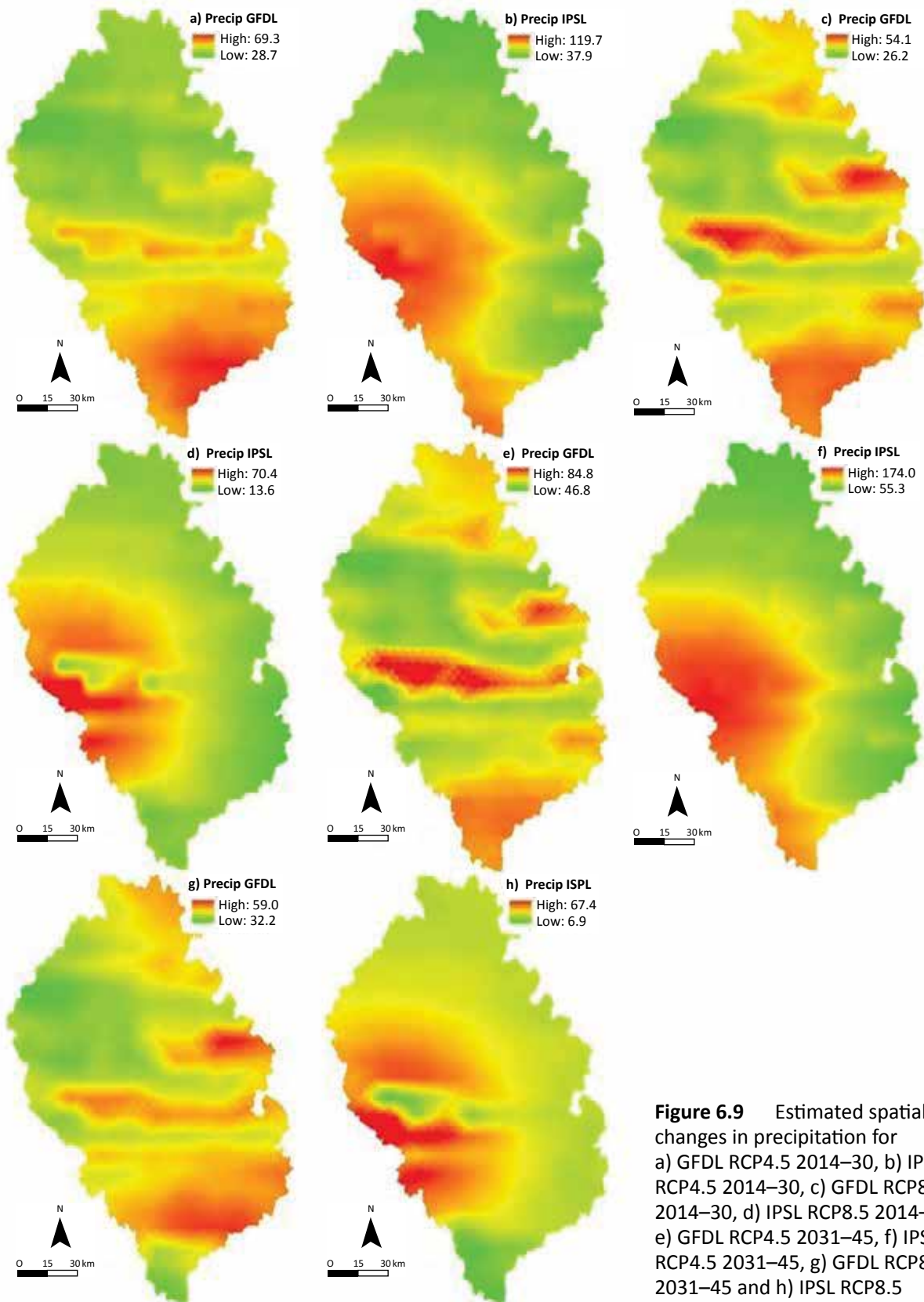


**Figure 6.9** Estimated spatial changes in precipitation for a) GFDL RCP4.5 2014–30, b) IPSL RCP4.5 2014–30, c) GFDL RCP8.5 2014–30, d) IPSL RCP8.5 2014–30, e) GFDL RCP4.5 2031–45, f) IPSL RCP4.5 2031–45, g) GFDL RCP8.5 2031–45 and h) IPSL RCP8.5 2031–45.

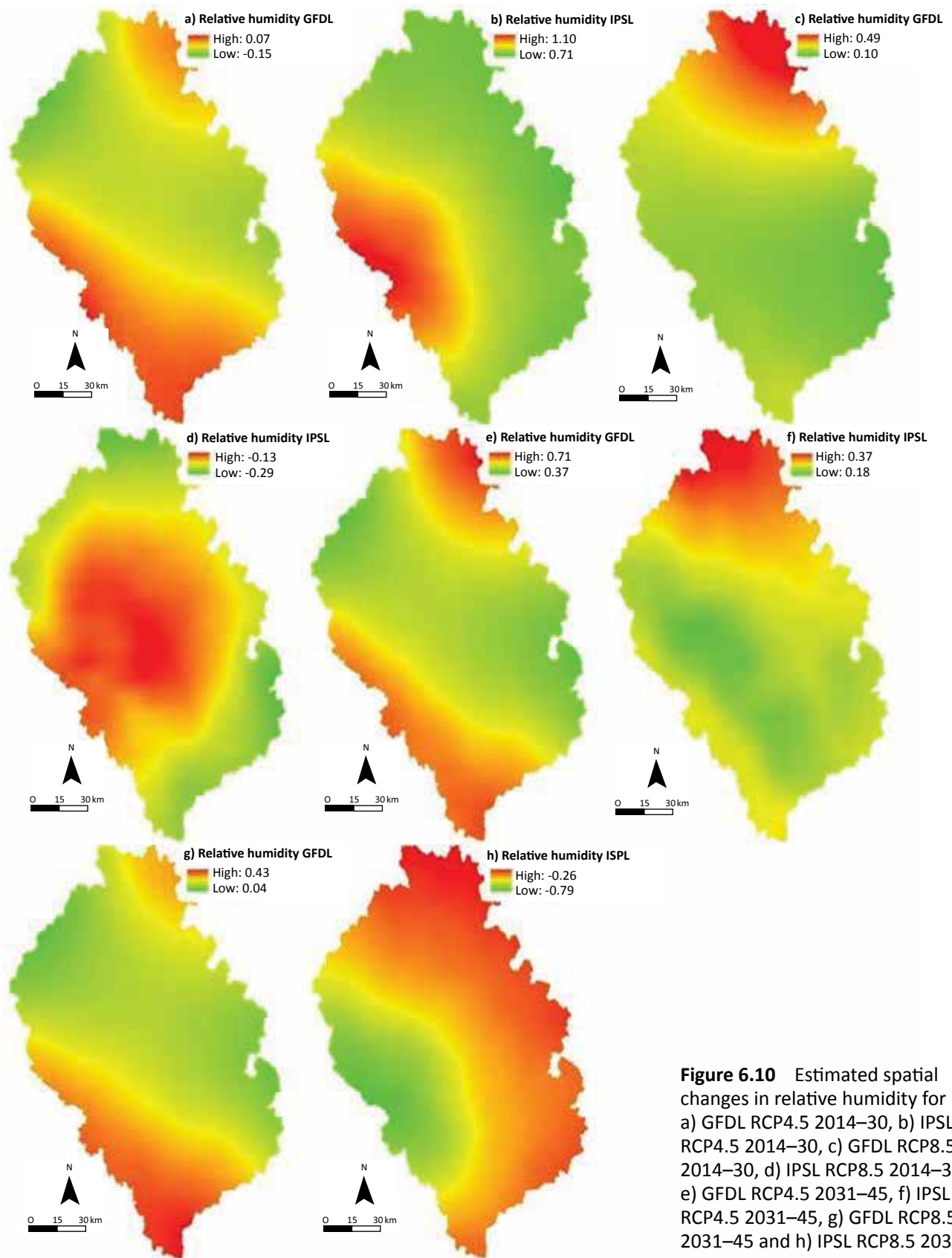


**Figure 6.10** Estimated spatial changes in relative humidity for a) GFDL RCP4.5 2014–30, b) IPSL RCP4.5 2014–30, c) GFDL RCP8.5 2014–30, d) IPSL RCP8.5 2014–30, e) GFDL RCP4.5 2031–45, f) IPSL RCP4.5 2031–45, g) GFDL RCP8.5 2031–45 and h) IPSL RCP8.5 2031–45.

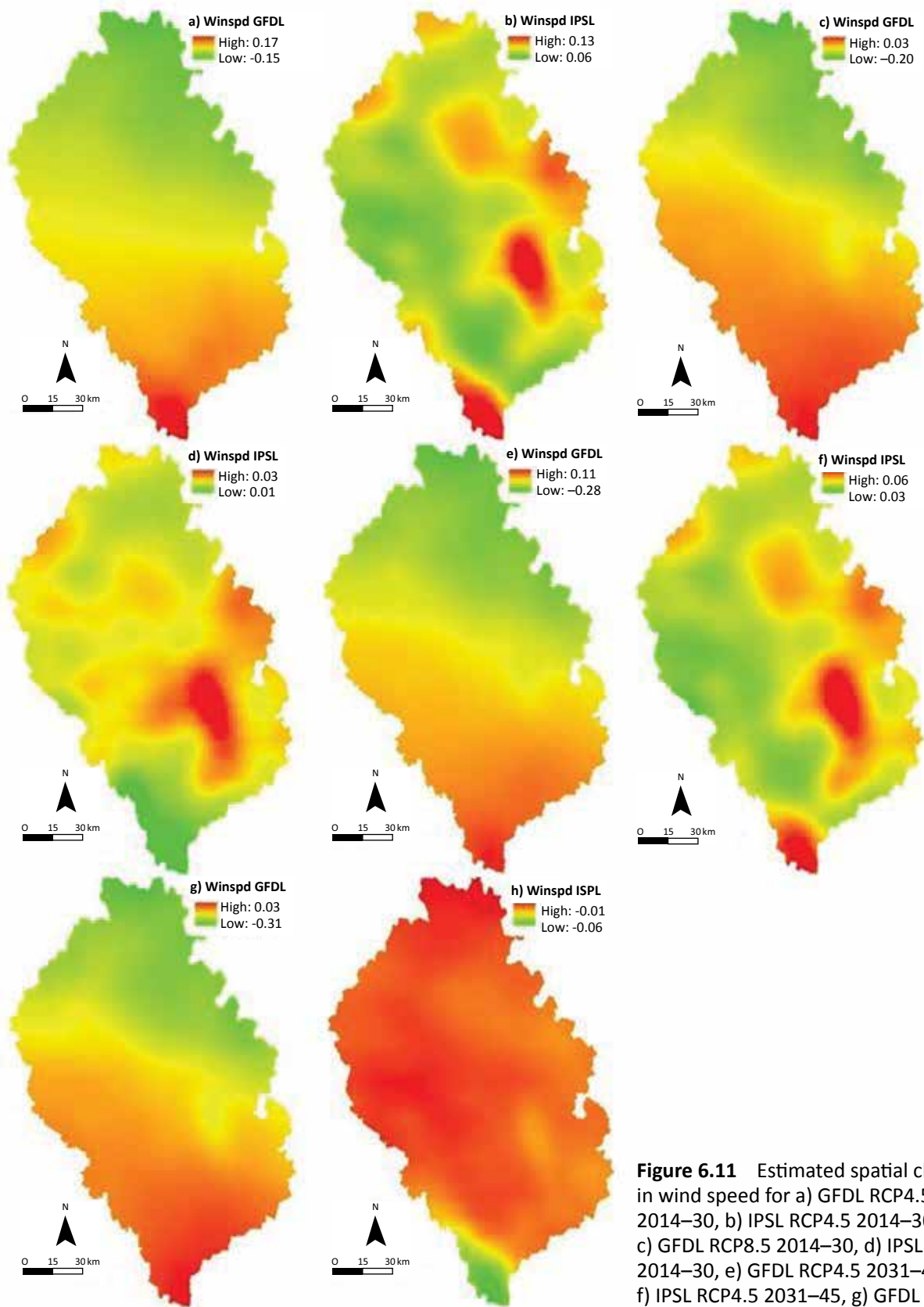


**Figure 6.11** Estimated spatial changes in wind speed for a) GFDL RCP4.5 2014–30, b) IPSL RCP4.5 2014–30, c) GFDL RCP8.5 2014–30, d) IPSL RCP8.5 2014–30, e) GFDL RCP4.5 2031–45, f) IPSL RCP4.5 2031–45, g) GFDL RCP8.5 2031–45 and h) IPSL RCP8.5 2031–45.

**6.3.1.3 Projected future air temperature changes in the Llewellyn and Willison glaciers**

The projected future changes (2014–30 and 2031–45) of maximum air temperature (Figure 6.12) and minimum air temperature (Figure 6.13) in the area of the Llewellyn and Willison glaciers were compared among GCMs. Results were grouped according to months of high ice melt (May to August) and lower to no ice melt (September to April; Figures 6.12 and 6.13). From May to August, both models and scenarios consistently estimated increases of maximum and minimum air temperature, with higher increases estimated for the RCP8.5 scenario than for the RCP4.5 scenario. Although large variability was estimated for September to April, the overall trend estimated increases in maximum and minimum air temperature for both models and both scenarios for future periods (2014–30 and 2013–45).

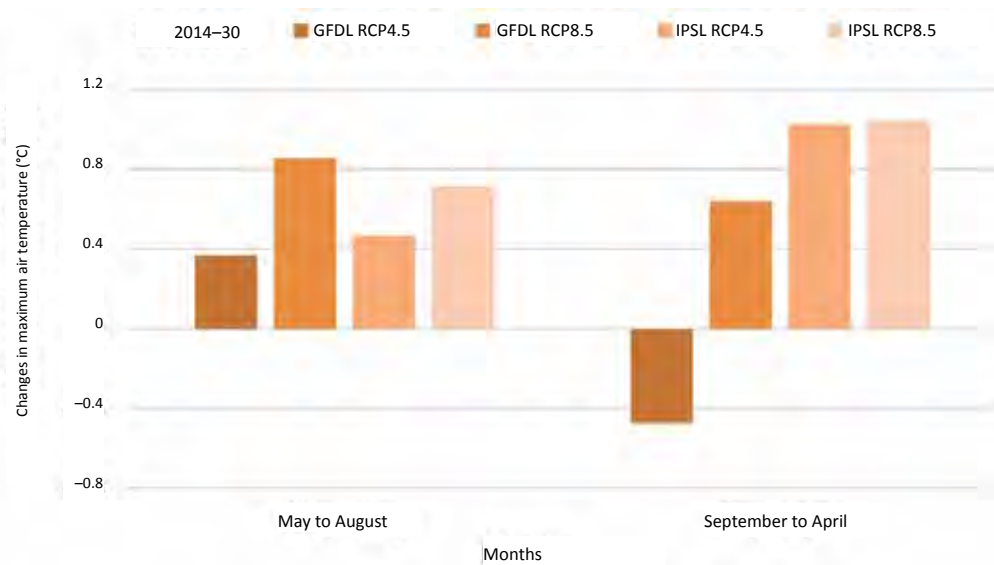


**Figure 6.12a** Estimated changes in maximum air temperature for 2014–30.

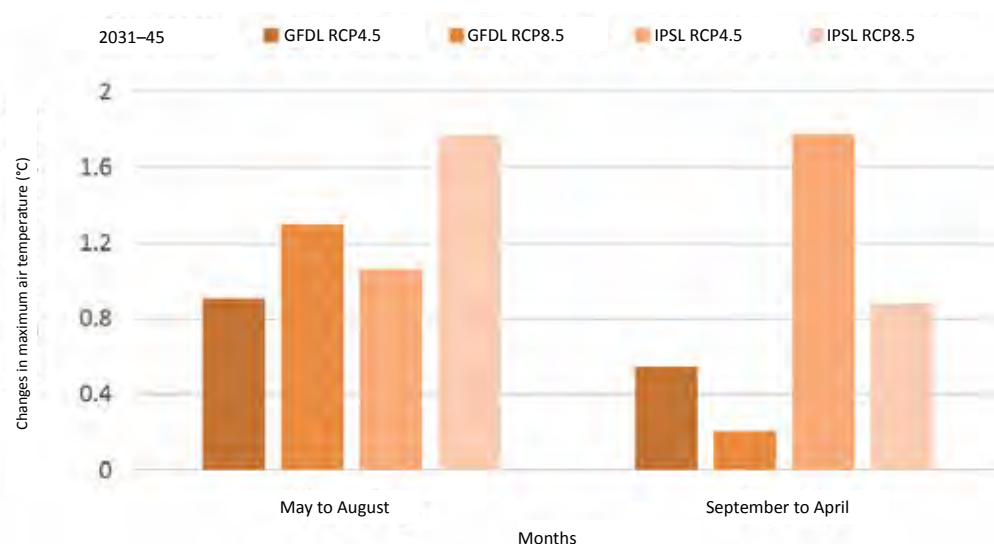


**Figure 6.12b** Estimated changes in maximum air temperature for 2031–45.

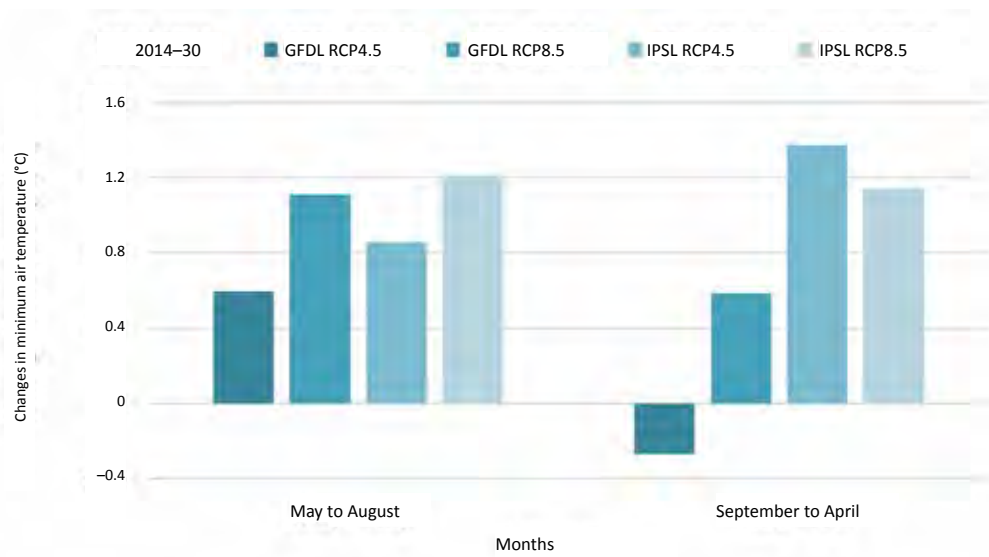


**Figure 6.13a** Estimated changes in minimum air temperature for 2014–30

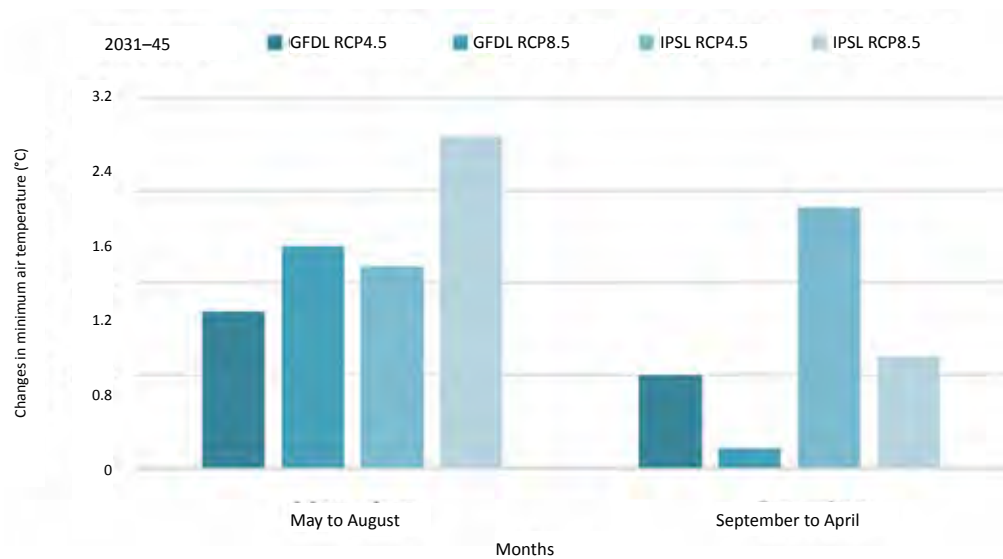


**Figure 6.13b** Estimated changes in minimum air temperature for 2031–45.

### 6.3.2 Estimates of future changes in glacier cover and volume

The extent of estimated glacier surface area and volume loss, which were predicted from initial ice thickness estimates, differed slightly among the various models and scenarios. The largest losses in glacier cover and volume were estimated to occur near the glacier terminus due to lower elevation and lower ice thickness in those areas (Figure 6.14).

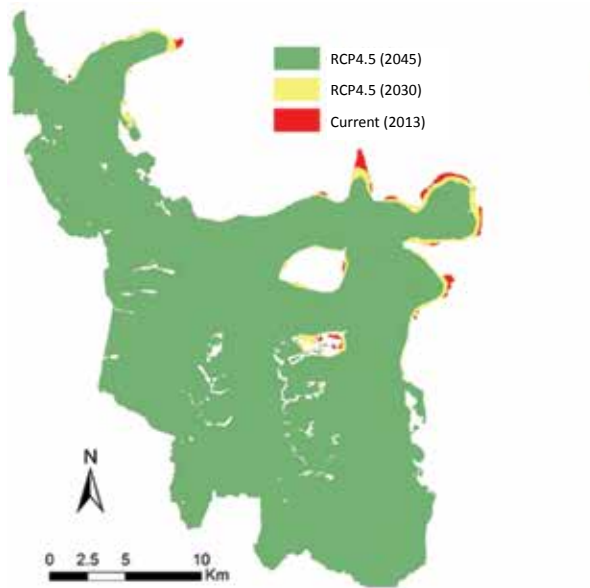


**Figure 6.14a** Estimated changes in extent of the Llewellyn and Willison glaciers using GFDL RCP4.5 climate model outputs in GCCM.

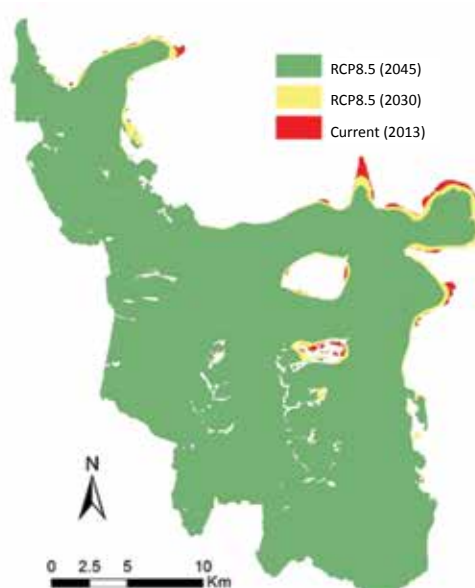


**Figure 6.14b** Estimated changes in extent of the Llewellyn and Willison glaciers using GFDL RCP8.5 climate model outputs in GCCM.

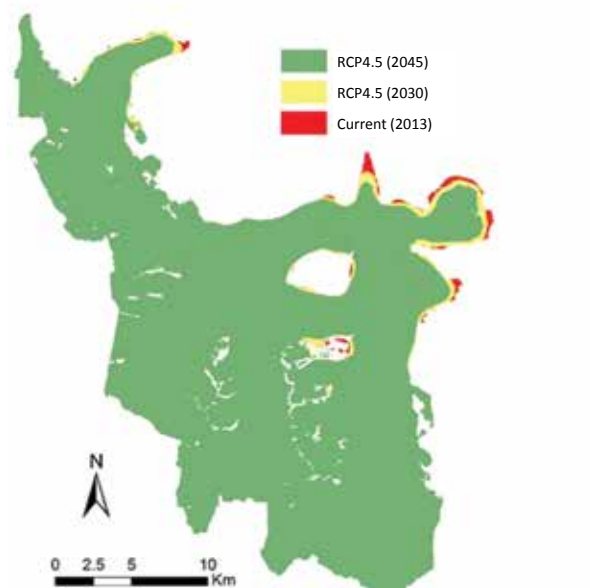


**Figure 6.14c** Estimated changes in extent of the Llewellyn and Willison glaciers using IPSL RCP4.5 climate model outputs in GCCM.

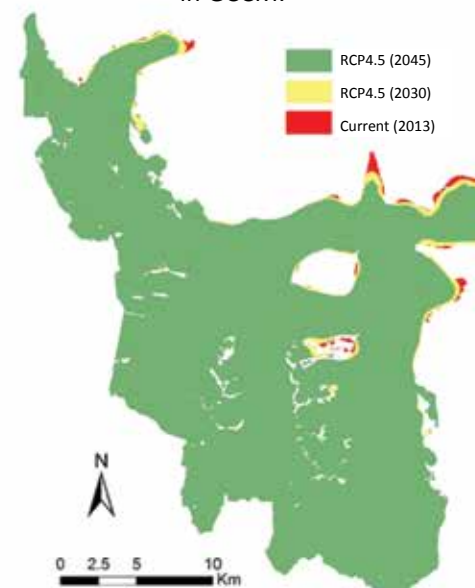


**Figure 6.14d** Estimated changes in extent of the Llewellyn and Willison glaciers using IPSL RCP8.5 climate model outputs in GCCM.

The RCP8.5 outputs both for the 2014–30 and 2031–45 periods estimated higher losses of glacier cover area and volume than the RCP4.5 outputs did, due to higher estimated increases in air temperature from May to August in the area of the Llewellyn and Willison Glacier (see Section 6.3.1.3).

**Table 6.3** Estimated changes in glacier surface area and volume and total surface area and volume for the Llewellyn and Willison glaciers for different time periods, models and scenarios.

Period	Model	Scenario	Glacier cover (Llewellyn and Willison Glaciers)			
			Estimated changes at the end of each period of analysis		Δ Change (current – future)	
			Area (km <sup>2</sup> )	Volume (km <sup>3</sup> )	Area (km <sup>2</sup> )	Volume (km <sup>3</sup> )
2014–30	GFDL	RCP45	508	131	–5	–10
		RCP85	507	127	–6	–14
	IPSL	RCP45	507	131	–6	–10
		RCP85	507	128	–6	–13
2031–45	GFDL	RCP45	497	120	–16	–21
		RCP85	493	112	–20	–29
	IPSL	RCP45	495	123	–18	–18
		RCP85	495	116	–18	–25

### 6.3.3 Contribution of climate related factors to changes in glacier cover and future flow

Sensitivity analysis is a technique used to determine how the values of an independent variable affect a dependent variable. In this case the independent variables are the climate variables and the dependent variables are glacier melt and river flow.

Sensitivity analysis was performed to examine the influence of the climate-related factors on long-term glacier cover and flow changes in the study basin. The analysis replaced a single climatic variable (e.g., precipitation, air temperature, relative humidity, and wind speed) for the period of 2006–13 with the GCM data for that variable. For example, a simulation was run in CRHM using precipitation, relative humidity and wind speed for the 2006–13 period and the mean air temperature estimated from the GCM data. It should be noted that for the sensitivity analysis, GCM data for the 2014–21 period was used instead of data for the 2014–30 period, in order to match the length of historical data records (2006–13). A total of 16 sensitivity analysis simulations were run in CRHM, including a “no change” simulation.

CRHM was found to be most sensitive to change in air temperature and precipitation (Figures 6.15 and 6.16). Ice melt values increased each time a change in air temperature was predicted; no strong difference was predicted when other climate variables were changed (Figure 6.15). For example, a change in air temperature (compared to the “No change” scenario) increased the ice melt values of the Llewellyn Glacier from approximately 2.3 m/year to 2.8 m/year at the 1,539–1,750 m elevation band and from approximately 4.6 m/year to 5.0 m/year at the 640–865 m elevation band (Figure

6.15). Only elevation bands in the ablation zone were considered, since ice melt does not occur in the accumulation zone. Ice melt is higher in the lowest ablation zone elevation band (640–865 m) than in the highest ablation zone elevation band (1,539–1,750 m).

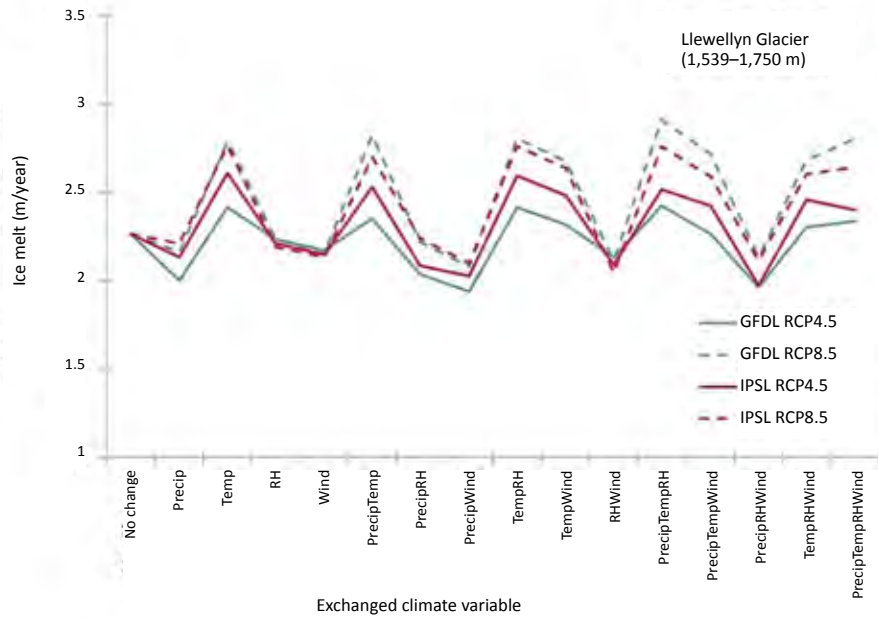


**Figure 6.15a** Sensitivity analysis of the influence of air temperature, precipitation, relative humidity and wind speed on changes in ice melt for the highest (1,539–1,750 m) ablation zone elevation bands.

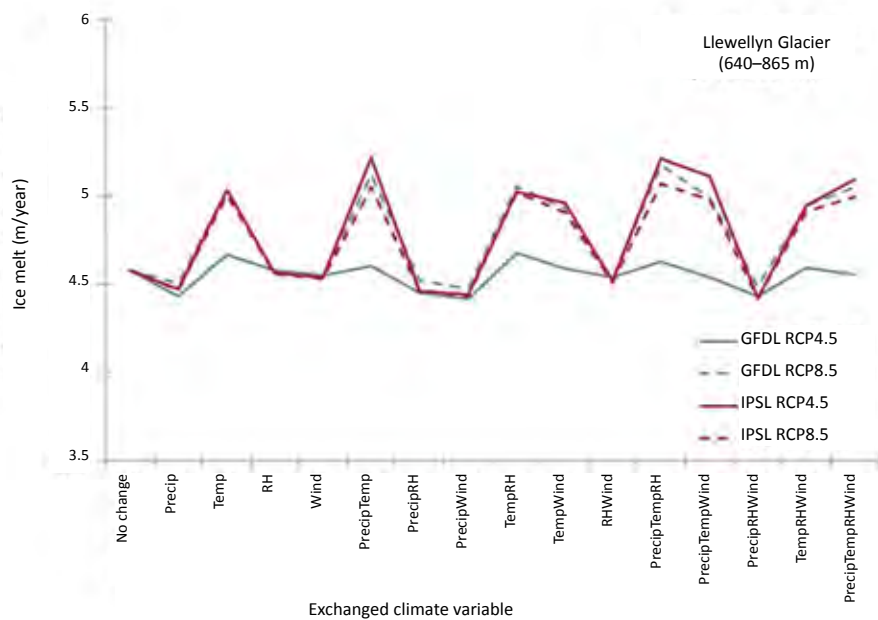


**Figure 6.15b** Sensitivity analysis of the influence of air temperature, precipitation, relative humidity and wind speed on changes in ice melt for the lowest (640–865 m) ablation zone elevation bands.

Flows in the Yukon River at Whitehorse outlet were influenced by changes in both air temperature and precipitation (Figure 6.16). Flows were more sensitive to changes in precipitation throughout most of the year, with the exception of April and July, where changes in both precipitation and air temperature influenced flow, and May and June, where only air temperature was found to influence flow. Here are some examples of changes, compared to the “No change” scenario:

- a change in precipitation in March increased flows from approximately 127 to 150 m<sup>3</sup>/second;
- a change in both air temperature and precipitation in April increased flows from approximately 116 to 135 m<sup>3</sup>/second; and
- a change in air temperature in May increased flows from approximately 130 to 181 m<sup>3</sup>/second.

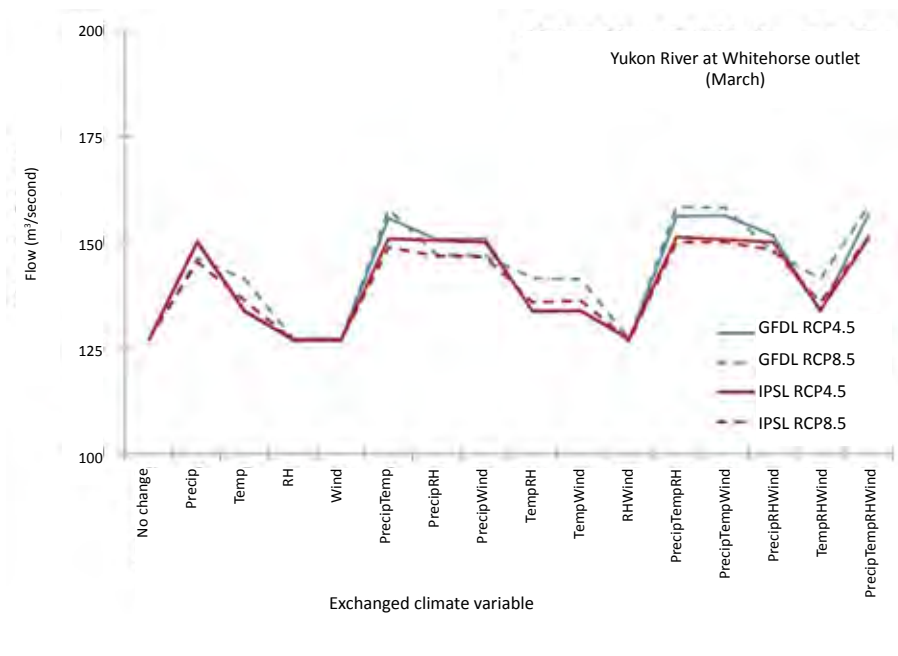


**Figure 6.16a** Sensitivity analysis of the influence of air temperature, precipitation, relative humidity and wind speed on changes in flow for the Yukon River at the Whitehorse outlet for the month of March.

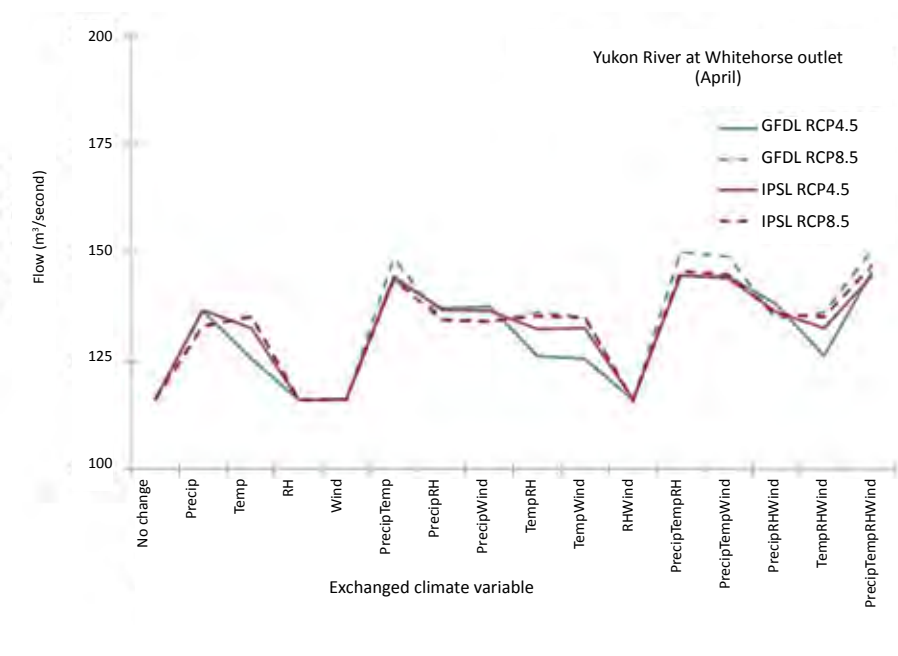


**Figure 6.16b** Sensitivity analysis of the influence of air temperature, precipitation, relative humidity and wind speed on changes in flow for the Yukon River at the Whitehorse outlet for the month of April.

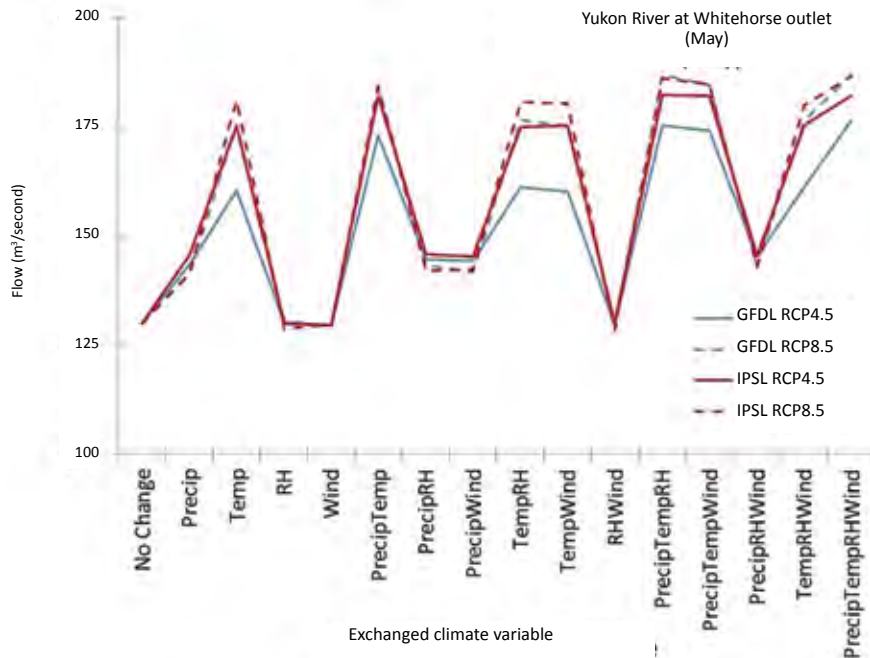


**Figure 6.16c** Sensitivity analysis of the influence of air temperature, precipitation, relative humidity and wind speed to changes in flow for the Yukon River at the Whitehorse outlet for the month of May.

Changes in air temperature and precipitation would have strong effects on increasing glacier wastage and glacier melts and therefore flows (Figure 6.17). All GCMs and scenarios estimate increases in glacier melt and wastage in the future (2014–30 and 2031–45), compared to the 2006–13 period (Figure 6.14), primarily due to changes in air temperature and precipitation. The increases in glacier wastage vary among GCMs and scenarios, from 15 to 65% and 30 to 90%; increases in glacier melt vary from 3 to 14% and 0 to 27% for 2014–30 and 2031–45, respectively.

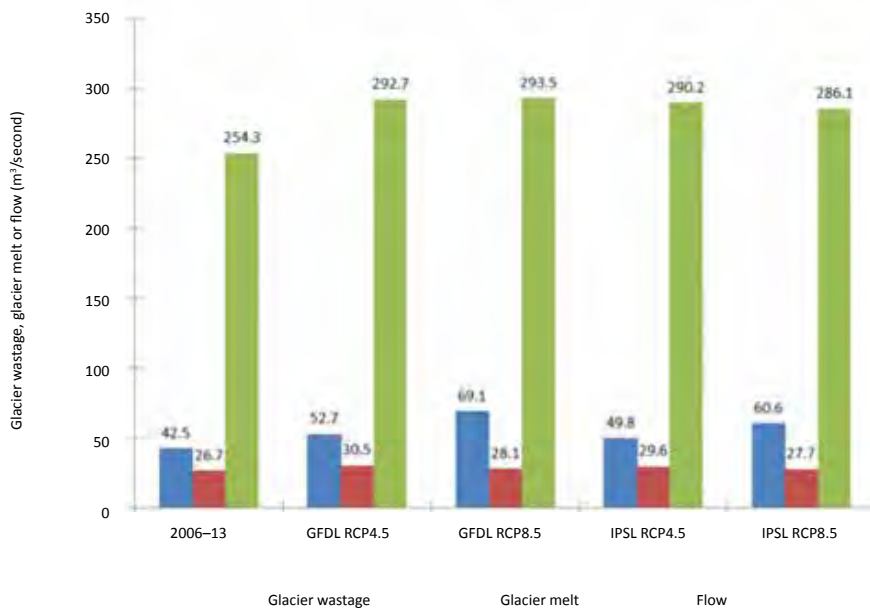


**Figure 6.17a** Comparison of annual glacier wastage, glacier melt and flows in the Yukon River at Whitehorse outlet for current (2006–13) and future periods (2014–30).

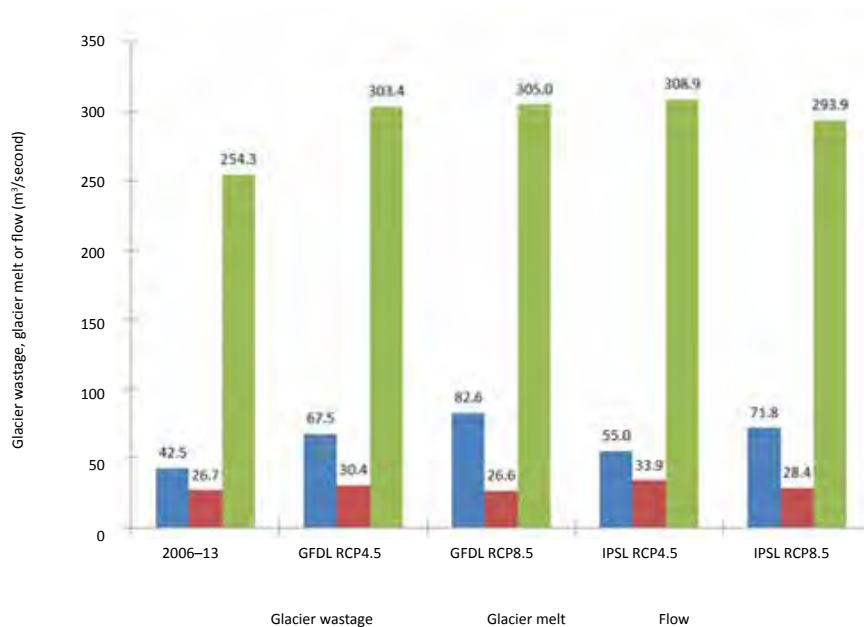


**Figure 6.17b** Comparison of annual glacier wastage, glacier melt and flows in the Yukon River at Whitehorse outlet for current (2006–13) and future periods (2031–45).

The estimated increase Yukon River flow at Whitehorse outlet varies among GCMs (Figure 6.17). Interestingly, flow projections for RCP 8.5 scenarios are not necessarily the highest. For example, for the period of 2031–45, IPSL RCP 4.5 resulted in higher estimated flow than IPSL RCP 8.5 due to the higher precipitation estimated by IPSL RCP4.5 (see Figure 6.4d). Flow was also more sensitive to changes in precipitation throughout most of the year, with the exception of May–June when temperature changes have a greater impact on flow.

Figure 6.18 compares the average glacier wastage, glacier melt, and subsurface flow for the 2006–13 and 2014–30 periods derived from GFDL for the RCP4.5 scenario. For the sake of simplicity, only the results of the GFDL RCP4.5 scenario for 2014–30 are plotted; the results from the other model, scenario and time period were similar.

Glacier wastage is the largest contributor to flow and is predicted to increase from mid-May to the beginning of October; this is likely attributed to changes in air temperature in the glacierized areas (Figure 6.15). Estimated changes in glacier melt are smaller than those for glacier wastage, and glacier melt is predicted to both increase and decrease relative to the current period. The increase in glacier melt can be attributed to warming air temperatures and to an estimated general increase in precipitation across the entire region (Section 6.3.1), which would increase snow accumulation and thus glacier melt. Subsurface flow is predicted to increase across all seasons, with the largest increases from April to December. This can be attributed to soil infiltration and runoff routing processes, which delay and attenuate subsurface flows throughout the year.

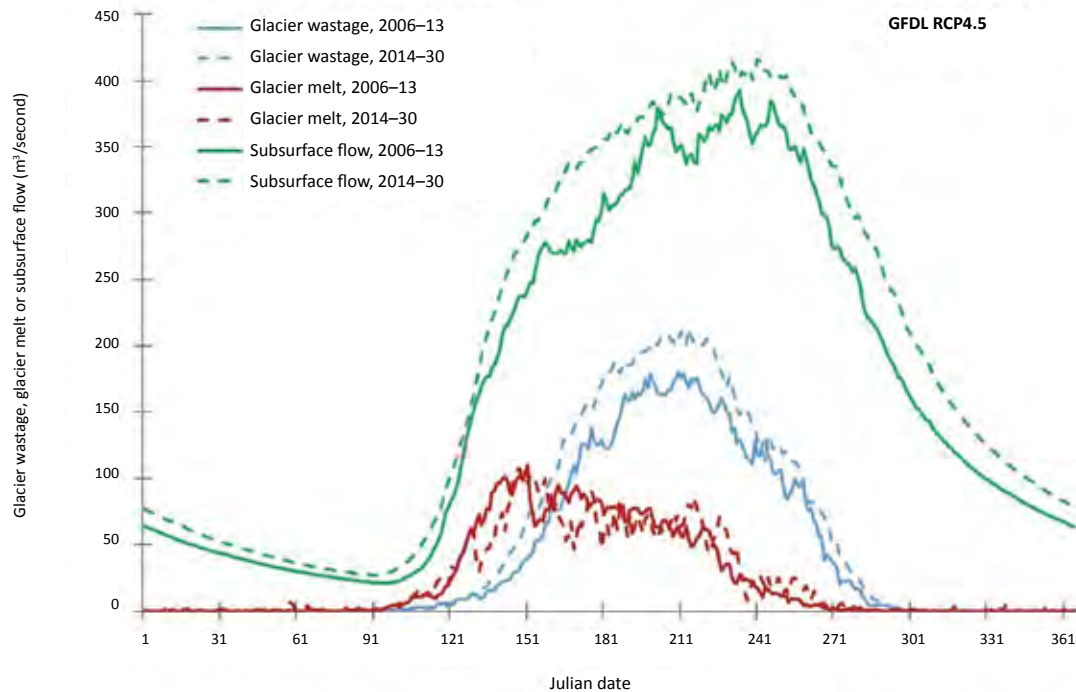


**Figure 6.18** Comparison of glacier melt, glacier wastages and subsurface flows for current (2006–13) and future periods (2014–30).

Note: Data are derived from the GFDL model, RCP4.5 scenario.

Increases in glacier melt, glacier wastage and subsurface flows result in estimated increases in river flow of approximately 15 to 18% for the 2014–30 period and 18 to 26% for the 2031–45 period, relative to the 2006–13 period (Figure 6.19). Higher changes were estimated during winter (DJF) and spring (MAM) than during summer (JJA) and autumn (SON), for both the 2014–30 and 2031–45 periods (Table 6.4). The future flow changes during spring, summer, autumn and winter flows, respectively averaging values for all two GCMs and two scenarios relative to the 2006–12 period, are 24%, 13%, 13% and 18% (for 2014–30) and 33%, 19%, 18%, and 22% (for 2031–45; see Table 6.4).

In addition, change in the timing of flow was estimated by computing the dates when the annual maximum flows occurred and the date when half of the total annual volume of water (i.e., centre of total annual flows) arrived in Whitehorse. In general, the timing of annual maximum flow and centre of total annual flow happen earlier, although timing of peak flow under GFDL RCP 8.5 is either unchanged or slightly later. The average date of both the annual maximum flow and the centre of total annual flow (i.e., averaging all values for the 2014–30 and 2031–45 periods and GCMs and scenarios) in Whitehorse are projected to shift approximately four days earlier relative to 2006–13 (Table 6.4). These results indicate that the future volume of water at the Whitehorse outlet will increase, but seasonal and annual flow patterns would not change substantially.

**Table 6.4** Percentage change of seasonal flow and timing changes of occurrences of annual maximum flows and centre of total annual flows (when half of total annual volume of water flowing into the Whitehorse outlet)

GCM	Seasonal changes				Annual changes		
	% change of flow (future vs. current periods)				% change of flow (future vs. current periods)	Average date of occurrence	
	MAM	JJA	SON	DJF	Annual flow	Annual maximum flow	Centre of total annual flow
Current period (2006–13)							
	—	—	—	—	—	20 Aug	9 Aug
Future period (2014–30)							
GFDL RCP4.5	22	14	14	20	17	15 Aug	6 Aug
GFDL RCP8.5	27	15	14	19	18	21 Aug	5 Aug
IPSL RCP4.5	23	13	14	18	17	10 Aug	6 Aug
IPSL RCP8.5	24	12	11	14	15	16 Aug	5 Aug
Average value for 2014–30	24	13	13	18	17	15 Aug	5 Aug
Future period (2031–45)							
GFDL RCP4.5	32	21	16	22	23	10 Aug	3 Aug
GFDL RCP8.5	36	20	17	22	24	25 Aug	3 Aug
IPSL RCP4.5	35	20	21	27	26	13 Aug	3 Aug
IPSL RCP8.5	26	14	17	17	18	21 Aug	6 Aug
Average value for 2031–45	33	19	18	22	23	17 Aug	3 Aug

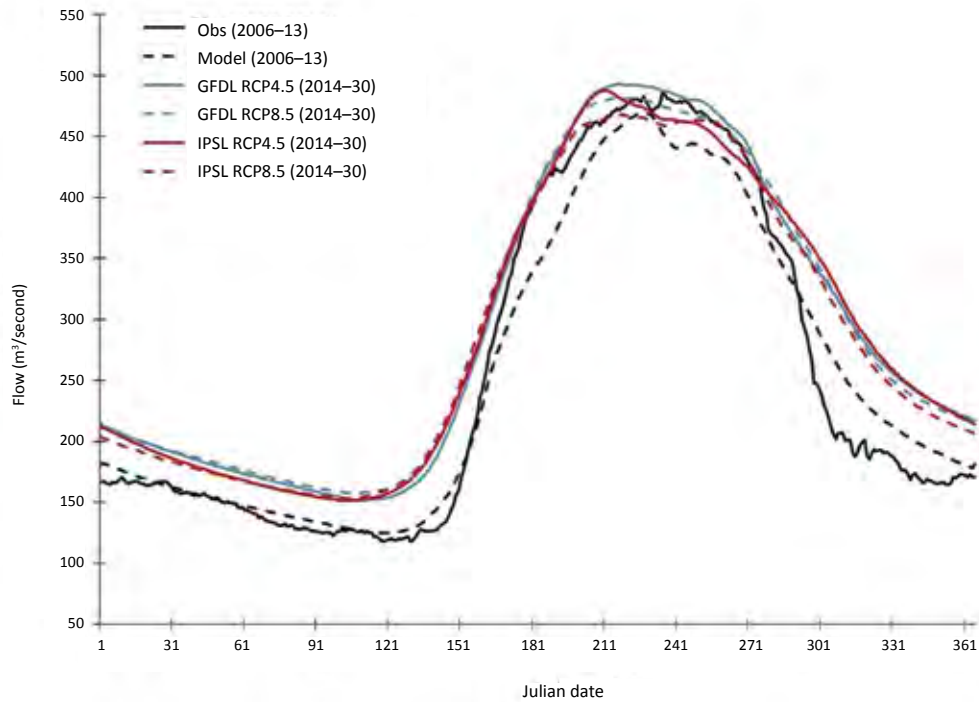


**Figure 6.19a** Comparison of flows at the Yukon River at the Whitehorse outlet for current (2006–13) and future periods (2014–30).

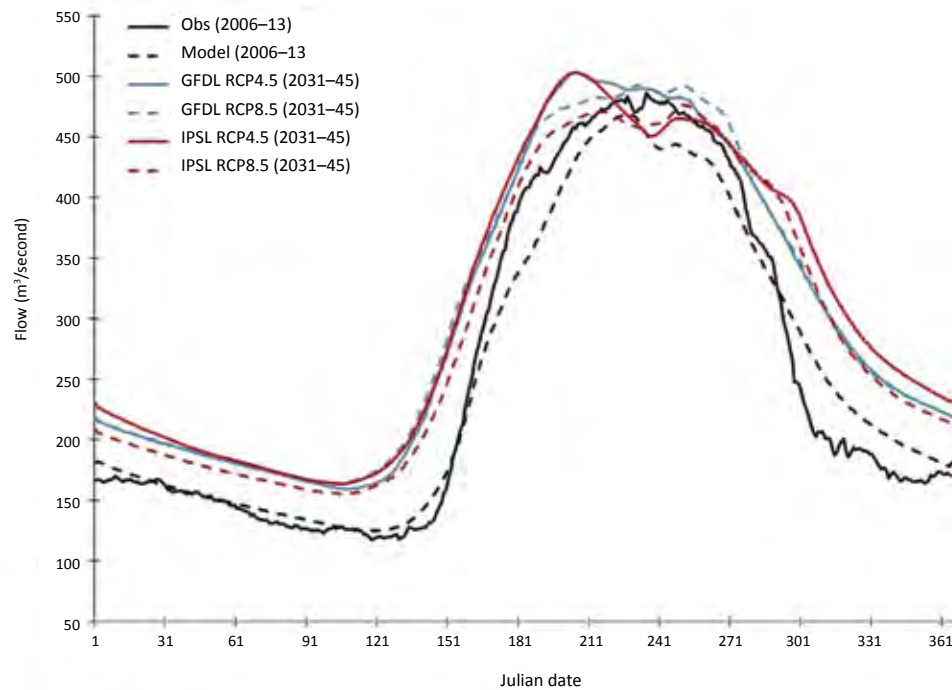


**Figure 6.19b** Comparison of flows at the Yukon River at the Whitehorse outlet for current (2006–13) and future periods (2031–45).

## 6.4 Conclusions

The CRHM was forced by GCM outputs derived from GFDL and IPSL models under the RCP4.5 and RCP8.5 scenarios to predict future climate change responses in the upper Yukon River basin for two time periods: 2014–30 and 2031–45. Projected changes in spatial and temporal climatic variables differed depending on the time period, model and scenario applied. Larger variabilities in climatic variables were found between models than between scenarios.

Spatially, both models predicted increases in maximum and minimum air temperature and in precipitation across the majority of the basin, relative to current conditions. Relative humidity was estimated to both increase and decrease across the basin relative to current conditions. The GFDL model predicted both increases and decreases in wind speed relative to current conditions, whereas the IPSL model estimated slight increases in wind speed. Temporal variations of the climate variables differed depending upon the scenario, model and time period.

Among the climate variables described above, particular attention should be paid to changes in air temperature and precipitation. As demonstrated by the sensitivity analysis (Section 6.3.3), change in air temperature is the dominant contributor to changes in glacier area/volume and glacier melt, although both air temperature and precipitation were found to strongly influence flows in the Yukon River at the Whitehorse outlet. Air temperature is the dominant contributor to changes in future flow in May and June. Air temperature and precipitation influenced flow in April and July, and precipitation was the dominant contributor to flow for the other months. Changes in air temperature and precipitation influence glacier wastage, glacier melt and subsurface flows, and thus river flow at the basin outlet. Both GCMs and scenarios estimated increases of flows in the Yukon River at the Whitehorse outlet; these ranged from 15 to 18% for the 2014–30 period and from 18 to 26% for the 2031–45 period, relative to the 2006–13 period. The increases of flows during spring, summer, autumn and winter averaging values of all GCMs and scenarios 24%, 13%, 13% and 18% (for 2014–30) and 33%, 19%, 18%, and 22% (for 2031–45), respectively. The timing of the annual maximum flows and the centre of annual volume of water at Whitehorse shift approximately four days earlier than those of the current period, with the variations of the shift of the centre of seasonal flows varying between zero and four days.

## 7. Considering uncertainties and recommendations for future work

This section suggests potential research avenues that can be explored to follow up on this project and outlines strategies for supporting future work by YEC on climate change adaptation.

### 7.1 Hydrological characteristics of the upper Yukon River basin

In order to predict future changes in river flow due to climate change, it is important to first understand the hydrological characteristics of the upper Yukon River basin (see Sections 1 and 5). The project's analysis allowed for an in-depth exploration of how climate, heterogeneous land cover, topography and glacierized areas along the Pacific mountainous regions in the west contribute to river flow. Based on sensitivity testing of the CRHM for the 2006–13 period, the complex combination of the spatial and temporal variability of climate and the spatial variability of topography and land-cover characteristics strongly control the timing and magnitude of hydrological variables, including snow and ice accumulation and melt. Any significant changes in climate and land cover relative to current conditions may cause appreciable changes in flow.

The study was successful in capturing basin-scale glacier melt, glacier mass balance and stream and river flows; thus, it provides a strong foundation for predicting future glacier cover and flow changes in upper Yukon River basin. It also expanded the weather, snowpack and climate monitoring infrastructure for the region, which will allow for better detection and tracking of changes in hydrological conditions over time. The decision to address glacier and climate changes as part of this study was guided by the understanding that these are the hydrological factors that have the greatest effect on the timing and volume of flow in the basin (Solomon et al. 2007; Hinzman et al. 2005; Woo et al. 1992). There are two key areas where further improvements in availability of data and understanding of hydrological processes will advance hydrological modelling:

- greater understanding of the role of permafrost in hydrology and of the distribution and characteristics of permafrost in the upper Yukon River basin. There is no high-resolution map of permafrost distribution in Yukon, and further work is required to fully understand how the many properties of permafrost affect hydrogeology and hydrology; and
- improvement in the spatial resolution of soil data and land-cover data. Higher resolution data in either of these variables might increase complexity of the model (by creating a need for more HRUs), but would also help decrease uncertainty.

Further work in either of these areas would help improve the ability of this implementation of CRHM for upper Yukon River basin to simulate current and future flow. For YEC, it is recommended that staff remain aware of research work by other organizations that may contribute to understanding in these key areas.

### 7.2 Anticipated climate changes

Since air temperature, precipitation, relative humidity and wind speed were used as the main climatic variables in CRHM, the analysis of future climate change focused on the spatial and temporal variation of these four variables. Particular attention should be paid to changes in air temperature and precipitation, since sensitivity analysis demonstrated that these two variables are the dominant contributors to increases in glacier melt and glacier wastage, which influences flow in the basin outlet.

In addition, larger differences between GCM outputs were found for air temperature and precipitation than for relative humidity and wind speed (Section 6). To help manage the uncertainty introduced by using GCM data, it is recommended that YEC monitor new releases and significant developments in the climate modelling field, and update the model input data accordingly. To run the model again using new climate projections, GCM data must be bias corrected with observational data prior forcing in CRHM. The bias-correction model software described in Section 6 can be used to correct GCM outputs. The model and its manual are delivered together with this project (NCE 2016).

### **7.3 Future glacier cover and changes in river flow**

Changes in climatic variables — particularly increases in air temperature — influence the timing and amount of snowmelt and ice melt, and thus affect glacier surface area and volume. For the Llewellyn and Willison glaciers, the two largest glaciers in the basin, the estimated average losses of surface area and volume from the end of 2013 to the end of 2045 were approximately 0.3–0.7 km<sup>2</sup>/year and 0.5–0.9 km<sup>3</sup>/year, respectively. At this time, there is no ongoing direct measurement of glacier mass balance. For YEC to understand and continually forecast the contributions of glaciers to river flow, methods to monitor glacier mass balance should be investigated and implemented.

The two GCMs and scenarios estimated higher future flow of the Yukon River at the Whitehorse dam, with increases ranging from 15 to 18% for the 2014–30 period and 18 to 26% for the 2031–45 period, relative to the 2006–13 period. The increase of flow is strongly related to the increase of glacier melt, glacier wastage and subsurface flows. However, it should be noted that the results may contain uncertainties because of the limited availability of observation data to be applied in CRHM (see Section 7.4). It is recommended that YEC consider adjusting the CRHM model only if there are major new findings (e.g., new mapping of permafrost and/or soil distribution and characteristics) from researchers working in this basin.

To estimate changes in glacier cover and subsequent changes in river flow entering the Whitehorse dam for time periods that differ from those used in this current study (2014–30 and 2031–45), the coupled Glacier Cover Change Model (GCCM) and CRHM (see Section 6.2.2) can be used by modifying the time period. However, the current version of the CRHM-GCCM model doesn't incorporate techniques to correct and update states of the hydrological model for a short period of time (see Section 7.5.5).

### **7.4 Model uncertainty**

Every modeling approach is subject to uncertainty. The complexity of natural systems and limits to our ability to measure and understand them presents challenges to even the best physically-based model. The quality of the CRHM outputs is determined by three factors:

- 1. Quality of input data and model parameters**

Model output uncertainties in this study can be caused by input data and model parameters (i.e., land-cover, elevation, soil, and meteorological data) that include high variability in both space and time, scarce data due to the limited amount of work that has been done in the region, and inaccurate determination of appropriate data and parameter values due to environmental complexity.

## **2. Selection of CRHM modules and mathematical description of physical processes**

Selection of CRHM modules for this study basin can cause model output uncertainty. Numerous equations and modules are available in CRHM. Modules that could provide better model outputs require a higher number of model parameters and additional observational data, which were limited for this basin. Mathematical description cannot fully describe physical processes in this basin. In addition, calibrated model parameters and/or model parameters derived from other regions might not accurately represent hydrological processes in the study basin and may cause uncertainty about model outputs. However, CRHM is always being improved and new modules might be developed in the future.

## **3. Use of other models and additional data to support simulating CRHM.**

Model output uncertainty can also be caused by the use of other models and additional data to support simulating CRHM. For example, this project used data-correction methods to correct GEM data with observational data and used an interpolation method to spatially distribute and temporally disaggregate meteorological data to specific points in the basin. Raw GEM data derived from modeling processes may contain uncertainties. Thus, the correction of GEM data and the use of additional models, given the limited availability of observational data and data records, can cause model output uncertainty.

For these reasons, it is not possible for the model to precisely reproduce observed streamflow, glacier mass balance, and SWE values and variation. All methods and input data for this study have been carefully chosen and evaluated. Based on the metrics used to evaluate model fit, the implementation of CRHM for the upper Yukon River basin appears to accurately reconstruct observed streamflow, mass balance characteristics, and SWE (see Section 5). Modelling efforts from the smaller Wolf Creek basin report similar fit (Rasouli et al. 2014), and models of small and large basins using CRHM and other hydrological models also report comparable fit (Zhou et al. 2014; Graham et al. 2007). However, it is still recommended that YEC remain aware of ongoing research work conducted in the region that may contribute to reducing uncertainty about model outputs.

## **7.5 Recommendations for future research**

The following recommendations for future research result from field observations, model development and model results. These recommendations are considered less crucial for the expected uses of the CRHM model by YEC, but would contribute to improvements in hydrological modelling. These recommendations were not implemented in the context of this study due to constraints in time, budget, personnel, data and/or software.

### **7.5.1 Reducing the uncertainty of climate projections**

The project applied interpolation, bias correction and disaggregation methods to correct the bias of the GCM outputs prior to using them for hydrological projections. This reduced the uncertainties associated with climate data by a minimum of 9% (relative humidity) and a maximum 335% (precipitation). Other data-correction methods could be used to further reduce uncertainty about predicting future climate change:

- statistical and physical downscaling methods or a combination of statistical, physical downscaling and bias correction methods; and
- more advanced bias correction approaches for correcting data on relative humidity and wind speed, although the availability of such approaches is limited at this time.

### 7.5.2 Improving estimates of spatial distribution of ice thickness and glacier cover

This project made progress in measuring the ice thickness of glaciers in the headwaters of the upper Yukon River basin. Estimates of ice thickness can be further improved in two ways:

- applying and comparing different models. There are several approaches to estimating glacier thickness, such as a combination of mass balance and ice-flow dynamics (Farinotti et al. 2009); a combination of mass balance, ice-flow dynamics and ground-measured data (Farinotti et al. 2013; Zekollari et al. 2013; Colgan et al. 2012); a combination of ice-flow model and photogrammetric data (Kääb 2000); a physically based volume-area power-law scaling relation (Bahr et al. 1997); a combination of field-measured data and regression techniques (Peduzzi et al. 2010; Clarke et al. 2009); and analytical models for the estimation of mass balance (Michel et al. 2013; Morlighem et al. 2011). Some methods require specific field observations (such as estimates of glacier velocity and ice flux), and some can be applied only to certain local glacial characteristics; and
- obtaining more field data to more accurately capture physical processes and increase model certainty. Expanding field observations (i.e., through GPR and ablation wires) to larger areas would improve estimates of the spatial distribution of ice thickness and glacier cover. The Willison Glacier and the northern portion of the Llewellyn Glacier, as well as other smaller glaciers in the basin, still require GPR surveys. It is recommended that ablation wire surveys be conducted on a regular basis over a range of elevations. Other field surveys, such as surface ice flow and strain rates, would also be beneficial in order to better understand glacier mass balance. However, these approaches are expensive and the results are highly dependable on weather, equipment used, and environmental conditions.

Estimates of glacier volume and surface area can be improved in two ways:

- further analysis of satellite imagery for improved interpretation of changes in glacier surface area; and
- finer resolution of elevation bands in CRHM and GCCM to obtain more accurate data on glacier surface area and volume losses — however, this approach could significantly increase the time required for model simulation and the number of parameters to be determined/calibrated/adjusted.

### 7.5.3 Improving the density of meteorological station networks

The low number and limited spatial distribution of meteorological stations in the study basin remain problematic, although this project has helped to address the issue. Visual inspections show that both the eastern and north-central regions of the basin would particularly benefit from additional meteorological stations. The basin is large and is heterogeneous in climate, land cover and topography; this requires a strong hydrometeorological network, particularly when applying a physically based distributed model such as CRHM. Additional meteorological data (GEM) was used in this study to fill the meteorological gaps; however, this data first had to be corrected to address data bias.

The Coupled Regionalization and Dual Entropy and Multi-Objective Optimization approach (Samuel et al. 2013) is a novel modeling method that can determine the ideal number of stations and placement locations. The approach is based on determining optimal trade-offs between the

maximum possible information content and the minimum amount of shared information among stations. It can serve as a guideline prior to installing new stations, although the final decision on new stations should consider many factors, such as cost, applicability, and local and/or regional needs and policies.

#### **7.5.4 Improving river flow estimates**

River flow estimates for current and future periods could be improved by coupling hydrological and 2D/3D hydraulic models. Hydrological models are used to estimate the total volumetric flow for a river, while hydraulic models compute lateral flows and their profiles, evaluate profiles at river confluences, and compute sediment transport. Coupled, these models may be able to improve hydrograph estimates, particularly for the upper Yukon River basin, which consists of a series of connected lakes and dynamic rivers. However, preparing the set-up and parameters for a hydraulic model could be challenging. For example, it requires information about river cross-section geometry and hydraulic structures, and extensive model calibration.

#### **7.5.5 Model limitations and model development**

This study uses a model that treats glaciers as static ice masses that melt in place and decrease in volume over time, with no lateral movement of the frozen mass. An initial idea was to couple an ice dynamic model and a physically distributed model, such as the one developed by Naz et al. (2014). That model uses a low-order ice dynamics model coupled with the Distributed Hydrology Soil Vegetation Model (Wigmosta et al. 1994) to dynamically adjust the glacierized areas and volume, depending on accumulation and ablation conditions at each time interval. Even though the model developed by Naz et al. shows promising results, it is computationally expensive and poorly suited for extensive regions with sparse climate data (B.S. Naz, pers. comm.). However, it has the potential to accurately model glacier mass balance dynamics and may be appropriate for smaller basins.

The developed model — which combines CRHM and GCCM— is currently applicable to long-term flow forecasts, and could be expanded for short-term forecasts. In order to do so, further study would be required to select the most appropriate forecasting data and the most appropriate ways to interpolate, correct and disaggregate the data. In addition, the hydrological states of the model would need to be updated and corrected prior to and after simulating each forecast because of the differences between observed and forecast meteorological data. Data assimilation approaches, which are commonly used for forecasting climate, have the capability to correct and update states of the hydrological model (Samuel et al. 2014; Moradkhani et al. 2005a and b). Since the CRHM, GCCM and data assimilation approaches require extensive computation and would have to be run simultaneously over a certain number of simulations, it would be important to carefully select a data assimilation model that fits best with the CRHM and GCCM. In addition, data assimilation parameters would need to be examined and adjusted accordingly. Development of an effective and efficient forecast model would require intensive discussions with CRHM and GCCM model developers, hydrologists and potentially, computer programmers.

## References

- Annandale, J.G., N.Z. Jovanovic, N. Benadé and R.G. Allen. 2002. "Software for missing data error analysis of Penman-Monteith reference evapotranspiration." *Irrigation Science* 21: 57–67. doi: 10.1007/s002710100047.
- Ayers, H.D. 1959. Influence of soil profile and vegetation characteristics on net rainfall supply to runoff. In: *Proceedings of Hydrology Symposium No.1: Spillway Design Floods*. Ottawa: Research Council Canada, pp. 198–205.
- Bahr, D.B., M.F. Meier and S.D. Peckham. 1997. "The physical basis of glacier volume-area scaling." *Journal of Geophysical Research* 102: 20,355–20,362. doi:10.1029/97JB01696.
- Berthier, E., E. Schiefer, G.K.C. Clarke, B. Menounos and F. Rémy. 2010. "Contribution of Alaskan glaciers to sea-level rise derived from satellite imagery." *Nature Geoscience* 3: 92–95.
- Beven, K.J. 2001. "How far can we go in distributed hydrological modelling?" *Hydrology and Earth System Sciences* 5(1): 1–12.
- Beven, K.J. 1985. Distributed modelling. In: Anderson, M.G. and T.P. Burt (eds.). *Hydrological Forecasting*. Chichester, UK: Wiley, pp. 405–435.
- Beven, K.J. and P.E. O'Connell. 1982. *On the Role of Physically-based Distributed Models in Hydrology*. Report No. 81. Wallingford, UK: Institute of Hydrology.
- Bitz, C.M. and D.S. Battisti. 1999. "Interannual to decadal variability in climate and the glacier mass balance in Washington, western Canada, and Alaska." *Journal of Climate* 12: 3,181–3,196.
- Boberg, F., P. Berg, P. Thejll and J.H. Christensen. 2007. *Analysis of Temporal Changes in Precipitation Intensities using PRUDENCE Data*. Danish Climate Centre Report 07-03. Denmark: Danish Meteorological Institute.
- Bonnaventure, P.P. and A.G. Lewkowicz. 2011. "Modelling climate change effects on the spatial distribution of mountain permafrost at three sites in northwest Canada." *Climatic Change* 105: 293–312. doi: 10.1007/s10584-010-9818-5.
- Brabets, T.P. and M.A. Walvoord. 2009. "Trends in streamflow in the Yukon River Basin from 1944 to 2005 and the influence of the Pacific Decadal Oscillation." *Journal of Hydrology* 371: 108–119.
- Braithwaite, R.J. 1995. "Positive degree-day factors for ablation on the Greenland ice sheet studied by energy-balance modelling." *Journal of Glaciology* 41(137): 153–160.
- Brock, B.E., B.B. Wolfe and T.W.D. Edwards. 2007. "Characterizing the hydrology of shallow floodplain lakes in the Slave River Delta, NWT, Canada, using water isotope tracers." *Arctic, Antarctic and Alpine Research* 39: 388–401.
- Bronk Ramsey, C. 2013. OxCal v. 4.2.4. <https://c14.arch.ox.ac.uk/login/login.php?Location=%2Foxcal%2FOxCal.html> [accessed October, 2015].
- Brooks, R.H. and A.T. Corey. 1964. *Hydraulic Properties of Porous Media*. Hydrology Papers 3. Fort Collins, CO: Colorado State University.
- Brown J., A. Kholodov, V. Romanovsky, K. Yoshikawa, S. Smith, H. Christiansen, G. Viera and J. Noetzli. 2010. "The Thermal State of Permafrost: the IPY-IPA snapshot (2007-2009)." In *Proceedings of the 63rd Canadian Geotechnical Conference and 6th Canadian Permafrost Conference*, Calgary, Canada, September 2010, 12–16.

- Cable, J., K. Ogle and D. Williams. 2011. "Contribution of glacier meltwater to streamflow in the Wind River Range, Wyoming, inferred via a Bayesian mixing model applied to isotopic measurements." *Hydrological Processes* 25: 2,228–2,236.
- Carey, S.K. and W.L. Quinton. 2004. "Evaluating snowmelt runoff generation in a discontinuous permafrost catchment using stable isotope, hydrochemical and hydrometric data." *Nordic Hydrology* 35: 309–324.
- Carey, S.K. and M-K. Woo. 2005. "Freezing of subarctic hillslopes, Wolf Creek Basin, Yukon." *Arctic, Antarctic and Alpine Research* 37: 1–10.
- Carey, S.K., D. Tetzlaff, J. Seibert, C. Soulsby, J. Buttle, H. Laudon, J. McDonnell, K. McGuire, D. Caissie, J. Shanley, M. Kennedy, K. Devito and J.W. Pomeroy. 2010. "Inter-comparison of hydro-climatic regimes across northern catchments: synchronicity, resistance and resilience." *Hydrological Processes* 24(24): 3,591–3,602. doi: 10.1002/hyp.7880.
- Chen, J., J.F. Franklin and T.A. Spies. 1993. "An empirical model for predicting diurnal air-temperature gradients from edge into old-growth Douglas-fir forest." *Ecological Modelling* 67: 179–198.
- Chen, J. and A. Ohmura. 1990. "Estimation of Alpine glacier water resources and their change since the 1870s." *International Association of Hydrological Sciences* No. 193: 127–135.
- Clague, J.J., J. Koch and M. Geertsema. 2010. "Expansion of outlet glaciers of the Juneau Icefield in northwestern British Columbia during the past two millennia." *The Holocene* 20(3): 447–461.
- Clark, C.O. 1945. "Storage and the unit hydrograph." *Proceedings of the American Society of Civil Engineering* 69: 1,419–1,447.
- Clarke, G.K.C, E. Berthier, C.G. Schoof and A.H. Jarosch. 2009. "Neural networks applied to estimating subglacial topography and glacier volume." *Journal of Climate* 22: 2,146–2,160. doi: 10.1175/2008JCLI2572.1.
- Colgan, W., W.T. Pfeffer, H. Rajaram, W. Abdalati and J. Balog. 2012. "Monte Carlo ice flow modeling projects a new stable configuration for Columbia Glacier, Alaska." *The Cryosphere* 6: 1,395–1,409. doi: 10.5194/tc-6-1395-2012.
- Coplen, T.B. 1996. "New guidelines for reporting stable hydrogen, carbon and oxygen isotope-ratio data." *Geochimica et Cosmochimica Acta* 60: 3,359–3,360.
- Coplen, T.B. 1994. "Reporting of stable hydrogen, carbon and oxygen isotopic abundances." *Pure and Applied Chemistry* 68 (2): 273–276.
- Côté J., J.G. Desmarais, S. Gravel, A. Méthot and A. Patoine. 1998a. "The operational CMC-MRB Global Environmental Multiscale (GEM) Model. Part II: Results." *Monthly Weather Review* 126(6): 1,397–1,418.
- Côté, J., S. Gravel, A. Méthot, A. Patoine, M. Roch and A. Staniforth. 1998b. "The operational CMC-MRB Global Environmental Multiscale (GEM) Model. Part I: Design considerations and formulation." *Monthly Weather Review* 126(6): 1,373–1,395.
- Craig, H. 1961. "Isotopic variations in meteoric waters." *Science* 133: 1,702–1,703.
- DeBeer, C.M., H.S. Wheeler, S.K. Carey and K.P. Chun. 2016. "Recent climatic, cryospheric and hydrological changes over the interior of western Canada: a review and synthesis." *Hydrology and Earth System Sciences* 20: 1,573–1,598. doi: 10.5194/hess-20-1573-2016.
- Déry, S.J., M.A. Hernández-Henríquez, J.E. Burford and E.F. Wood. 2009. "Observational evidence of an intensifying hydrological cycle in northern Canada." *Geophysical Research Letters* 36: L13402. doi: 10.1029/2009GL038852.

- Dornes, P.F., J.W. Pomeroy, A. Pietroniro, S.K. Carey and W.L. Quinton. 2008. "Influence of landscape aggregation in modelling snow-cover ablation and snowmelt runoff in a sub-arctic mountainous environment." *Hydrological Sciences Journal* 53: 725–740.
- Edwards, T.W.D., B.B. Wolfe, J.J. Gibson and D. Hammarlund. 2004. Use of water isotope tracers in high-latitude hydrology and paleohydrology. In Pienitz, R, M. Douglas and J.P. Smol (eds.). *Long-term Environmental Change in Arctic and Antarctic Lakes*. Dordrecht, The Netherlands: Kluwer Academic Publishers, pp. 187–207.
- Ellis, C.R. and J.W. Pomeroy. 2007. "Estimating sub-canopy shortwave irradiance to melting snow on forested slopes." *Hydrological Processes* 21 (19): 2,581–2,593. doi: 10.1002/hyp.6794.
- Ellis, C.R., J.W. Pomeroy, T. Brown and J. MacDonald. 2010. "Simulation of snow accumulation and melt in needleleaf forest environments." *Hydrology and Earth System Sciences* 14: 925–940. doi: 10.5194/hess-14-925-2010.
- ESRI (Environmental Systems Research Institute). 2011. Arc Hydro Tools Tutorial. Redland, CA: ESRI.
- Essery, R. 1997. "Modelling fluxes of momentum, sensible heat and latent heat over heterogeneous snow cover." *Quarterly Journal of the Royal Meteorological Society* 123 (543): 1,867–1,883.
- Fang X., J.W. Pomeroy, C.R. Ellis, M.K. MacDonald, C.M. DeBeer and T. Brown. 2013. "Multi-variable evaluation of hydrological model predictions for a headwater basin in the Canadian Rocky Mountains." *Hydrology and Earth System Sciences* 17: 1,635–1,659. doi: 10.5194/hess-17-1635-2013.
- Fang, X., J.W. Pomeroy, C.J. Westbrook, X. Guo, A.G. Minke and T. Brown. 2010. "Prediction of snowmelt derived streamflow in a wetland dominated prairie basin." *Hydrology and Earth System Sciences* 14: 991–1,006. doi: 10.5194/hess-14-991-2010.
- Farinotti, D., H. Corr and G.H. Gudmundsson. 2013. "The ice thickness distribution of Flask Glacier, Antarctic Peninsula, determined by combining radio-echo soundings, surface velocity data and flow modelling." *Annals of Glaciology* 54: 18–24. doi: 10.3189/2013AoG63A603.
- Farinotti, D., M. Huss, A. Bauder and M. Funk. 2009. "An estimate of the glacier volume in the Swiss Alps. Global Planet." *Global and Planetary Change*. 68(3): 225–231. doi: 10.1016/j.gloplacha.2009.05.004.
- Fleming, S.W. and G.K.C. Clarke. 2003. "Glacial control of water resource and related environmental responses to climatic warming: empirical analysis using historical streamflow data from northwestern Canada." *Canadian Water Resources Journal* 28: 69–86.
- Fleming, S.W., R.D. Moore and G.K.C. Clarke. 2006. "Glacier-mediated streamflow teleconnections to the arctic oscillation." *International Journal of Climatology* 26: 619–636.
- Garnier, B.J. and A. Ohmura. 1970. "The evaluation of surface variations in solar radiation income." *Solar Energy* 13: 21–34.
- Gibson, J.J. and T.W. Edwards. 2002. "Regional water balance trends and evaporation-transpiration partitioning from a stable isotope survey of lakes in northern Canada." *Global Biogeochemical Cycles* 16 (2): 10-1 to 10-14.
- Graham L.P., J. Andréasson and B. Carlsson. 2007. "Assessing climate change impacts on hydrology from an ensemble of regional climate models, model scales and linking methods – a case study on the Lule River basin." *Climatic Change* 81: 293–307.
- Granger, R.J. and D.M. Gray. 1990. "A new radiation model for calculating daily snowmelt in open environments." *Nordic Hydrology* 21: 217–234.

- Granger, R.J. and D.M. Gray. 1989. "Evaporation from natural non-saturated surfaces." *Journal of Hydrology* 111: 21–29.
- Granger, R.J. and J.W. Pomeroy. 1997. Sustainability of the western Canadian boreal forest under changing hydrological conditions. Part II: Summer energy and water use. In: Rosjberg, D., N. Boutayeb, A. Gustard, Z. Kundzewicz and P. Rasmussen (eds.). *Sustainability of Water Resources under Increasing Uncertainty*. Wallingford, UK: IAHS Press, pp. 243–250.
- Gray, D.M and P.G. Landine. 1987. "Albedo model for shallow prairie snow covers." *Canadian Journal of Earth Sciences* 24(9): 1,760–1,768.
- Guay, R., R. Gagnon and H. Morin. 1992. "A new automatic method and interactive tree-ring measurement system based on a line scan camera." *Forestry Chronicle* 68: 138–141.
- Haddeland, I., J. Heinke, F. Voß, S. Eisner, C. Chen, S. Hagemann and F. Ludwig. 2012. "Effects of climate model radiation, humidity and wind estimates on hydrological simulations." *Hydrology and Earth System Sciences* 16: 305–318.
- Haeberli, W. and M. Hoelzle. 1995. "Application of inventory data for estimating characteristics of and regional climate-change effects on mountain glaciers: a pilot study with the European Alps." *Annals of Glaciology* 21: 206–212.
- Hinzman, L.D., N.D. Bettez, W.R. Bolton, F.S. Chapin, M.B. Dyurgerov, C.L. Fastie, B. Griffith, R.D. Hollister, A. Hope, H.P. Huntington, A.M. Jensen, G.J. Jia, T. Jorgenson, D.L. Kane, D.R. Klein, G. Kofinas, A.H. Lynch, A.H. Lloyd, A.D. McGuire, F.E. Nelson, W.C. Oechel, T.E. Osterkamp, C.H. Racine, V.E. Romanovsky, R.S. Stone, D.A. Stow, M. Sturm, C.E. Tweedie, G.L. Vourlitis, M.D. Walker, D.A. Walker, P.J. Webber, J.M. Welker, K. Winker and K. Yoshikawa. 2005. "Evidence and implications of recent climate change in northern Alaska and other Arctic regions." *Climatic Change* 72: 251 –298.
- Hock, R. 2003. "Temperature index melt modelling in mountain areas." *Journal of Hydrology* 282: 104–115.
- Hock R. and C. Tijn-Reijmer. 2013. *Program documentation and Users Manual. Version 31: A mass-balance, glacier runoff and multi-layer snow model, DEBAM AND DETIM, Distributed Energy Balance Model and Distributed Enhanced Temperature-Index Model*. Fairbanks, AK: University of Alaska.
- Hinzman, L.D., N.D. Bettez, W.R. Bolton, F.S. Chapin, M.B. Dyurgerov, C.L. Fastie, B. Griffith, R.D. Hollister, A. Hope, H.P. Huntington, A.M. Jensen, G.J. Jia, T. Jorgenson, D.L. Kane, D.R. Klein, G. Kofinas, A.H. Lynch, A.H. Lloyd, A.D. McGuire, F.E. Nelson, W.C. Oechel, T.E. Osterkamp, C.H. Racine, V.E. Romanovsky, R.S. Stone, D.A. Stow, M. Sturm, C.E. Tweedie, G.L. Vourlitis, M.D. Walker, D.A. Walker, P.J. Webber, J.M. Welker, K. Winker and K. Yoshikawa. 2005. "Evidence and implications of recent climate change in northern Alaska and other Arctic regions." *Climatic Change* 72: 251–298.
- Hubbard, B. and N.F. Glasser. 2005. *Field Techniques in Glaciology and Glacial Geomorphology*. West Sussex, England: John Wiley & Sons Ltd.
- Hyndman, R.J. and A.B. Koehler. 2006. "Another look at measures of forecast accuracy." *International Journal of Forecasting* 22(4): 679–688. doi: 10.1016/j.ijforecast.2006.03.001.
- IP3 (Improving Processes and Parameterization for Prediction in Cold Regions Hydrology). 2010. *Improving Processes & Parameterization for Prediction in Cold Regions Hydrology*. Accessed December, 2011. <http://www.usask.ca/ip3/index.php>.

- IPCC (Intergovernmental Panel on Climate Change). 2013. Climate Change 2013: The Physical Science Basis. In Stocker, T.F., D. Qin, G.-K. Plattner, M. Tignor, S.K. Allen, J. Boschung, A. Nauels, Y. Xia, V. Bex and P.M. Midgley (eds.). *Contribution of Working Group I to the Fifth Assessment Report of the Intergovernmental Panel on Climate Change*. Cambridge, UK and New York, NY, USA: Cambridge University Press, 1,535 pp.
- Janowicz, J.R. 2008. "Apparent recent trends in hydrologic response in permafrost regions of northwest Canada." *Hydrology Research* 39(4): 267–275.
- Janowicz, J.R., S. Krogh, J.W. Pomeroy, T. Williams, S. Carey and C. Beaudry. 2016. Sensitivity of Dempster Highway Hydrological Response to Climate Warming: Final Report. Report to Indigenous and Northern Affairs Canada. Government of Yukon.
- Jianqi, S. and W. Huijun. 2006. "Relationship between arctic oscillation and pacific oscillation on decadal timescale." *Chinese Science Bulletin* 51(1): 75–79.
- Kääb, A. 2000. "Photogrammetric reconstruction of glacier mass-balance using a kinematic ice-flow model, a 20-year time-series on Grubengletscher, Swiss Alps." *Annals of Glaciology* 31: 45–52. doi: 10.3189/172756400781819978.
- Kim, S.J., G.M. Flato, G.J. Boer and N.A. McFarlane. 2002. "A coupled climate model simulation of the Last Glacial Maximum, Part 1: transient multi-decadal response." *Climate Dynamics* 19: 515–537.
- Klock, R., E. Hudson, D. Aihoshi and J. Mullock. 2011. *The Weather of the Yukon, Northwest Territories and Western Nunavut: Graphic Area Forecast 35*. Ottawa, ON: NAV Canada.
- Leavesley, G.H., R.W. Lichty, B.M. Troutman and L.G. Saindon. 1983. *Precipitation-runoff Modelling System: User's Manual*. Reston, VA: United States Geological Survey.
- Lewkowicz, A.G., P.P. Bonnaventure, S.L. Smith and Z. Kuntz. 2012. "Spatial and thermal characteristics of mountain permafrost, northwest Canada." *Geografiska Annaler: Series A, Physical Geography* 94(2): 195–213. doi: 10.1111/j.1468-0459.2012.00462.x.
- Liang, X., D.P. Lettenmaier, E.F. Wood and S.J. Burges. 1994. "A simple hydrologically based model of land surface water and energy fluxes for GCMs." *Journal of Geophysical Research* 99(D7): 41,415–41,428.
- Linsbauer, A., F. Paul and W. Haeberli. 2012. "Modeling glacier thickness distribution and bed topography over entire mountain ranges with GlabTop: application of a fast and robust approach." *Journal of Geophysical Research* 117: 1–17. doi:10.1029/2011JF002313.
- López-Moreno, J.I., J.W. Pomeroy, J. Revuelto and S.M. Vicente-Serrano. 2012. "Response of snow processes to climate change: spatial variability in a small basin in the Spanish Pyrenees." *Hydrological Processes* 27: 2,637–2,650. doi: 10.1002/hyp.9408.
- Mahfouf, J.F., B. Brasnett and S. Gagnon. 2007. "A Canadian Precipitation Analysis (CaPA) project: description and preliminary results." *Atmosphere-Ocean* 45(1): 1–17.
- Matott, L.S. 2007. *An Optimization Software Tool: Documentation and User's Guide*. Buffalo, NY: State University of New York at Buffalo.
- Matthews, J.A. and K.R. Briffa. 2005. "The 'Little Ice Age': re-evaluation of an evolving concept." *Geografiska Annaler* 87A (1): 17–36.
- MacDonald, M.K., J.W. Pomeroy and A. Pietroniro. 2009. "Parameterising redistribution and sublimation of blowing snow for hydrological models: tests in a mountainous subarctic catchment." *Hydrological Processes* 23(18): 2,570–2,583. doi: 10.1002/hyp.7356.

- McCartney, S.E., S.K. Carey and J.W. Pomeroy. 2006. "Intra-basin variability of snowmelt water balance calculations in a subarctic catchment." *Hydrological Processes* 20(4): 1,001–1,016.
- Michel, L., M. Picasso, D. Farinotti, A. Bauder, M. Funk and H. Blatter. 2013. "Estimating the ice thickness of mountain glaciers with an inverse approach using surface topography and mass balance." *Inverse Problems* 29: 1–23. doi: 10.1088/0266-5611/29/3/035002.
- Moore, R.D. and M.N. Demuth. 2001. "Mass balance and streamflow variability at Place Glacier, Canada, in relation to recent climate fluctuations." *Hydrological Processes* 15(18): 3,473–3,486.
- Moore, R.D., S.W. Fleming, B. Menounos, R. Wheate, A. Fountain, K. Stahl, K. Holm and M. Jakob. 2009. "Glacier change in western North America: influences on hydrology, geomorphic hazards and water quality." *Hydrological Processes* 23: 42– 61.
- Moradkhani, H., K. Hsu, H. Gupta and S. Sorooshian. 2005a. "Uncertainty assessment of hydrologic model states and parameters: Sequential data assimilation using the particle filter." *Water Resources Research* 41: W05012. doi.org/ 10.1029/2004WR003604.
- Moradkhani, H., S. Sorooshian, H.V. Gupta and P.R. Houser. 2005b. "Dual state parameter estimation of hydrological models using ensemble Kalman filter." *Advances in Water Resources* 28: 135–147.
- Morlighem, M., E. Rignot, H. Seroussi, E. Larour, H. Ben Dhia and D. Aubry. 2011. "A mass conservation approach for mapping glacier ice thickness." *Geophysical Research Letters* 38: 1–6. doi: 10.1029/2011GL048659.
- Nachtergaele, L., H.V. Velthuisen, L. Verelst and D. Wiberg. 2012. *Harmonized World Soil Database, Version 1.2*. Rome: FAO/IIASA/ISRIC/ISS-CAS/JRC.
- Narod, B.B. and G.K.C. Clarke. 1994. "Miniature high-power impulse transmitter for radio-echo sounding." *Journal of Glaciology* 40(134): 190–194.
- Nash, J.E. and J.V. Sutcliffe. 1970. "River flow forecasting through conceptual models. Part I: A discussion of principles." *Journal of Hydrology* 10 (3): 282–290.
- Naz, B.S., C.D. Frans, G.K.C. Clarke, P. Burns and D.P. Lettenmaier. 2014. "Modeling the effect of glacier recession on streamflow response using a coupled glacio-hydrological model." *Hydrology and Earth System Sciences* 18: 787–802.
- NCE (Northern Climate Exchange). 2016. *Data Retrieval Software Manual*. Whitehorse, YT: Northern Climate Exchange, Yukon Research Centre.
- NCE (Northern Climate Exchange). 2014. *Projected future changes in glaciers and their contribution to discharge of the Yukon River at Whitehorse*. Whitehorse, YT: Northern Climate Exchange, Yukon Research Centre.
- Neal, E.G., M.T. Walter and C. Coffeen. 2002. "Linking the pacific decadal oscillation to seasonal stream discharge in southeast Alaska." *Journal of Hydrology* 263: 188–197.
- Østrem, G. and M.M. Brugman. 1991. *Glacier Mass-Balance Measurements: A manual for field and office work*. National Hydrology Research Institute, Science Report No. 4. Ottawa: Ministry of Supply and Services.
- Pattyn, F. and W. Van Huelde. 1998. "Power law or power flaw?" *Earth Surface Processes and Landforms* 23: 761–767.

- Peduzzi, P., C. Herold and W. Silverio. 2010. "Assessing high altitude glacier thickness, volume and area changes using field, GIS and remote sensing techniques: the case of Nevado Coropuna (Peru)." *The Cryosphere* 4: 313–323. doi: 10.5194/tc-4-313-2010.
- Pietroniro, A., V. Fortin, N. Kouwen, C. Neal, R. Turcotte, B. Davison, D. Versegny, E.D. Soulis, R. Caldwell, N. Evora and P. Pellerin. 2007. "Development of the MESH modelling system for hydrological ensemble forecasting of the Laurentian Great Lakes at the regional scale." *Hydrology and Earth System Sciences* 11: 1,279–1,294.
- Pomeroy, J.W and L. Li. 2000. "Prairie and Arctic aerial snow cover mass balance using a blowing snow model." *Journal of Geophysical Research* 105(D21): 26,619–26,634.
- Pomeroy, J.W., D.M. Gray, N.R. Hedstrom and J.R. Janowicz. 2002. "Prediction of seasonal snow accumulation in cold climate forests." *Hydrological Processes* 16: 3,543–3,558.
- Pomeroy, J.W., D.M. Gray, T. Brown, N.R. Hedstrom, W.L. Quinton, R.J. Granger and S.K. Carey. 2007. "The cold regions hydrological model: a platform for basing process representation and model structure on physical evidence." *Hydrological Processes* 21: 2,650–2,667. doi: 10.1002/hyp.6787.
- Pomeroy, J.W., O.M. Semenova, X. Fang, Y.B. Vinogradov, C. Ellis, T.A. Vinogradova, M. MacDonald, E.E. Fisher, B.V. Sochava, P. Dornes, L. Lebedeva and T. Brown. 2010. *Wolf Creek Cold Regions Model Set-up, Parameterization and Modelling Summary*. Report No. 8. Saskatoon: Centre for Hydrology, University of Saskatchewan.
- Porparto, A. and L. Ridolfi. 1998. "Influence of weak trends on exceedance probability." *Stochastic Hydrology and Hydraulics* 12(1): 1–15.
- Prowse, T.D. and C. Furgal. 2009. "Northern Canada in a changing climate: major findings and conclusions." *Ambio* 38 (5): 290–292.
- Prowse, T.D., F.J. Wrona, J.D. Reist, J.J. Gibson, J.E. Hobbie, L. Lévesque and W.F. Vincent. 2006. "Climate change effects on hydroecology of arctic freshwater ecosystems." *Ambio* 35(7): 347–358.
- Rasouli, K., J.W. Pomeroy, J.R. Janowicz, S.K. Carey and T.J. Williams. 2014. "Hydrological sensitivity of a northern mountain basin to climate change." *Hydrological Processes* 28: 4,191–4,208.
- Reimer, P.J., E. Bard, A. Bayliss, J.W. Beck, P.G. Blackwell, C. Bronk Ramsey, C.E. Buck, H. Cheng, R.L. Edwards, M. Friedrich, P.M. Grootes, T.P. Guilderson, H. Hafliðason, I. Hajdas, C. Hatté, T.J. Heaton, D.L. Hoffmann, A.G. Hogg, K.A. Hughen, K.F. Kaiser, B. Kromer, S.W. Manning, M. Niu, R.W. Reimer, D.A. Richards, E.M. Scott, J.R. Southon, R.A. Staff, C.S.M. Turney and J. van der Plicht. 2013. "IntCal13 and Marine13 radiocarbon age calibration curves 0-50,000 years cal BP." *Radiocarbon* 55(4): 1,869–1,887.
- Rouse, W.R., M.S. Douglas, R.E. Heckey, A.E. Hershey, G.W. Kling, L. Lesack, P. Marsh, M. McDonald, B.J. Nicholson, N.T. Roulet and J.P. Smol. 1997. "Effects of climatic change on the freshwaters of Arctic and Subarctic North America." *Hydrological Processes* 11: 873–902.
- Samolczyk, M., S. Laxton and J.J. Clague. 2016. Late Holocene fluctuations of the north lobe of Llewellyn Glacier, Upper Yukon River Basin. In: K.E. MacFarlane and M.G. Nordling (eds.). *Yukon Exploration and Geology 2015*. Whitehorse: Yukon Geological Survey.
- Samuel, J., P. Coulibaly and R.A. Metcalfe. 2012. "Evaluation of future flow variability in ungauged basins: Validation of combined methods." *Advances in Water Resources* 35: 121–140.
- Samuel, J., P. Coulibaly, G. Dumenah and H. Moradkhani. 2014. "Assessing model state variation in hydrologic data assimilation." *Journal of Hydrology* 513: 127–141.

- Samuel, J., P. Coulibaly and J. Kollat. 2013. "CRDEMO: Combined regionalization and dual entropy-multiobjective optimization for hydrometric network design." *Water Resources Research* 49: 1-20. doi: 10.1002/2013WR014058.
- Serreze, M.C., J.E. Walsh, E.C. Chapin, T. Osterkamp, M. Dyurgerov, V. Romanovsky, W.C. Oechel, J. Morison, T. Zhang and R.G. Barry. 2000. "Observation evidence of recent change in the northern high-latitude environment." *Climatic Change* 46: 159–207.
- Shea, J.M., R.D. Moore and K. Stahl. 2009. "Derivation of melt factors from glacier mass-balance records in western Canada." *Journal of Glaciology* 55(189): 123–130.
- Shepard, D. 1968. A two-dimensional interpolation function for irregularly-spaced data. *Proceedings of the 1968 ACM National Conference*, pp. 517–524. doi: 10.1145/800186.810616.
- Sicart, J.E., J.W. Pomeroy, R.L.H. Essery and D. Bewley. 2006. "Incoming longwave radiation to melting snow: observations, sensitivity and estimation in northern environments." *Hydrological Processes* 20: 3,697–3,708. doi: 10.1002/hyp.6383.
- Smith, C.A.S., J.C. Meikle and C.F. Roots (eds.). 2004. *Ecoregions of the Yukon Territory - Biophysical Properties of Yukon Landscapes*. Summerland, BC: Agriculture and Agri-Food Canada, PARC Technical Bulletin 04–01.
- Solomon, S., D. Qin, M. Manning, Z. Chen, M. Marquis, K.B. Averyt, M. Tignor and H.L. Miller. 2007. *Climate Change 2007 - The Physical Science Basis: Contribution of Working Group I to the Fourth Assessment Report of the Intergovernmental Panel on Climate Change*. Cambridge, United Kingdom: Cambridge University Press.
- Soulis, E.D., K.R. Snelgrove, N. Kouwen, F. Seglenieks and D.L. Verseghy. 2000. "Towards closing the vertical water balance in Canadian atmospheric models: coupling of the land surface scheme CLASS with the distributed hydrological model WATFLOOD." *Atmosphere-Ocean* 38 (1): 251–269.
- Stahl, K. and R. Moore. 2006. "Influence of watershed glacier coverage on summer streamflow in British Columbia, Canada." *Water Resources Research* 42: 1–5.
- Theakstone, W.H. 1988. "Temporal variations of isotopic composition of glacier-river water during summer: Observations at Austre Okstindbreen, Okstindan, Norway." *Journal of Glaciology* 34: 309–317.
- Tolson, B.A. and C.A. Shoemaker. 2007. "Dynamically dimensioned search algorithm for computationally efficient watershed model calibration." *Water Resources Research* 43: W01413. doi: 10.1029/2005WR004723.
- Trenberth, K.E. 1990. "Recent observed interdecadal climate changes in the northern hemisphere." *Bulletin of the American Meteorological Society* 71(7): 988–993.
- Turner, K.W., B.B. Wolfe and T.W. Edwards. 2010. "Characterizing the role of hydrological processes on lake water balances in the Old Crow Flats, Yukon Territory, Canada, using water isotope tracers." *Journal of Hydrology* 386 (1-4): 103–117.
- Vincent, L.A., X.L. Wang, E.J. Milewska, H. Wan, F. Yang and V. Swail. 2012. "A second generation of homogenized Canadian monthly surface air temperature for climate trend analysis." *Journal of Geophysical Research* 117: D18110. doi: 10.1029/2012JD017859.
- WC2N (Western Canadian Cryospheric Network). 2010. Western Canadian Cryospheric Network. Accessed December 2011. <http://wc2n.unbc.ca>.
- Whitfield P. and A. Cannon. 2000. Recent climate moderated shifts in Yukon hydrology. In: D.L. Kane (ed.). *Water Resources in Extreme Environments*. Proceedings of the American Water Resources Association Spring Specialty Conference, Anchorage, Alaska, May 1 –3, 2000. Middleburg, VA: American Water Resources Association, pp. 257–262.

Wigmosta, M.S., L.W. Vail and D.P. Lettenmaier. 1994. "A distributed hydrology-vegetation model for complex terrain." *Water Resources Research* 30: 1,665–1,680.

Wilby, R.L., C.W. Dawson and E.M. Barrow. 2002. "SDSM – a decision support tool for the assessment of regional climate change impacts." *Environmental Modelling and Software* 17: 145–157.

Woo, M.K., A.G. Lewkowitz and W.R. Rouse. 1992. "Response of the Canadian permafrost environment to climatic change." *Physical Geography* 13: 287–317.

Yeh, K.S., J. Côté, S. Gravel, A. Méthot, A. Patoine, M. Roch and A. Staniforth. 2002. "The CMC-MRB Global Environmental Multiscale (GEM) model. Part III: Nonhydrostatic formulation." *Monthly Weather Review* 130: 339–356.

Zekollari, H., P. Huybrechts, J.J. Fürst, O. Rybak and O. Eisen. 2013. "Calibration of a higher-order 3-D ice-flow model of the Morteratsch glacier complex, Engadin, Switzerland." *Annals of Glaciology* 54: 343–351.  
doi: 10.3189/2013AoG63A434.

Zhao, L. and D.M. Gray. 1999. "Estimating snowmelt infiltration into frozen soils." *Hydrological Processes* 13: 1,827–1,842.

Zhou, J., J.W. Pomeroy, W. Zhang, G. Cheng, G. Wang and C. Chen. 2014. "Simulating cold regions hydrological processes using a modular model in the west of China." *Journal of Hydrology* 509: 13–24.





